Electrospun Soy Protein-based Scaffolds for Skin Tissue Engineering and Wound Healing

A Thesis

Submitted to the Faculty

of

Drexel University

by

Leko Lin

in partial fulfillment of the

requirements for the degree

of

Doctor of Philosophy

February 2011

Dedications

To my mother

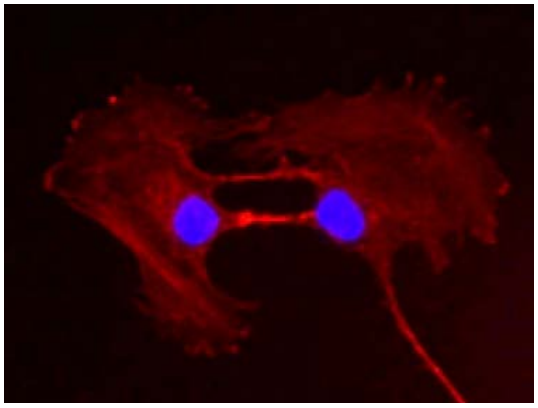

Acknowledgments

First and foremost, I would like to express my heartfelt gratitude to my advisor, Prof. Peter Lelkes, for his guidance and generosity throughout my time at Drexel. It is my honor to be a part of carrying out the research that moved this project forward since it began as his vision for using plant proteins in tissue engineering. With his patience and insight, he has taught me to approach problems critically and to keep an open mind, and many skills to succeed in research and in life. As a mentor, he has inspired an enduring passion for science, and he has been most understanding and supportive during a time of difficult circumstances in my life; for all of these things I am very grateful to him.

I would also like to thank my co-advisor, Dr. Dara Woerdeman, who also had a vision for this project and shared with me a lot of knowledge about plant proteins and their behavior, and who often guided me to look at research problems from a wider perspective;

Prof. Elisabeth Papazoglou for sharing her expertise in wound healing and animal studies, for the collaboration from her and her team in the functional near infrared (fNIR) spectroscopy studies, and for being a member of my committee;

Prof. Fred Allen, Prof. Cezary Marcinkiewicz and Prof. Philip Lazarovici, for their guidance, expertise and critical input into this project, and for being on my committee.

I am very grateful to Prof. Yury Gogotsi for accepting me into the Integrative Graduate Education and Research Traineeship (IGERT) program, which provided me with financial support (NSF-IGERT, DGE-0221664 and DGE-0654313) and valuable learning experiences beyond my field of research.

This project has also received funding from the Nanotechnology Institute of Southeastern Pennsylvania, the Louis and Bessie Stein Family Foundation, and the Wallace H. Coulter Foundation.

I would like to thank Dr. Julie Mostov and the Office of International Programs for granting me an International Travel Award to present at the World Biomaterials Congress in Amsterdam, 2008; and Dr. Teck-Kah Lim and the Graduate Studies Office for granting me a Travel Subsidy Award and a Dissertation Fellowship; and Prof. Banu Onaral and Prof. Rahamim Seliktar for support from the School of Biomedical Engineering, Science and Health Systems.

Gratitude is owed to the following individuals:

Dr. David Moscatello (Coriell Institute for Medical Research) for his generous gift of primary normal human epidermal keratinocytes, and for his advice on working with them.

Prof. J. Yasha Kresh, Prof. Gregg Johannes, Prof. Mark Stearns, Prof. Jane Azizkhan-Clifford, Prof. Karen Winey (University of Pennsylvania) and Dr. Boris Polyak for granting me use of their laboratory equipment.

Kimberly Wasko, CVT, VTS, RLATG, SRS for her tireless and enthusiastic work in the animal studies, and always looking for innovative solutions to research and technical problems. The raw data on the aged rat and splinted (ring) model in this thesis are courtesy of Kim.

Michael Weingarten, MD, FACS for his work in the animal studies and expertise in wound healing.

Piotr Krecioch, MD for his help with the animal studies.

Janet Schulenberg for training me to work with rats and teaching me about their dispositions.

Dee Breger and Dr. Ed Basgall for their assistance and training on the scanning electron microscope (SEM).

Xiang Mao, Joshua Samuels and Michael Neidrauer for their work in taking measurements and data analysis as part of the “wound healing team”.

Sin Chung Park for helping me with machining parts to fit with various lab equipment setups.

Dr. Mohammad Moniruzzaman and Dr. Arun Kota for assistance with the Instron in Prof. Karen Winey’s lab.

Lelkes Lab past and present:

Dr. Anat Katsir, who taught me a lot about research, cell culture and lab culture from the time I first joined the Lelkes Lab and throughout the time I was there. She has helped me greatly, teaching me many lab skills, providing a lot of encouragement and perspective, and believing in me.

Dr. Mengyan Li, who helped me through a rough period during my PhD with her valuable advice, encouragement, support and friendship.

Dr. Ie Uttayarat, who also helped me with advice, example and friendship.

Sirma Koutzaki, who taught me a lot about histology and took the time to help me even when she was busy.

Dr. Donald Simons, Dr. Mark Mondrinos, and Dr. Vishal Kamat for their help, advice, and interesting conversation in the lab.

Dr. Qingwei Zhang for helping me with SEM and EDAX data acquisition, and especially for her contagious enthusiasm and wonderful friendship!

Dr. Jingjia Han, who first welcomed me to the Lelkes Lab with a tour and introduced me to electrospinning, and who has been my labmate, office-mate, fellow group member in class, and great friend during the time I've been at Drexel. She has helped me in numerous aspects of lab life and with experiments, as well as outside the lab.

Devika Varma, who worked diligently on the electrospinning of zein and the characterization and cell culture experiments on electrospun zein. She is a keen learner and a pleasure to work with.

Rosemary Bastian, who kindly and patiently guided me through the processes of RNA isolation, cDNA synthesis, and RT-PCR.

Brittany Pattinson, Depinder Khaira and Vy Nguyen for helping me with experiments—thank you and I hope the experience was worthwhile for you.

Anant Chopra, Anusha Rajan, Aybike Saglam, Collin Stabler, Diane Keene, Gözde Şenel, Gregory Botta, Haibo Gong, Igor Zabrodin, Jessica Falcon, Michael Frohbergh, Nidhi Sheth, Pimchanok Pimton, Sean Devlin, Seda Karamil—thank you for your help and for making the lab a cheerful and friendly place.

Susan Sullivan, who always made sure things ran smoothly for the lab and was there to help with anything when we needed it, as well as being a great friend.

Lisa Williams, Caryn Glaser, Natalia Broz and Danielle Crocker in the Biomed Office, who took care of everything administrative.

I would like to thank my long-time, long-distance mentors, Dr. Esther Hanna, Alfreda and Gordon Hanna, and the late Geraldine Huhnke, who have provided much wisdom and helped me to grow in faith and perseverance.

My friends Tyra, Fuhan, Eyal, Seeni, Lydia and Iris, who made my time in Philly memorable and have added a lot of depth to some of the most important years of my life. We celebrated and commiserated and grew together through many experiences, and I wish you all the best.

I am indebted to my family for their enduring and unconditional support, and I am blessed to be able to share this journey with my fiancé, Ho-Lung, to whom I am grateful for his love, patience, kindness and support in so many ways.

Table of Contents

List of Tables

List of Figures

Abstract

Electrospun soy protein-based scaffolds for
skin tissue engineering and wound healing

Leko Lin

Peter I. Lelkes, Ph.D.

In order to bypass some of the limitations of currently available skin substitutes and wound dressings, we explored the use of bioactive scaffolds made of plant-derived proteins. We hypothesized that these “green” materials may confer bioactive properties to enhance wound healing and skin regeneration. We optimized the parameters for electrospinning fibrous scaffolds from soy protein isolate (SPI) with addition of 0.05% poly(ethylene oxide) (PEO) dissolved in 1,1,1,3,3,3-hexafluoro-2-propanol, and characterized these scaffolds based on their physical and mechanical properties, degradation behavior, and *in vitro* biocompatibility. SPI/PEO scaffolds remained stable without further cross-linking, possessing mechanical properties similar to those reported for human skin, and supported the adhesion and proliferation of cultured primary human dermal fibroblasts alone and in organotypic co-culture with primary human epidermal keratinocytes. Using targeted PCR arrays and qPCR validation, we found similar gene expression profiles of fibroblasts cultured for 2h and 24h on SPI substrates and on collagen type I at both time points. On both substrates there was a pronounced time-dependent up-regulation of

several genes related to extracellular matrix (ECM) remodeling, including MMP-10, MMP-1, collagen VII, integrin-α2 and laminin-β3, indicating that both plant- and animal-derived materials induce similar responses from the cells after initial adhesion, degrading substrate proteins and depositing ECM in a “normal” remodeling process.

Electrospun SPI/PEO scaffolds were evaluated *in vivo* against Tegaderm™ wound dressing, a standard in wound care, in a full-thickness excision wound model in the hairless rat. SPI/PEO scaffolds promoted a slightly but not significantly faster initial wound closure than Tegaderm™. The similar quantitative response in both groups was corroborated by non-invasive optical measurements using functional near infrared spectroscopy (fNIR). Electrospun SPI/PEO scaffolds provided qualitative benefits over Tegaderm™, including greater compliance to the wound shape, and the tendency to absorb wound exudates. SPI/PEO scaffolds integrated well with the wound and detached naturally with the formed encrustation at day 7 that occurred in both treatment groups. SPI/PEO scaffolds are therefore promising as a new type of treatment for non-healing wounds, and further studies will help to elucidate potential mechanisms by which it promotes wound healing at a cellular and/or molecular level.

Executive Summary

The work proposed in this thesis is focused on the ***long-term goal*** of developing a novel, acellular, plant protein-based scaffold for skin tissue engineering and wound healing applications. Non-healing wounds afflict millions of people worldwide and translate into billions of dollars in healthcare costs each year. Currently available skin substitutes have only limited clinical success and present several disadvantages including the risk of immune rejection or disease transfer from allogeneic or xenogeneic sources, long (2-6 weeks) culture times where cellular components are involved, mismatching mechanical properties, and high cost. We explore the use of soy protein isolate (SPI) as a "green" raw material to bypass some of these limitations associated with animal-derived and/or synthetic materials. Soy protein is abundant, produced from renewable sources, and has well documented bioactivity *in vitro* and *in vivo*. It is also a versatile biomaterial that can be fabricated into various forms of scaffold including fibrous scaffolds, hydrogels and films. Our ***overall hypothesis*** is that soy protein-based scaffolds will promote a cellular and wound healing response similar to or better than other well-established biomaterials.

Toward our long-term goal, three ***specific aims*** are proposed: 1) Fabricate a novel soy protein-based electrospun fibrous scaffold and characterize its mechanical properties,

degradation behavior and *in vitro* biocompatibility. 2) Identify initial adhesion mechanisms of human dermal fibroblasts to SPI/PEO. 3) Evaluate electrospun SPI/PEO scaffolds *in vivo* using a rat wound healing model.

For Specific Aim 1, we chose electrospinning as our fabrication technique based on its ability to produce biomimetic structures. We discovered that SPI alone in solution could not be electrospun into fibers, but that a minimal addition of the inert synthetic polymer, poly(ethylene oxide) (PEO), enabled fiber formation by virtue of increased chain entanglements. The optimal solvent was determined to be 1,1,1,3,3,3 Hexafluoro-2-propanol (HFP), which produced stable solutions with indefinite shelf lives. Importantly, resultant electrospun fibers were resistant to hydrolysis in aqueous media without further cross-linking. Electrospun SPI/PEO scaffolds were ductile and their mechanical and tactile properties became more “skin-like” in hydrated condition. Although hydrolysis-resistant, SPI/PEO scaffolds were able to be degraded proteolytically. SPI/PEO scaffolds promoted the attachment and proliferation of primary human dermal fibroblasts in a similar manner to scaffolds electrospun from more well-established materials such as poly(lactic-*co*-glycolic acid) (PLGA) and gelatin.

Specific Aim 2 was proposed to address the mechanistic question of “how” mammalian cells

attached to and interacted with foreign materials, and we approached it with the hypothesis that *initial cellular adhesion to foreign substrates such as SPI was at least partially mediated by integrins and/or other cell adhesion molecules*. Human dermal fibroblasts were seeded onto substrates coated with SPI and collagen type I, to compare the cellular response to SPI with a native ECM protein. A global analysis of gene expression related to human ECM and adhesion molecules, using targeted PCR arrays, was followed by validation with PCR analysis of specific genes up-regulated or highly expressed by fibroblasts on these substrates after 2 h and 24 h of seeding. Surprisingly, no substrate-significant differences were found at either time point. However, on both substrates, certain genes were similarly up-regulated at 24 h compared to 2 h. MMP-10 was the most highly up-regulated, approx. 1152-fold on SPI and 471-fold on collagen I. MMP-1 was also very highly up-regulated, 54-fold on SPI and 37-fold on collagen I. ECM proteins collagen and laminin, as well as integrin subunit α2, the predominant cell surface receptor for collagen, were also up-regulated at 24 h. Taken together, these results point to an aggressive remodeling response by the fibroblasts to their immediate extracellular environment. Importantly, SPI elicited a similar gene expression profile as the native ECM protein collagen and also on the synthetic PLGA, suggesting that SPI as a biomaterial may be as suitable as these other well-established materials.

Specific Aim 3 was fulfilled at a preliminary level in evaluations that were carried out to the end of study at complete wound closure. Electrospun SPI/PEO scaffolds were evaluated against Tegaderm™ wound dressing, a standard in wound care, as a control in a full-thickness excision wound model in the hairless rat. SPI/PEO scaffolds promoted a slightly but not significantly faster initial wound closure than the control, although wounds in both groups healed completely by post-operative day 18, while the neodermis continued to be replaced by thicker scar tissue up to the end of our study at day 31. The similar quantitative response in both groups was corroborated by non-invasive optical measurements using functional near infrared spectroscopy (fNIR).

Electrospun SPI/PEO scaffolds provided qualitative benefits over the control, including greater compliance to the wound shape, and the tendency to absorb wound exudates thus preventing irritation at the wound site. SPI/PEO scaffolds integrated well with the wound and detached naturally with the formed encrustation at day 7 that occurred in both treatment groups. These scaffolds provide a “breathable” interface between the wound and the external environment, which allow for a normal course of healing without the disadvantages of occlusive dressings that do not come in direct contact with the open wound. By design as a permanent scaffold, electrospun SPI/PEO is able to present structural and molecular cues to the cells in a

regenerating wound environment. It is therefore promising as a new type of treatment for non-healing wounds, and further studies will help to elucidate potential mechanisms by which it promotes wound healing at a cellular and/or molecular level.

Chapter 1. Background and Introduction

1.1. Skin

1.1.1. Anatomy

Skin is the largest organ in the vertebrate body and makes up approximately one-tenth of the body mass in humans (Metcalfe and Ferguson, 2007). Skin (Figure 1.1) consists of two main cell layers, the upper being stratified epidermis and the lower being the dermis, connected to the subcutaneous fatty layer separating the skin from the rest of the body. The two layers are separated by a basement membrane (BM) comprising BM-specific extracellular matrix (ECM) proteins such as laminin and collagen IV. The epidermis can be further divided into fine layers of progressively differentiated keratinocytes—the *stratum basale* or *stratum germinativum*, *stratum spinosum*, *stratum granulosum* and *stratum corneum*, with the uppermost *stratum corneum* being the most differentiated and first to slough off. Keratinocytes (KC) are the major cell type of the epidermis and make up approximately 95% of the total cell population. Also scattered throughout the epidermis are melanocytes, which secrete melanin and account for the pigmentation of skin. The dermis consists of fibroblasts, which confer the tensile strength and connective tissue function of the skin (McGrath et al., 2004). 70% - 80% of the dry weight of dermis is comprised of collagens, mainly type I collagen, with the ratio of collagen type III to type I increasing with age (Waller and Maibach, 2006). While both collagen I and collagen III are

fibril-forming collagens, collagen I is a heterotrimer that contributes to tensile stiffness in tissues, and collagen III is a homotrimer that contributes to elasticity (Gelse et al., 2003). Elastin is the other predominant protein, responsible for the resilience and suppleness of skin, but accounts for only a small proportion (2-4%) of the bulk volume of dermis (Waller and Maibach, 2006). Embedded within the dermis are also other functional components such as eccrine (sweat) glands, sebaceous glands, vasculature, nerves and hair follicles (McGrath et al., 2004).

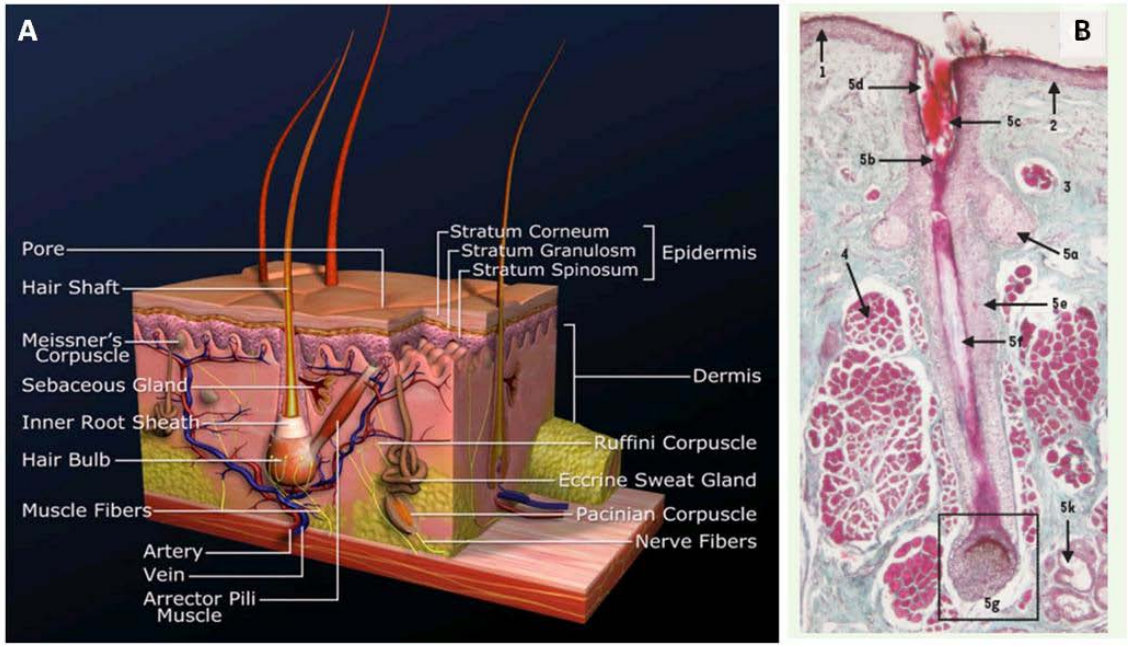

Figure 1.1. Various components of human skin. a) Schematic diagram of skin cross-section (Taken from http://en.wikipedia.org/wiki/Image:3DScience_skin_section_labeled.jpg) b) Histological section of cellular components of human skin from the eyelid; 1) epidermis, 2) dermo-epidermal junction, 3) dermis (collagen fibers stained green), 4) striated skeletal muscle, 5a) sebaceous gland, 5b) isthmus of hair follicle, 5c) hair shaft, 5d) infundibulum, 5e) external follicular sheath, 5f) hair root, 5g) hair bulb (taken from Prost-Squarcioni, 2006).

Dermal fibroblasts show differences in matrix molecule production depending on their region. Fibroblasts in the superficial, papillary dermis produce low levels of the proteoglycan versican and high levels of decorin. Conversely, fibroblasts in the deeper, reticular dermis produce high levels of versican and low levels of decorin (Nolte et al., 2008). Versican is a large proteoglycan with a 265 kDa core protein attached to 12-15 chondroitin sulfate type glycosaminoglycans (GAGs), and appears in the basal layer of adult skin epidermis as well as in association with elastic fibers in the dermis. By contrast, decorin is a small proteoglycan with a 36 kDa core protein attached to a single GAG, usually of the dermatan sulfate type, and is found in association with dermal collagen fibers (Carrino et al., 2000). Decorin is also a crucial mediator of collagen fibrillogenesis, as it binds to collagen near the C-terminus of a newly forming fibril, regulating lateral fusion and maintaining uniform interfibrillar spacing. It also binds to transforming growth factor-β (TGF-β) and inhibits fibrotic stimulation of collagen production by TGF-β (Reed and Iozzo, 2002).

Dermal fibroblasts may be grouped into two major populations based on their mitotic status. The first, replicative progenitor fibroblasts, are mitotically active and in human, rat and mouse skin has been shown both *in vivo* and *in vitro* to differentiate along this lineage until spontaneous terminal differentiation into irreversible postmitotic fibrocytes. These fibrocytes

produce approximately 5-8 times more total collagen than the replicative fibroblasts and maintain the homeostasis of interstitial tissues by maintaining the correct ratio of collagens (Nolte et al., 2008).

Epidermal keratinocytes are connected by various intercellular junctions that are responsible for signaling between epithelial cells. Desmosomes bridge adjacent keratinocytes by anchoring the cell membrane with keratin intermediate filaments, and space adjacent cells by approx. 30 nm. Adherens junctions also link adjacent keratinocytes via the transmembrane glycoprotein E-cadherin. Within the cell, they associate with the actin cytoskeleton mainly through α-catenin. Gap junctions connect adjacent keratinocytes with each other and other cells in the form of clusters of intracellular channels known as connexons. Gap junctions permit ion exchange and the passing of low molecular mass (<1000 Da) metabolites between cells. Tight junctions are intercellular proteins that regulate barrier permeability and include occludin, junction adhesion molecule and claudins (McGrath et al., 2004).

A small population of different stem cells exist within the skin, located in clusters at the bulge region of hair follicles. Keratinocyte stem cells divide infrequently, and some become transient amplifying cells that proliferate before undergoing terminal differentiation. The stem cells show

increased β1 integrin expression as well as high levels of Notch ligand Delta 1 (McGrath et al., 2004). Neighboring cells may express Notch 1 but not Delta 1, and be committed to differentiation into mature keratinocytes. Delta 1 inhibits Notch 1 receptor expression in the same cells but activate neighboring transit amplifying cells which express Notch 1 but not Delta 1; thus, cells expressing only Notch 1 are "responding cells" (Thélu et al., 2002). Notch-Delta signaling is absent during the temporary hyperproliferative phase of wound healing in the epidermis, but is restored once the epidermis is regenerated and stratified, with keratinocytes once again committed to differentiation (Thélu et al., 2002).

1.1.2. Function

The skin serves to protect the underlying layers from exposure to the outside environment, a function fulfilled mainly by the epidermis. The tight packing of corneocytes (anucleated, flattened cells) to each other, as well as the arrangement of lipids in the uppermost stratum corneum prevents transepidermal water loss (TEWL). The skin also protects against other exogenous stressors, which include ultraviolet radiation, chemicals and mechanical forces. The dermis plays an active role in wound healing as dermal fibroblasts synthesize new collagen and also produce proteolytic enzymes necessary for remodeling. Underneath the dermis, the hypodermis consists of well-vascularized adipose tissue that also contributes to the mechanical

properties of the skin as well as the ability of the skin to regulate body temperature (Metcalfe and Ferguson, 2007).

1.2. Wound healing

Wound healing of the injured skin is divided into three main phases: hemostasis and inflammation, re-epithelialization and granulation tissue formation, and finally tissue remodeling (Figure 1.2). Hemostasis begins locally at the site of the wound, as bleeding occurs from the disrupted blood vessels and platelets are activated. Soluble fibrinogen is cleaved by thrombin to form insoluble fibrin fibers, which bind to platelets to form a fibrin clot to stop the bleeding and serve as a provisional matrix (Toriseva and Kähäri, 2009). The first inflammatory response will be induced by the resident mast cells in the wound, which help recruit neutrophils by signaling with tumor necrosis factor (TNF) and leukotrienes, which also stimulate vasodilation during inflammation (Baum and Arpey, 2005). Within two days of the injury in humans, monocytes are also recruited and become activated macrophages, which secrete transforming growth factors (TGF-β and TGF-α), basic fibroblast growth factor (bFGF) and platelet-derived growth factor (PDGF). During re-epithelialization, keratinocytes migrate from the wound edge into the wound bed and proliferate. A few days after injury, dermal fibroblasts are stimulated by growth factors such as TGF-β and PDGF to proliferate and migrate, and to secrete extracellular matrix (ECM)

proteins, initially fibronectin and hyaluronan, and later proteoglycans and collagens I and III, when the wound is more stable. Fibroblasts also adopt a myofibroblast phenotype to contract and create mechanical tension, which serves to physically close the wound gap (Toriseva and Kähäri, 2009).

Both keratinocytes and fibroblasts secrete matrix metalloproteases (MMPs), which degrade disrupted ECM and whose proteolytic activity is necessary for angiogenesis in the remodeled wound site. The remodeling process in humans may take several months, as initially there may be an excess deposition of ECM proteins that will need to be removed. Proteolytic cleavage of the ECM also serves to release soluble bioactive factors such as basic fibroblast growth factor (bFGF), vascular endothelial growth factor (VEGF) and insulin-like growth factor (IGF) to the cells, making them available to stimulate further wound healing processes (Toriseva and Kähäri, 2009).

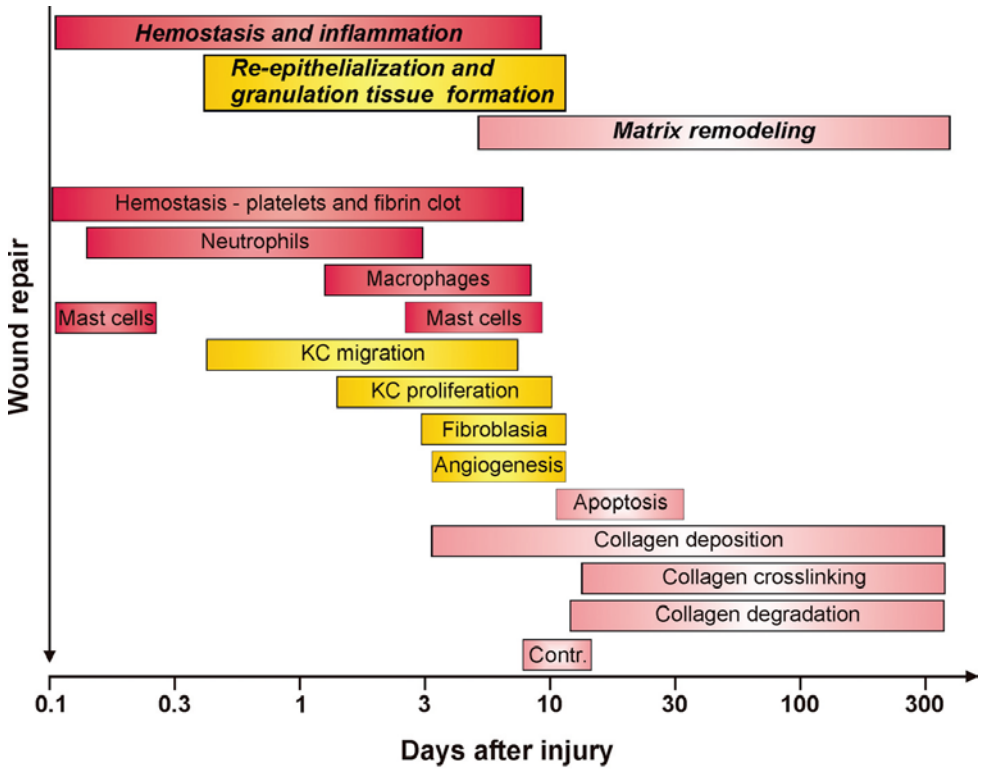

Figure 1.2. Timeline for normal human cutaneous wound healing (image taken from Toriseva and Kähäri, 2009). KC = keratinocyte, Contr. = contraction.

1.3. Non-healing wounds

Non-healing skin wounds afflict nearly 5 million Americans each year, and translate into multi-billion dollar healthcare costs, with global wound care expenditures amounting to $13 to $15 billion annually (Fonder et al., 2008). In Europe, their treatment accounts for an estimated 2 – 4% of the total healthcare budget (Gottrup et al., 2010). Clinically, non-healing wounds include venous leg ulcers, pressure sores and diabetic foot ulcers. The pathogenesis of these wounds is not fully understood; they encompass abnormalities in the healing processes of

inflammation, cell migration and remodeling. Sustained inflammation and bacterial infection are key players in the chronicity of such wounds (Pukstad et al., 2010). For example, wound fluids from non-healing venous leg ulcers have higher levels of interleukins IL-1α and IL-1β and lower levels of IL-8 than healing wounds (Pukstad et al., 2010).

In normal healing wounds, activated neutrophils do not persist after 72 hours—however, in the continuous inflammatory state of non-healing wounds, activated neutrophils are constantly present, leading to excessive amounts of MMPs, especially MMP-8, and neutrophil-derived elastase (Menke et al., 2007). The MMPs are not balanced by adequate amounts of tissue inhibitors of matrix metalloproteases (TIMPs), leading to a pattern of abnormally high wound degradation (Menke et al., 2007). Inflammatory cytokines such as tumor necrosis factor alpha (TNF-α) are increased and proliferation-promoting growth factors such as platelet-derived growth factor (PDGF) and matrix deposition stimulators such as transforming growth factor beta (TGF-β) are reduced. Not only is new matrix formation hindered, fibroblasts also become abnormal in the non-healing wound, undergoing premature senescence and lowered responsiveness to growth factors (Menke et al., 2007). Figure 1.3 schematically shows the abnormal progression of the healing processes in chronic, non-healing wounds.

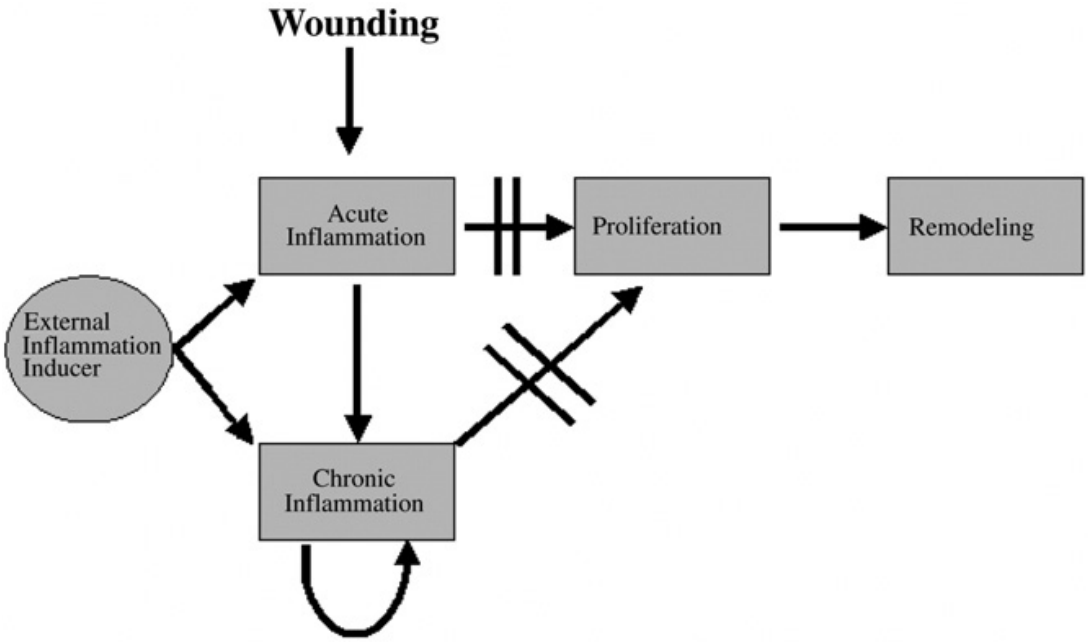

Figure 1.3. Abnormal progression of healing processes in impaired wound healing (figure taken from Menke et al., 2007).

1.4. State of the art in skin substitutes and bioactive wound dressings

The lack of structural and molecular cues to promote normal healing in pathological wound scenarios as discussed above, and the lack of availability of donor tissue to replace damaged or lost skin, points to the need for bioengineered skin substitutes and/or bioactive wound dressings that can deliver these cues exogenously. They may present a matrix on which cells can attach, as well as deliver cells and/or growth factors *in situ* ("smart matrix technology") (Metcalfe and Ferguson, 2007). This section details advances in these technologies.

1.4.1. Commercially available skin substitutes

Tissue engineering approaches using cell-based dermal substitutes (e.g. Dermagraft and Transcyte) and epidermal (e.g. Epicel, Laserskin, EpiDex and Myskin) or full-thickness (e.g. Apligraf and OrCel) skin substitutes to treat acute burn wounds and chronic diabetic ulcers have shown clinical success; however, their limitations include long culture times, restricted availability and/or the risk of immune rejection of cell sources (Metcalfe and Ferguson, 2007; Shevchenko et al., 2010). The majority of currently available skin substitutes and bioactive wound dressings (Table 1.1) use acellular collagen scaffolds alone or in conjunction with fibroblasts and/or keratinocytes (Powell et al., 2008). Epicel®, Epidex™ and Myskin™ are epidermal cell sheets cultured from autologous keratinocytes, often grown in the presence of murine feeder fibroblasts. Apligraf® and Orcel® are composite skin substitutes, used mostly for chronic wounds and consist of cellularized layers containing human allogeneic keratinocytes and fibroblasts. AlloDerm®, Integra® and Matriderm® are acellular dermal substitutes that are incorporated directly into the wound bed (Böttcher-Haberzeth et al., 2010). Since these acellular skin substitutes incorporate animal-derived de-cellularized extracellular matrix (ECM), they possess an intrinsic disease transfer risk (Metcalfe and Ferguson, 2007). These treatments also come at a very high cost—for example, Apligraf costs $28 per cm^2 (Shevchenko et al., 2010). As another obstacle to the use of such skin substitutes, certain segments of the population needing

treatment may also be barred by religious or ethical restrictions from using components involving, for example, bovine, porcine, fetal or cadaver derived material, which comprise many commercially available skin substitutes (Enoch et al., 2005). Synthetic polymers do not bridge this need gap due to incompatible biodegradation profiles of synthetic components as well as the lack of biochemical signals to the cells (Metcalfe and Ferguson, 2007).

Besides the efficacy of the treatment itself, the surgical requirements for the application of such treatment must also be taken into account. It is preferable both for the surgeon and the patient to be able to apply the treatment in one surgical intervention as opposed to many. Dermal and epidermal substitutes may be applied separately, 3-4 weeks apart, especially where the dermal component is thicker than 1mm, as in the case of Integra® and Matriderm®. This is in order to allow for vascularization of the dermal component to ensure perfusion to the epidermal component, to avoid epidermal necrosis. However, cultured epidermal substitutes have shown disappointing results in the “take” rate onto dermal matrices, with an average of 50% or less. Other disadvantages are the long (approximately 3 weeks) culture times, fragility of handling and high production costs (Böttcher-Haberzeth et al., 2010).

Table 1.1. Examples of commercially available skin substitutes and their components (table adapted from Böttcher-Haberzeth et al., 2010).

	Product	Company	Type	Cellular/ Acellular	Natural component(s)	Synthetic component(s)
Epidermal	Epicel®	Genzyme Corp.	Autograft	cellular	keratinocytes	
	Epidex™	Euroderm GmbH	Autograft	cellular	outer root sheath hair follicle cells	
	Myskin™	Celltran Ltd.	Autograft	cellular	keratinocytes	
	ReCell®	Clinical Cell Culture (C3), Ltd.	Autologous cell suspension	cellular	keratinocytes	
Dermal	AlloDerm®	LifeCell Corp.	Allograft	acellular	acellular dermis	
	Dermagraft®	Advanced BioHealing Inc.	Allogeneic/ synthetic	cellular	neonatal fibroblasts	polyglactin mesh
	Integra®	Integra LifeSciences Corp.	Xenogeneic/ synthetic	acellular	bovine collagen I and shark chondroitin-6-sulfate	polysiloxane (silicone)
	Matriderm®	Dr. Suwelack Skin & Health Care AG	Xenogeneic	acellular	bovine collagen I, III, V and elastin	
Composite	Apligraf®	Organogenesis Inc.	Allogeneic	cellular	neonatal keratinocytes; bovine collagen I containing neonatal fibroblasts	
	OrCel®	Forticell Bioscience, Inc.	Allogeneic	cellular	neonatal keratinocytes; bovine collagen sponge containing neonatal fibroblasts	

1.4.2. Experimental research in novel skin scaffolds

With the need for reproducibility, “off-the-shelf” availability, and reduction in regulatory and cost burdens, companies are increasingly interested in acellular scaffolds (Böttcher-Haberzeth et al., 2010). Several research groups are actively investigating new synthetic materials with improved properties for skin tissue engineering. Poly(lactic-*co*-glycolic acid) (PLGA) has been used in recent years due to its biocompatibility and the ability to control degradation rate according to copolymer composition. PLGA scaffolds have been electrospun for dermal tissue

engineering purposes (Blackwood et al., 2008; Kumbar et al., 2008). Poly(D,L-lactide) (PDLLA), which degrades at a slower rate than PLGA, has also been of interest since it is also approved by the Food and Drug Administration (FDA) for clinical applications, shows excellent biocompatibility, and its degradability can be tailored by varying the ratios of D- and L-lactides, with increased D-lactides increasing hydrolytic degradability (Kluger et al., 2010; Leong et al., 2010). Poly(caprolactone) (PCL) has recently become a popular choice of scaffold material either alone or as part of a hybrid due to the ability to tailor its physical properties (Powell and Boyce, 2009; Chen et al., 2011). Chen et al. (2011) created electrospun chitosan-*graft*-poly (ε-caprolactone)/poly (ε-caprolactone) scaffolds that combine the benefits of mechanical properties and fiber-forming ability of poly (ε-caprolactone) (PCL) with the antibacterial and wound healing activity of natural chitosan, while counterbalancing the shortcomings of poor hydrophilicity of PCL and poor electrospinnability and brittleness of chitosan. Synthetic polymers such as polyurethane do not confer biological benefit by themselves, but may be considered as carriers for biologically active agents, such as growth factors. Li et al. (2009) incorporated PDGF into molded polyurethane scaffolds and showed that the addition of PDGF promoted significantly greater granulation tissue formation and polymer resorption accompanied by replacement with new collagenous tissue than polyurethane alone in a rat excisional wound model. Table 1.2 provides a brief summary of recent research developments in scaffolds for skin

tissue engineering and wound healing applications.

Table 1.2. Recently developed scaffolds intended for skin tissue engineering.

Materials	**Form of scaffold**	**Cell type used for biocompatibility testing**	**Special properties**	**Reference**
polyurethane	Reactive liquid molded	MC3T3 mouse osteoblast precursor cells	Platelet-derived growth factor (PDGF) incorporated	Li et al. (2009)
collagen-poly(caprolactone)	Electrospun	Primary human dermal fibroblasts and epidermal keratinocytes	PCL can inhibit contraction of scaffold	Powell and Boyce (2009)
synthetic human elastin	Electrospun	Primary human dermal fibroblasts		Rjnak et al. (2009)
poly-N-acetyl glucosamine	Filtered and dried nanofibers	HUVECs; human gingival fibroblasts		Scherer et al. (2009)
collagen-chitosan	Freeze-dried	Primary rat dermal fibroblasts		Wang et al. (2009)
chitosan-*graft* -poly (ε–caprolactone)/poly (ε–	Electrospun	L929 mouse fibroblasts		Chen et al. (2010)
poly(D/L-lactide-*co* -L-lactide) (50:50)	Electrospun	Primary human dermal fibroblasts	Porous fiber surface	Kluger et al. (2010)
poly(D,L-lactide)	Electrospun	Porcine esophageal epithelial cells and smooth muscle cells	Bilayer with top layer being more porous to allow for culture of two or more cell types separated by a basement membrane	Leong et al. (2010)
chitosan-gelatin	Electrospun	N/A		Dhandayuthapani et al. (2010)
collagen-chitosan/fibrin glue	Freeze-dried	Primary human dermal fibroblasts and HaCaT keratinocytes	Different pore sizes on either side (5-20μm on top layer, 80-150μm on bottom layer)	Han et al. (2010)
collagen-chondroitin sulfate	Freeze-dried	Primary human epidermal keratinocytes		Liang et al. (2010)
collagen/chondroitin sulfate/hyaluronic acid	Freeze-dried	Primary rat dermal fibroblasts		Wang et al. (2010)
rat abdominal wall fasciocutaneous flap	Decellularized	N/A	Vascular structure intact with a pedicle containing inflow and outflow channels	Henderson et al. (2010)
silk fibroin/chitosan-hyaluronic acid	Pressed microparticles	Primary human dermal fibroblasts		Chung and Chang (2010)
pullulan-collagen	Hydrogel	Primary human dermal fibroblasts; primary mouse mesenchymal stem cells; bEnd.3 mouse brain endothelial cells	KCl crystallization-induced pore formation	Wong et al. (2010)
collagen-chitosan/silicone membrane	Freeze-dried	Human umbilical vein endothelial cells (HUVECs)	DNA incorporated	Guo et al. (2011)

1.5. Methods of scaffold preparation

1.5.1. Electrospinning

Electrospinning has gained widespread popularity in the area of scaffold fabrication, and more and more advanced setups have been developed for specific structural needs or for the incorporation of other components such as microspheres for drug or growth factor delivery. The most typical setup is a horizontal electrospinning setup (Figure 1.4) that produces non-woven, randomly oriented fibers. Here, the path of the extruded fiber is horizontal between the needle tip and the target. Another common setup is vertical or orthogonal, where gravity helps pull the fiber toward the target. Aligned fibers can be obtained by using a high-speed (approximately 4500 rpm or higher) rotating mandrel as the target. This arrangement has been preferred for vascular graft fabrication, as it provides the ability to tailor graft vessel wall thickness and promotes cellular alignment and migration along the direction of the fibers. Fibers with a core-shell structure can be created using a co-axial dual capillary spinneret. The usefulness of this structure is that drugs or enzymes can be incorporated in the core, and release profiles can be controlled by the degradation rates of the shell, or the shell surface can be functionalized with bioactive or inductive molecules (for a recent review, see Cui et al., 2010).

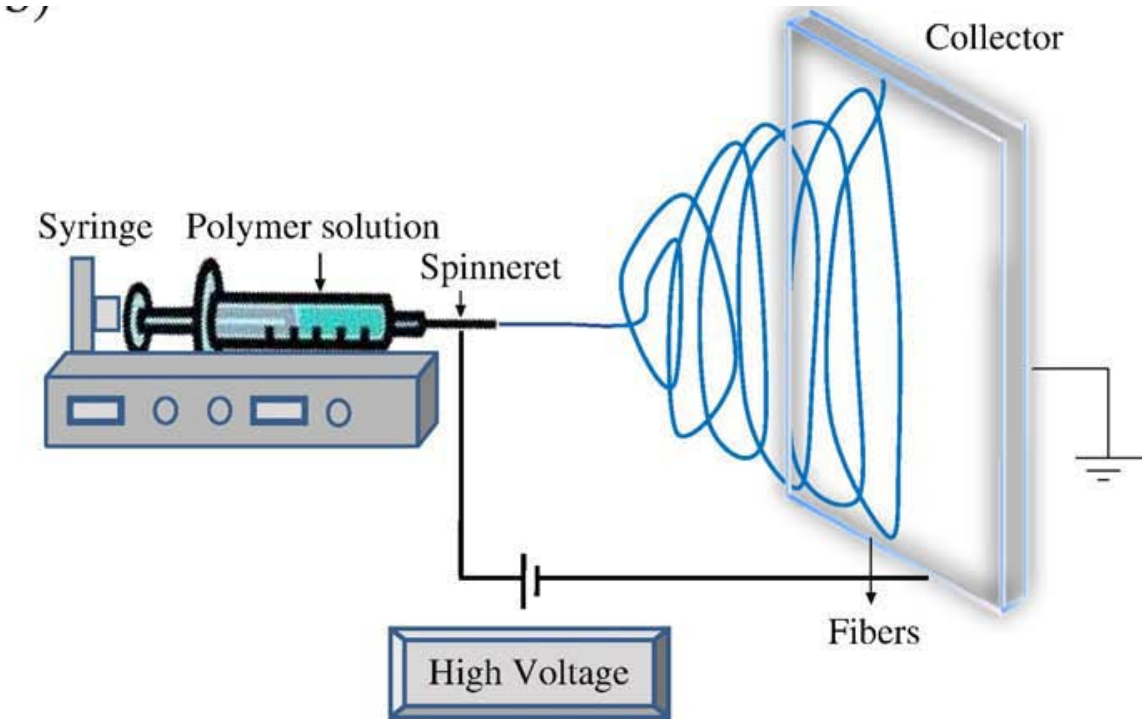

Figure 1.4. Horizonal electrospinning setup (image taken from Bhardwaj and Kundu, 2010).

Electrospinning has been a highly desirable platform technology in scaffold fabrication due to the ability to tailor fiber diameter and architecture by varying simple parameters such as polymer solution viscosity, applied voltage, solution flow rate, and the air gap distance between the needle tip and the target (Li et al., 2005, 2006; reviews by Lelkes et al., 2008; Cui et al., 2010; Bhardwaj and Kundu, 2010). The morphology of electrospun fibrous scaffolds mimics the structure of native extracellular matrix (ECM), allowing for enhanced cellular interaction with the scaffold (Li et al., 2005, 2006; Lelkes et al., 2008; Han et al., 2011). In order to increase the porosity of electrospun scaffolds, Leong et al. (2006) developed a technique termed “cryogenic

electrospinning", in which ice crystals are allowed to form continuously on a chilled mandrel, onto which the polymer is electrospun. The scaffold is then freeze-dried to remove the embedded ice crystals, resulting in large pore diameters ranging from approx. 34 to 80 µm to improve cellular infiltration and vascularization compared to typical electrospun scaffolds with average pore diameter ~5 µm (Leong et al., 2006, 2009).

From a process standpoint, electrospinning is advantageous in being relatively mild and thus able to change the form of a material (from solution to fibrous) while preserving the molecular structure and bioactivity (Cui et al., 2010). For instance, the monomers of collagen remain intact after electrospinning, and do not become fragmented like gelatin, the denatured form of collagen (Sell et al., 2009). Even living cells have been shown to remain viable after undergoing the electrospinning process (van Aalst et al., 2008). Human fibroblasts either in suspension or mixed in solution with poly(vinyl alcohol) (PVA) were electrosprayed (alone) or incorporated with electrospun PVA fibers, and remained intact in both cases (van Aalst et al., 2008). For drug delivery applications, electrospun fibers can serve as carriers for antibiotics or other drugs that are mixed in with the polymer solution, if a burst release profile is desired. Alternatively, microspheres encapsulating the drugs can be co-electrospun with the fibers, either in the same solution or co-axially with a dual or multiple syringe setup (Wang et al., 2009; Zabrodin, 2009).

In the past, our laboratory have thoroughly optimized electrospinning of natural proteins such as collagen and elastin (Li et al., 2005, Lelkes et al., 2008). Larger fiber diameters generally correspond to greater porosity and thus, greater ease of cell infiltration. Han et al. (2011) demonstrated that in co-electrospun blends of PLGA, gelatin and elastin, the elastin content did not significantly affect the mechanical properties of the hybrid scaffold, while increased PLGA content increased the tensile properties and conversely, increased gelatin content increased the elasticity, fiber diameters and also effective pore area, allowing for greater cell penetration. However, submicron to nano-scale fibers are desirable for our intended applications in skin tissue engineering, as a greater surface area-to-volume ratio of the fibers provides more topology for cellular support for a more organized, continuous epithelium (Powell and Boyce, 2007). Powell et al. (2008) investigated differences in cellular behavior and wound contraction between freeze-dried and electrospun bovine collagen skin substitutes, and found that while cellular proliferation and organization *in vitro* were similar, electrospun scaffolds had shrunk significantly less than freeze-dried grafts at 8 weeks post-grafting (68.8 ± 2.8% vs. 39.2 ± 8.8% of original area, respectively). Fibrous scaffolds are superior to conventional collagen gel scaffolds for skin equivalent culture, in terms of reduced shrinkage and increased stability leading to prolonged culture times, with keratinocytes continuing to proliferate and differentiate after 12

weeks on electrospun structures while collagen gel-based structures degenerate after only 3 weeks (Stark et al., 2006). From a biological vantage point, expression of collagen types I and III in fibroblasts bears closer resemblance to the pattern of collagen expression in native dermis when cultivated on a hyaluronan-based fibrous scaffold, than when cultured on pre-formed collagen gels (Stark et al., 2006). These findings support the use of electrospun material in designing skin substitutes.

1.5.2. Hydrogels

Scaffolds for soft tissue engineering can take the form of pliable, hydrophilic hydrogels, of which a large proportion of the composition is water (Van Tomme et al., 2008). Hydrogels can either be pre-formed before implantation, or injected as a liquid for gelling *in situ*. *In situ* polymerizing systems provide the advantage of conforming to the shape of the defect. These systems include photopolymerizable hydrogels and self-assembling hydrogels, which may be cross-linked enzymatically or chemically or through ionic or hydrophobic interactions or by stereocomplexation (Van Tomme et al., 2008). Bell et al. (1979) developed the original collagen hydrogel for human dermal fibroblast culture. While this system promoted cell growth and served as a platform for numerous studies on cellular contraction and physiological behavior, it was always functionally limited by poor mechanical properties. Helary et al. (2010) revisited

collagen hydrogels by increasing its initial concentration, from the low concentration (0.66 mg/ml) of “classical” collagen gels to 1.5, 3 and 5 mg/ml. They found 3 mg/ml to be optimal, with little benefit of increasing to 5 mg/ml since at such a high concentration, the gels were non-homogeneous and tended to creep and be less elastic. Collagen gels at 3 mg/ml promoted a higher growth rate of human dermal fibroblasts between days 7 and 14 of culture than gels of 1.5 mg/ml or 0.66 mg/ml. The major advantage of this higher concentration hydrogel is the reduction in contraction and increase in stiffness, allowing it to be able to be sutured onto a wound bed and more importantly, provide sufficient porosity for neovascularization to occur after implantation. This potentially elevates its usefulness from a temporary dressing to a permanent scaffold for wound healing. However, the outcome benefits of hydrogels are often derived from the cells that they carry, i.e. the cytokines and growth factors that these cells secrete, rather than from the hydrogels themselves.

Zawko and Schmidt (2010) developed a “crystal templating” technique to fabricate hydrogels with dendritic pore networks, a structure found naturally in the human body in the form of the microvasculature within tissues. Hyaluronic acid (HA) was photocrosslinked around dendritic urea crystals, which were subsequently dissolved to yield the dendritic porous structure. The disadvantage was that these scaffolds had to be coated with poly-L-lysine in order to become

cell adhesive; human dermal fibroblasts and epidermal keratinocytes both showed strong adhesion and cytotypic morphology on the coated scaffolds.

Completely synthetic hydrogels have also been researched for tissue engineering, such as RADA16 (PuraMatrix™), a synthetic peptide material made of 1% amino acid and 99% water. It consists of the standard amino acids arginine (R), aspartic acid (D), and alanine (A) and has a short, 16–amino acid sequence with alternating hydrophobic and hydrophilic side chains. The RAD motif is similar to the cell adhesion ligand RGD. RADA16 self-assembles into a fibrous scaffold upon pH changes. Kao et al. (2009) developed a synthetic dermis by mixing human dermal fibroblasts with the peptide hydrogel, and cultured 3-5 layers of keratinocytes on top to form an epidermal component. However, the process of polymerization requires changing the pH to 3 and then de-acidifying the solidified gel, damaging many of the fibroblasts during preparation.

1.5.3. Freeze-drying

Where high porosity is desired, freeze-drying may be employed as a scaffold fabrication method. Freeze-dried scaffolds are suitable in applications where thicker defects need to be filled, such as cartilage or bone. Porous scaffolds are formed by phase separation, where the mixture is

separated into frozen solvent and concentrated polymer. The ice crystals of the frozen solvent become sacrificial material, leaving behind pores of their size after ice sublimation. Cao et al. (2010) developed a porous scaffold based on a freeze-dried mixture of poly(L-glutamic acid) and chitosan, with chitosan being the more hydrophilic material. They attributed a greater tendency for swelling in the scaffolds with higher chitosan content to its greater hydrophilicity. These freeze-dried scaffolds supported the culture of articular chondrocytes for 2 weeks, although they were distributed unevenly throughout the structure. Coimbra et al. (2011) combined the properties of negatively charged pectin and positively charged chitosan in a polyelectrolyte complex to produce a freeze-dried scaffold for bone tissue engineering, supporting the culture of human osteoblasts. The advantage of the phase separation technique followed by freeze drying is the tight control over pore size and structure depending on the porogen—however, problems include residual porogen not being thoroughly extracted, and limited ability to scale up production (Ayres et al., 2010).

1.6. Plant proteins and their uses in regenerative medicine

Given the limitations of animal-derived and synthetic materials in tissue engineering applications, as discussed in Section 1.4.1, plant proteins are a particularly attractive potential alternative class of biomaterial. Plant proteins are abundantly available from renewable sources, are

non-toxic and biodegradable, and are versatile in their ability to be formed into different structures such as films, fibers and gels (Lelkes et al., 2008). They also offer the benefit of being intrinsically bioactive as edible nutritive sources (e.g. Miyoshi et al., 1991; Holzbeierlein et al., 2005), and it is reasonable to hypothesize that this bioactivity may potentially be harnessed in *in vitro* applications.

1.6.1. Soy protein

Soybean-derived products have been consumed in Asian diets for centuries, and strong correlations have been made between this consumption and a lower incidence of various cancers in the Asian population compared to Western populations (Holzbeierlein et al., 2005). This observation led to extensive *in vitro* studies trying to identify some of the individual bioactive components within soybean products that might inhibit cancer formation or metastasis. The best-characterized amongst these are trypsin inhibitors, such as Bowman Birk inhibitor (BBI) and Kunitz trypsin inhibitor (KTI) (Armstrong et al., 2003), the peptide lunasin (de Lumen, 2005), and some of the isoflavones, particularly genistein, daidzein and glycitein (Magee and Rowland, 2004). The biologic effects of these compounds is discussed in Section 1.6.1.1.

Soy protein isolate (SPI) is commercially purified to a purity of greater than 90% and consists of

two main fractions of protein, namely a 7S fraction comprising mostly β-conglycinin and an 11S fraction which is pure glycinin, as well as small quantities of γ-conglycinin, lipoxygenases, α-amylases, and hemagglutenins (Nielsen, 1985). The molecular weights of the 7S and 11S fractions are roughly 180 and 350 kDa (Hua et al., 2005). SPI can be processed into films (Jiang et al., 2007) and gels (Mauri and Añon, 2006; Maltais et al., 2007, 2010; Caillard et al., 2008, 2010), and extruded into fibers (Zhang et al., 2003).

1.6.1.1. Bioactivity of soy protein

Soy protein isolate contains approximately 6.92 ± 0.14 mg lunasin/g protein (Wang et al., 2008b). Wang et al. (2008a) found that after simulated gastrointestinal digestion, 3% of lunasin was still active. Interestingly, gastrointestinal enzyme digestion greatly increased cytotoxicity of soy protein for L1210 leukemia cells. At 7 mg/ml, soy protein hydrolysate from simulated digestion inhibited cell growth by ~ 80 %, whereas a negative control of nonhydrolyzed soy protein isolate (from the same defatted soy flour) and nonhydrolyzed defatted soy flour itself showed no inhibition. This “indicated that bioactive peptides released from the hydrolysis might be important for the observed cytotoxicity of soy on L1210 leukemia cells” (Wang et al., 2008a). These authors also determined that the isoflavones may have been partially responsible for the observed cytotoxicity, but the peptides lunasin and BBI had only a “modest effect” at the

concentrations they tested. When purified lunasin (98%) and BBI (95%) were tested, they found a dose-dependent inhibition of L1210 cell growth, with IC_{50} values of 78 μg/ml (13.9 μM) for lunasin and 180 μg/ml (22.5 μM) for BBI. Wang et al. suggested that β-conglycinins, the 150 – 200 kDa trimer fraction of soy protein, contained more bioactive, tryptic peptides than glycinins, the 320 – 375 kDa hexamer fraction, due to possessing more acidic and basic amino acids as well as aromatic amino acids, compared to glycinins, which have more sulfur-containing amino acids. However, purified β-conglycinins and glycinins showed lower cytotoxity to L1210 leukemia cells than soy flour hydrolysates, suggesting that other active compounds such as isoflavones are also responsible.

Park et al. (2007) suggest that BBI may help to protect lunasin from gastric digestion, since lunasin in soy protein was found to be resistant to *in vitro* digestion by simulated gastric and intestinal fluids, but purified or synthetic lunasin was not. By contrast, pure BBI was stable even up to 120 minutes of digestion. They saw this protective effect above lunasin/BBI ratios of 1:20, but conceded that the Kunitz trypsin inhibitor may also have played a role, although this was not measured. Of potential relevance to our applications, both lunasin and BBI were found to be able to be internalized into the nuclei of NIH3T3 mouse fibroblasts after simulated digestion (Park et al., 2007). Of particular interest, soy protein already contains an Arg-Gly-Asp (RGD) motif

in its 43-amino acid bioactive peptide lunasin, which has been identified as responsible for the internalization of lunasin into the nuclei of NIH3T3 mouse fibroblasts (Hernández-Ledesma et al., 2009).

When lunasin was removed from BBI, the BBI showed significantly reduced ability to inhibit the carcinogenic transformation of mouse embryo-derived C3H lymphocytes. Also, lunasin was found to be more potent (effective as low as 10 nM) than BBI in preventing carcinogen-induced tumor formation. This strongly suggests that lunasin "is a major if not the major active chemopreventive molecule" in BBI concentrate (BBIC) (de Lumen and Galvez, 2002). Deletion of the acidic carboxyl end and the RGD cell adhesion motif of lunasin also removes the inhibition effect, indicating that the bioactivity of lunasin is dependent on these domains. Internalization into the cell also only occurs when the RGD motif is present. Once inside the nucleus, lunasin binds to the core histones and repress transcription, thus preventing carcinogen-induced transformation (de Lumen and Galvez, 2002).

In a comprehensive study on the chemopreventive property of lunasin, Galvez et al. (2001) showed that C3H cells transfected with the viral oncogene E1A became apoptotic if treated with 20 μM lunasin for 24 h before transfection, whereas treatment of normal C3H or NIH3T3 cells

did not affect cell proliferation or morphology. In the female SENCAR mouse model, shaved dorsal skin was treated with lunasin dissolved in 250 µl of ethanol at three doses, low (2.5 µg/week), medium (25 µg/week), and high (250 µg/week), twice/week for 1 week before application of the initiator DMBA to induce skin tumorigenesis. This was followed by treatment with lunasin twice a week for 19 weeks. It was shown that the highest lunasin dose (250 µg/week) reduced skin tumor incidence by 70% ($p < 0.01$), decreased tumor yield/mouse ($p < 0.005$), and delayed the appearance of tumors by 2 weeks relative to the positive control (no lunasin treatment). The lower doses did not show a statistically significant difference.

BBI has also been shown to confer resistance to radiation-induced terminal differentiation in normal human fibroblasts, when they were pre-treated for 2 h with 10 µM of BBI before continuing culture without BBI for 8 days and then irradiated. However, this protective effect was not observed when the same treatment was given to transformed human fibroblasts (Dittmann et al., 1995).

Genistein derived from soy was shown by Sienkiewicz et al. (2008) to protect human dermal fibroblasts from oxidative stress that inhibits collagen biosynthesis. Genistein can modulate insulin-like growth factor-I (IGF-I) receptor signaling via inhibition of tyrosine kinases. It was

found that incubation for 1 h per day with 1 μM of genistein blocked the inhibitory effect of oxidative stress on collagen synthesis. However, increasing the dose to 10 μM and 100 μM decreased collagen synthesis to approximately 60% and 40% of the control, respectively. A similar decrease was seen with IGF-I receptor expression at those doses (55% and 46% of the controls, respectively). This suggests that at low doses, genistein serves a protective function by preventing disturbances to the IGF-I receptor-mediated pathway and phosphorylated ERK, but at higher doses, the tendency of genistein to inhibit tyrosine kinases may outweigh its protective effects.

In terms of combating inflammation in chronic diseases, soy protein peptides and isoflavones have also been shown to inhibit inducible nitric oxide synthase (iNOS)/nitric oxide (NO) and cyclooxygenase-2 (COX-2)/prostaglandin E2 (PGE2) inflammatory pathways in lipopolysaccharide-stimulated macrophages (Dia et al., 2008). BBI can prevent the release of oxygen free radicals, and genistein has also been reported to reduce reactive oxygen species (ROS) by decreasing the expression of ROS-producing enzymes. The activity is also synergistic. The mix of soy isoflavone glycosides (84% genistein glucoside, ~16% daidzein glucoside, and 0.3% glycitein glucoside) was more potent than any of the three isoflavones alone, followed by either genistein or daidzein alone (Dia et al., 2008).

The protective effects of soy isoflavones on skin directly, as well as against systemic inflammation as discussed in this section, all support the use of soy-derived biomaterials in skin tissue engineering and wound healing. Recently, soy genistein has been shown to accelerate skin wound healing directly in an ovariectomized (Ovx) mouse model treated with subcutaneous injections of genistein, via suppressing inflammatory activity of neutrophils and macrophages, and accelerating re-epithelialization via interaction with the estrogen receptor (Emmerson et al., 2010). It is reasonable to surmise that these effects may be translated in soy-derived scaffolds for wound healing.

1.6.1.2. Use of soy protein in regenerative medicine

The suitability of soy protein for biomedical applications has been well demonstrated by Vaz et al. (2003a, b, c) and Silva et al. (2003, 2005). Vaz et al. compared cast films made from soy protein with those made from gelatin, casein and sodium caseinate, and found that soy films were most resistant to hydrolysis whether they were crosslinked or not. This was attributed to the globular structure of soy protein, unlike the coiled or helical structure of other proteins (Vaz et al., 2003a). Soy protein matrices formed by melt extrusion and injection molding have shown the ability for controlled drug release in single (Vaz et al., 2003c) or bilayer skin-core (Vaz et al., 2004)

formations. Soy films supported the spreading and proliferation of mouse L929 fibroblast cells (Silva et al., 2003), as did chitosan/soy blend films but not chitosan films alone (Silva et al., 2005). The suitability of SPI films for use in a controlled release drug delivery system has also been investigated (Chen et al., 2008). More recently, others and we developed the methodology to electrospin soy proteins (Lelkes et al., 2008; Vega-Lugo and Lim, 2008; Fung et al., 2010).

Soy protein isolate has also been shown to increase the viability of L929 mouse fibroblasts cultured on cellulose/SPI composite sponges compared to the same cells cultured on cellulose sponges alone (Luo et al., 2010). The authors attributed this effect to SPI hydrolysis in the cell culture medium, both rendering the sponges more porous for cell infiltration and providing nutrients in the form of SPI degradation products. Lee et al. (2008) have also demonstrated that soybean protein hydrolysates provide a source of nutrients for adherent primary human epidermal keratinocytes in culture at low concentrations (1 g/L) and stimulated cell proliferation by approx. 200%. Soybean protein in the form of non-woven fabric promoted epithelialization of full-thickness skin excisional wounds in a Wistar rat model when used as the upper layer in a bilayer composite wound dressing with a genipin-crosslinked chitosan film as the lower layer (Liu et al., 2008). As a biofilm by itself, SPI crosslinked with formaldehyde has been shown to support the culture of normal human fibroblasts and keratinocytes for 4 days, although viability of

fibroblasts decreased with increasing concentrations of formaldehyde (Curt et al., 2009). SPI has also been formed into a hydrogel with poly(ethylene glycol) (PEG) (Snyders et al., 2007) and shown to have an elastic modulus of 1-16 kPa, although no cell culture studies were done with these gels. Reddy and Yang (2009) developed soy protein fibers using wet spinning without additives or crosslinking. These fibers with diameters 50-150 μm supported the growth of mouse fibroblasts for 7 days.

1.6.2. Zein

Zein is the major storage protein of corn, isolated directly from corn gluten meal as an industrial polymer. It comprises roughly 6% of the corn kernel and under polyacrylamide gel electrophoresis (PAGE) analysis shows strong protein bands at 21 kDa with a main band at 18 kDa, and minor bands at 12, 46, 41 kDa (Selling et al., 2004). Zein comprises mainly α and β fractions from 14-24 kDa (Shukla and Cheryan, 2001).

Corn zein has been shown to be suitable as a biomaterial in the form of films (Sun et al., 2005) and porous scaffolds (Wang et al., 2007), and has been electrospun by different groups (Yao et al., 2007; Selling et al., 2007; Jiang et al., 2010) using a variety of solvents. The water stability of electrospun zein scaffolds, as well as the ability to promote cell attachment and proliferation,

can be enhanced by crosslinking with citric acid (Jiang et al., 2010). The ability of zein to be formed into hydrophobic coatings and its antibacterial activity has led to its increased use in the food industry and these benefits may be conferred to biomedical applications (Shukla and Cheryan, 2001).

As a film, zein has been shown to promote the adhesion of HL-7702 human liver cells to a greater extent than a collagen coating, and its degradation products were shown to stimulate proliferation of HL-7702 cells when added to cell culture medium (Sun et al., 2005). Rat mesenchymal stem cells (MSCs) have been shown to grow and differentiate towards osteoblasts on a porous zein scaffold (Gong et al., 2006). Microspheres formed by homogenizing zein in an ethanol-water mixture have shown capability for sustained drug release (Liu et al., 2005; Lai and Guo, 2011). Microspheres of soy protein, zein, and blends of both have been created for nutraceutical delivery, with soy/zein complex being optimal as it is capable of near zero-order release kinetics, while soy or zein microspheres alone released too rapidly in the presence of simulated gastric fluid (Chen and Subirade, 2009; Chen et al., 2010). Tablets based on zein microspheres are capable of sustained delivery of the drug ivermectin via oral administration, with bioavailability of the drug ~133% that of commercial formulations (Gong et al., 2010). Zein has been combined with PLGA to form hybrid microspheres to deliver amoxicillin for root canal

disinfection, with zein contributing to the ability of the matrix to diffuse the drug (Sousa et al., 2010).

A porous 3-D scaffold prepared by salt leaching was seen to promote healing of bone defects in rabbits by 12 weeks, with the effect much more pronounced and full when combined with MSCs (Tu et al., 2009). Xu et al. (2010) recently developed a porous zein gel for periodontal tissue engineering, and observed that periodontal ligament cells grow along the edges of the pores.

Zein has also been hydrolyzed to yield the bioactive angiotensin converting enzyme (ACE) inhibiting peptide (Miyoshi et al., 1991), which incidentally can also be derived from soy protein (Mallikarjun Gouda et al., 2006). Of relevance to wound healing, ACE upregulation has been implicated in fibrotic remodeling in pathologic scars as it appears to have significantly higher activity in fibrotic scars than in normal and wounded skin tissue (Morihara et al., 2006). Hence, we surmise that wound dressings made of plant proteins might suppress scar formation and contribute to a more natural healing process with reduced scarring

1.6.3. Wheat gluten

Gluten is the protein, starch, and lipid nutrient storage component of grain endosperm cells. Commercial wheat gluten is highly heterogeneous, with a large range of molecular weight from 10^4-10^6 Da where the high molecular weight glutenin polymers and low molecular weight gliadin monomers in wheat gluten exist as coiled or folded chains (Lelkes et al., 2008). Wheat gluten was most likely the first plant protein to have been electrospun (Woerdeman et al., 2005), paving the way for fabrication of nanofibrous or submicron fibrous scaffolds from other plant-derived proteins. Gliadin as wet spun fibers (Reddy and Yang, 2007) and glutenin as films have been investigated for tissue engineering applications, with glutenin potentially more suitable as gliadin has been found to be cytotoxic (Reddy et al., 2010).

1.7. Plant cell signaling mechanisms

Signal transduction in plant cells is mediated by pathways that are surprisingly similar to some of those in mammals, including humans. Among these are calcium-based signaling, G-protein-mediated signaling and inositol phospholipid influenced signaling (review by Clark et al., 2001). The calcium-binding protein calmodulin was found to be necessary for pollen tube growth and could stimulate cell wall regeneration and cell division in protoplasts. The ECM of light-grown plants has been shown to contain a NTPase that binds calmodulin and belongs to the

ecto-apyrase family of NTPases, which in animal counterparts is responsible for turning off the hormonal activity of extracellular ATP and ADP. Another similarity between animal and plant cells is the role of annexins, which are distributed throughout the endomembrane and associated with the cytoskeleton, ECM and nucleus in animals, and associated with the plasma membrane, Golgi membranes, the ECM and nuclei in plants. Annexin is an important Ca^{2+} regulatory motif in plants, and has F-actin binding ability. Heteromeric GTP-binding proteins (G proteins) are activated when they bind GTP and dissociate into subunits that transmit downstream intracellular signals. Well characterized in animals, they have also later been found in plants, with roles in the regulation of pollen germination and tube growth and possibly of inwardly-rectifying K^+ channels controlling stomatal opening (review by Clark et al., 2001).

Of particular interest in our case, plants possess cell adhesion sites termed plasmalemmal control centers that are similar to integrin clusters in animals. Plants, like animals, perceive mechanical stresses such as tension and compression through the ECM-cytoskeletal interface. While plant integrin-like receptors have not been well characterized, RGD-binding sites have been identified in certain plants such as the small flowering plant *Arabidopsis*. Plant RGD receptors have also been shown to cross-react with animal anti-β1 integrin antibodies. Plants also possess fibronectin- and vitronectin-like protein sequences (Clark et al., 2001). Soybean root

cells possess a 70-72 kDa RGD-binding polypeptide that cross-reacts with antibodies against human vitronectin receptor but not human fibronectin receptor, and promotes cell membrane-cell wall attachment (Schindler et al., 1989). As mentioned earlier, soy protein also contains an RGD motif in its peptide lunasin (Hernández-Ledesma et al., 2009).

The plasmalemmal reticulum, which connects the cortical cytoplasm to the cell wall, is home to adhesion sites that resemble animal cell adhesion sites. *Arabidopsis thaliana* contains an ortholog of β1-integrin, as well as extracellular proteins which are functionally similar to animal ECM proteins. Adhesion can be disrupted by exogenous RGD peptide as it is in animal cells (review by Pickard, 2008). *Arabidopsis* also has epidermal growth factor (EGF) repeats in its wall associated domain, which may be involved in ligand recognition. In addition to similarities between plant and animal cells with respect to ECM and adhesion molecules, plants also possess matrix metalloproteases (MMPs), which may be implicated in pathogen defense, senescence, growth and flowering (review by Brownlee, 2002). For example, the *GmMMP2* gene in soybean (*Glycine max*) is upregulated in the soybean plant in response to pathogen infection as well as wounding and dehydration, but not in correlation to senescence or programmed cell death (Liu et al., 2001).

Given the parallels—or at least analogies—between plant and mammalian signal transduction mechanisms, it is not unreasonable to surmise that mammalian cells may interact with plant ECM similarly to how they interact with mammalian ECM.

1.8. Mammalian integrins

Mammalian cells attach to natural substrates (e.g. extracellular matrix proteins) mainly via a class of transmembrane receptors called integrins (Ingber, 1991; Assoian and Klein, 2008). So far, 18 α and 8 β subunits have been identified, which assemble into 24 different integrins each having a specific, nonredundant function (Hynes, 2002). Specifically, dermal fibroblasts attach to extracellular matrix (ECM) proteins predominantly with β1 integrin subunits, specifically α2β1 for collagen and α5β1 for fibronectin, and these integrin-ligand interactions play a key role in contraction during wound healing (Sethi et al., 2002). Impaired α2β1 function, as can occur in aged fibroblasts, can correlate to poor migration and thus deficient wound healing (Reed et al., 2001). Specific to the wound matrix, fibroblasts have been shown to bind to fibrinogen via integrin αvβ3 independently of fibronectin in the matrix (Gailit et al., 1997), and fibroblast binding to the provisional matrix protein vitronectin has been shown to be inhibited by antibodies to αvβ3 and αvβ5 when used together (Gailit and Clark, 1996). Integrin subunit αv has also been seen to be up-regulated in subepidermal fibroblasts, papillary dermis, and blood

vessels in the wounds of human skin (Noszczyk et al., 2002). Up-regulation of integrin subunits occurs concurrently with up-regulation of their corresponding ECM ligands (Noszczyk et al., 2002).

In the epidermis, α6β4 is crucial for basal keratinocyte adhesion to the underlying basement membrane. It is concentrated in the keratin-rich trailing edge in re-epithelializing wounds. The ubiquitous subunit β1 mediates keratinocyte adhesion and proliferation, although its absence may be compensated for by α6β4. Integrin α2β1 is required for keratinocyte adhesion to collagens *in vitro*, but no epidermal defects are seen in mice lacking this integrin. Integrins α2β1, α3β1 and α6β4 are highly expressed by epidermal stem cells, which are characterized by rapid adhesion *in vitro* (Margadant et al., 2010). Table 1.3 shows combinations of integrin subunits and their expression in the epidermis.

Table 1.3. Integrin subunits and their respective ECM ligands in the epidermis (adapted from Margadant et al., 2010).

Integrin	Ligand	Expression in epidermis
β1		
α2	Collagens	Constitutive, up-regulated during wound healing
α3	Laminins	Constitutive, up-regulated during wound healing
α5	FN	Induced during wound healing
α6	Laminins	Uncertain
α8	RGD	In developing HFs and the arrector pili muscle
α9	RGD, mainly of FN and TN	Weak constitutive, up-regulated during wound healing
αv		
β1	RGD	Uncertain
β5	RGD, mainly of VN	Weak constitutive, up-regulated during wound healing
β6	RGD, mainly of FN, TN and LAP-1/-3	In stem cells in HF, induced during wound healing in interfollicular epidermis
β8	RGD, mainly of VN and LAP-1/-3	Weak, suprabasal
α6β4	Laminins	Constitutive

β-ig-h3, TGF-β-inducible gene-h3; FN, fibronectin; HF, hair follicle; LAP, latency-associated protein; RGD, arginine-glysine-aspartate; TN, tenascin; VN, vitronectin.

In the native extracellular matrix environment, cells attach to ECM proteins via various discrete adhesion motifs. The advantage of preferential attachment to specific peptides, mediated by integrins, can be harnessed in the functionalization of scaffold surfaces. For example, Lee et al. (2006) showed that PPy functionalized with a carboxylic acid group by which an RGD motif was grafted promoted greater attachment and spreading of human umbilical vascular endothelial cells. Wang et al. (2010) grafted RGD-containing peptides onto electrospun chitosan nanofibrous scaffolds and observed significantly greater viability of NIH3T3 cells on RGD-modified scaffolds compared to non-modified scaffolds at 3 and 5 days post-seeding.

1.9. Matrix metalloproteases (MMPs) and their role in wound healing

Matrix metalloproteases (MMPs) play a versatile role in wound repair, with functions including proteolytic degradation of ECM as well as activation of other proteases, cytokines and growth factors. They are further categorized as collagenases, gelatinases, stromelysins, matrilysins, and membrane-type MMPs (Toriseva and Kähäri, 2009). Their activity is blocked by endogenous tissue inhibitors of matrix metalloproteases (TIMPs). Figure 1.5 shows the MMPs and TIMPs secreted during wound healing, and their cell sources. MMP expression is also mediated by growth factors; for example MMP-1 expression in human fibroblasts is up-regulated by PDGF and down-regulated by TGF-β (Toriseva and Kähäri, 2009).

Intact skin shows low constitutive expression of MMPs. In normally healing skin wounds, collagenases MMP-1 and MMP-8, gelatinases MMP-2 and MMP-9, stromelysins MMP-3 and MMP-10, metalloelastase MMP-12, MT1-MMP, MMP-19, MMP-26 and MMP-28, as well as TIMP-1, -2 and -3, but not TIMP-4, have been reported (Toriseva and Kähäri, 2009). MMP-1 is expressed by fibroblasts in granulation tissue, and may also aid in wound healing by cleaving collagen to reveal “cryptic binding sites” for integrins such as αv to increase binding and promote cell survival in the new matrix. It also promotes human keratinocyte migration on fibrillar collagen, and is induced in wound basal keratinocytes to move off the basement membrane by

ligation of α2β1 integrin with dermal collagen (Chen and Parks, 2009). MMP-8 was found to be the most abundant collagenase in human excisional wounds, mainly expressed by neutrophils. MMP-26, the smallest MMP, was expressed during re-epithelialization in the epithelial tip of both normally healing acute wounds as well as chronic ulcers, but not in granulation tissue (Toriseva and Kähäri, 2009).

In terms of TIMPs, the regulators of MMPs, expression also varies with the type of wound. TIMP-1 has been detected in wound fibroblasts, whereas TIMP-2 and TIMP-3 has been found in skin epithelial cells as well as fibroblasts. TIMP-4 expression has not been detected in acute human wounds, but has been in fibroblasts from chronic ulcers (Toriseva and Kähäri, 2009).

ADAMs, a disintegrin and metalloproteinase, are a special family of transmembrane proteins, most of which have both adhesive and proteinase activity. Their substrates are mainly cell membrane associated proteins. In humans, ADAMs 9, 10 and 15 may aid cell migration or release growth factors from ECM by cleaving fibronectin and type IV collagen. ADAMTS proteases, a disintegrin and metalloproteinases with thrombospondin type 1 motifs, are secreted, rather than transmembrane proteins, and their substrates are ECM proteins. Only ADAMTS-1 has been specifically associated with cutaneous wound healing—it is first

up-regulated in dermal wound macrophages, and by day 5 the expression shifts to the granulation tissue fibroblasts (Toriseva and Kähäri, 2009).

In wound fluid from chronic ulcers, MMP-2, -9, -1, and -8 levels have been found to be elevated. MMP-13 expression is “a distinct feature” of chronic ulcer fibroblasts, and appears to be elevated in keloid tissues as well. Intriguingly, MMP-13 is expressed by human fetal wound fibroblasts and may be involved in activation of TGF-β3, which plays an important role in scarless wound healing (Toriseva and Kähäri, 2009).

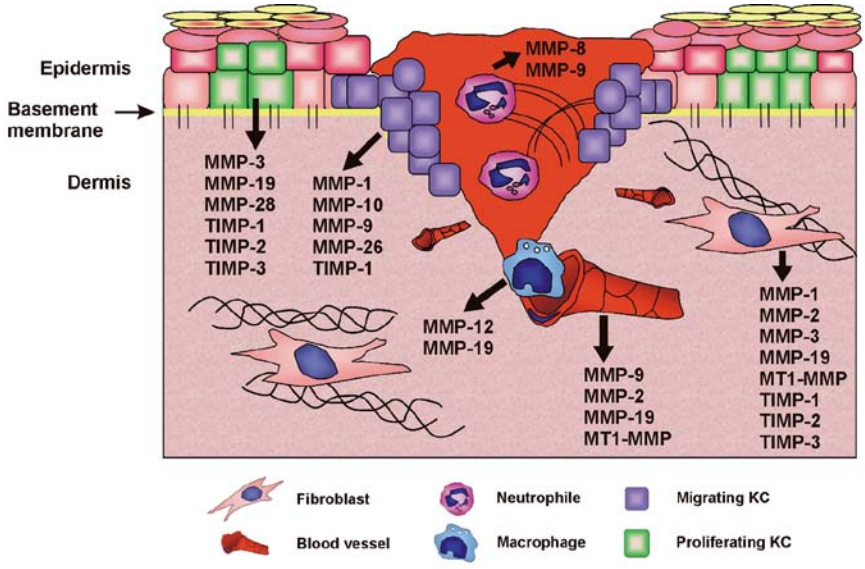

Figure 1.5. Diagram of cellular expression of MMPs and TIMPs in an acute cutaneous wound (taken from Toriseva and Kähäri, 2009).

1.9.1. Interaction between MMPs and soy protein

The major bioactive polypeptide component of soy protein, the Bowman-Birk inhibitor (BBI), is both a metalloprotein (containing magnesium, calcium and zinc) and concomitantly a metalloproteinase inhibitor that inhibits not only the serine proteases trypsin and chymotrypsin but also human MMPs. BBI inhibits trypsin at its Lys_{16}-Ser_{17} domain and chymotrypsin at its Leu_{43}-Ser_{44} domain. BBI also contains four Glu and seven Asp residues that bind metals, especially zinc. BBI dose-dependently inhibited the MMP-1 hydrolysis of gelatin, with complete inhibition at 115 nM for mineralized BBI and 30 nM for demineralized BBI (Losso et al., 2004). BBI not only inhibits the activity of MMP-1 but also the activation of pro-MMP-1, as well as pro-MMP-9 (Bawadi et al., 2004). The ability of BBI concentrate (BBIC), a soybean extract enriched in BBI, to reduce the activity of MMP-2 and MMP-9 has been investigated for the treatment of multiple sclerosis in a rat model (Gran et al., 2006). Hence BBI might be an important soy-derived regulator of MMP1 activity *in vivo* and as such a modulator of wound healing.

1.10. Animal models

The information that *in vitro* and *in silico* experiments can give us is limited to the specific interactions that we target, by isolating chosen variables with specific conditions that we define.

However, our intended applications in biomedical engineering are almost always in a dynamic interface with the human body in all its intricacy. Thus, a living organism is required to test any medical product before it can be deemed safe and effective in humans.

Different species offer different advantages in studying wound healing, both scientific and practical. The pig is classically considered to have the most similarities to humans in physiology and certain anatomical features, such as the attachment of skin to subdermal tissues (Sullivan et al., 2001), in contrast to rodents (Cross et al., 1995; Dorsett-Martin and Wysocki, 2008). However, pigs have the disadvantages of a slower life cycle and large size, making them more difficult and costly to maintain. Rats are a convenient species that allow for comparisons between treatment modalities. Table 1.4 lists some of the advantages and disadvantages of different species.

Table 1.4. Summary of commonly used animal models and their relative advantages and disadvantages (adapted from Lindblad, 2008).

Animal	Advantages	Disadvantages
Rat/Mouse	Small; genetic mutants readily available; easy to handle; low cost	Heal mainly by contraction, dissimilar to human skin
Rabbit	Useful in fetal studies	No large benefit over the cheaper, smaller rodent model
Pig	Greater similarity to human skin in structure and physiology; larger size allows for fewer animals to generate statistically significant results; useful in fetal studies	Large size increases difficulty in housing and handling; expensive
Human	Most accurate	Ethical limitations

No animal model exists that can perfectly replicate the complexity of human wounds. However, different animal models approximate different aspects of wound healing more closely than others. To investigate the effects of external treatments, the physical similarity between the animal skin and human skin will be important. To determine the role of a certain endogenous growth factor or pathway on wound healing, knockout studies may be employed in more genetically controllable models such as the mouse (Reid et al., 2004). Parameters that are analyzed to measure the degree of wound healing include wound contraction, re-epithelialization, vascularization, inflammatory response, macroscopic and histological appearance of the scar, and mechanical strength of the scar (Birch et al., 2005).

Several models attempt to simulate chronic impairment, including chemically induced diabetes (Davidson, 1998; Weingarten et al., 2006), genetic mutations for diabetes, ischemia, glucocorticoid administration, immune deficiency, malnutrition, aging, radiation and bacterial infection (Davidson, 1998). Each of these has limitations for example in systemic effects or variability in the model. In choosing an animal model for the desired aspect of wound healing to study, cost and convenience also often play a large role, especially since the ability of researchers to accommodate the animals and perform the studies depends on institutional approval and availability of facilities.

Chapter 2. Research Aims and Objectives

Pairing the need for readily available, "off-the-shelf" affordable bioactive scaffolds from renewable sources with the potential for inexpensive plant proteins to confer bioactivity and interact favorably with human skin at a cellular and molecular level, our long-term goal is to develop an *acellular*, plant protein-derived scaffold for skin tissue engineering and wound repair. We have chosen soy protein due to its versatility in processing, its abundance, and its long history of dietary benefits and recently documented *in vitro* anti-carcinogenic, anti-inflammatory and anti-oxidative properties as described in Chapter 1. We hypothesize that soy protein as a raw material will promote skin wound healing in a manner similar to or better than currently available treatments.

Toward this long-term goal, the work in this thesis addresses three specific aims:

1) Fabricate a novel soy protein-based electrospun fibrous scaffold and characterize its mechanical properties, degradation behavior and *in vitro* biocompatibility.

2) Identify initial adhesion mechanisms of human dermal fibroblasts to SPI/PEO.

3) Evaluate electrospun SPI/PEO scaffolds *in vivo* using a rat wound healing model.

For Specific Aim 1, we chose electrospinning as our fabrication method for soy protein-based scaffolds based on the desirability of the biomimetic structure it produces. This method is also especially suitable for thin layer defects such as can be found in the skin. For Specific Aim 2, we investigated the initial cellular adhesion response to our scaffold material, as this will determine how well the scaffold integrates with the cell-mediated wound environment in later interactions. Finally, for Specific Aim 3, we evaluated the wound healing response to our SPI/PEO scaffold in a well-established full-thickness skin excision model in the hairless rat.

Chapter 3. Fabrication and Characterization of Soy Protein-Based Scaffolds

3.1. Introduction

Our initial desired approach was to form an electrospun scaffold based on soy protein isolate (SPI) alone, without any additives. Thus, a variety of solvents were explored to find one most suitable to dissolve SPI, and concentrations of SPI were varied to achieve a solution with the viscosity of “corn syrup” in order to electrospin consistent, bead-free fibers. However, it was found that SPI alone at any concentration in any solvent we tested would yield electrospraying behavior at best. This may be due to soy protein being a globular protein and tending to form gel networks when aggregated (Curt et al., 2009), instead of interconnected chains. Therefore, the synthetic inert polymer poly(ethylene oxide) (PEO) was added to increase chain entanglements in solution (Shenoy et al., 2005) and enable the formation of continuous fibers. We then optimized the fabrication of SPI/PEO scaffolds by varying the key electrospinning parameters of SPI concentration, ratio of SPI to PEO, syringe pump delivery rate, accelerating voltage, and air gap distance between the ejection needle tip and the target collector. SPI/PEO scaffolds were then characterized based on morphology, fiber diameters, tensile properties, and degradation behavior in various aqueous media with and without a proteolytic component.

3.2. Materials and Methods

3.2.1. Production of the scaffolds

3.2.1.1. Preparation of protein solutions: Initially, soy protein isolate (SPI) (obtained from Cargill Health and Food Technologies, Minneapolis, MN) was dissolved without any additives in a variety of aqueous and organic solvents (Table 3.1) to determine the most suitable solvent for electrospinning.

Table 3.1. Solvents investigated for dissolving SPI for electrospinning.

Solvent type	Solvent	Dissolve?	Remarks
Aqueous	Acetic acid	No	
	Ethanol	No	
	Acetic acid/ethanol (50/50)	No	
	Hydrochloric acid	No	
	Acetone	No	
	Sodium hydroxide	Yes	Solution unstable
	Ammonium hydroxide	Yes	
	Water	No	
Organic	Dimethylformamide (DMF)	No	Evaporated very quickly
	Tetrahydrofuran (THF)	No	Evaporated very quickly
	1,1,1,3,3,3 Hexafluoro-2-propanol (HFP)	Yes	Solution stable indefinitely

It was found that pure SPI solutions would not electrospin into fibers—they only yielded electrospraying behavior. A range of concentrations between 3 – 20% (w/v) SPI was tested. Therefore, poly(ethylene oxide) (PEO) (Sigma, St. Louis, MO) was added to the solutions and the amount parametrically adjusted between 0.01% (w/v) to 2% (w/v) to determine the minimal amount required to yield an electrospinnable solution.

The first “optimal” solution consisted of 10% (w/v) SPI and 1% (w/v) PEO in 0.1 N sodium hydroxide (NaOH). However, due to limitations discussed in the Results section (Section 3.3), the concentrations were re-optimized using 1,1,1,3,3,3 Hexafluoro-2-propanol (HFP) (Sigma) as the solvent of choice. SPI was varied between 5 – 10% (w/v) and PEO between 0.05 – 0.2% (w/v).

Once the “optimal” amount of PEO was determined by characterization of resultant fibers to be 0.05% (w/v) (see Results, Section 3.3), solutions were made by first dissolving 0.5% (w/v) PEO in HFP and adding appropriate volumes from this stock solution to 5, 6, 7, and 8% (w/v) SPI in HFP respectively. Blend solutions were left to stir at RT for at least 48 h and up to approximately 2 weeks before electrospinning to ensure complete and homogeneous dissolution, although the quality of resultant electrospun fibers was not reduced when solutions were left to stir for more than 2 weeks.

For comparison in cell culture experiments, corn zein (obtained from Freeman Industries LLC, Tuckahoe, New York) was dissolved at 35%, 40% and 45% (w/v) in glacial acetic acid (Fisher Scientific, Pittsburgh, PA) and left to stir at least 3 h and up to approximately 1 week before electrospinning. Solutions were not kept for longer as bead formation was observed when solutions older than 1 week were electrospun. Fabrication and characterization of zein scaffolds were performed by Devika Varma.

3.2.1.2. Electrospinning of protein solutions: Fibers were electrospun in a horizontal setup, as previously described (Li et al., 2005) (Figure 3.1). In brief, a precision syringe pump (KD Scientific Single Syringe Infusion Pump, Fisher) was used to eject solution from a disposable 3 ml syringe (BD Biosciences, Franklin Lakes, NJ) through a blunt 18-gauge needle. Parametric studies were conducted to identify optimal settings that would yield consistent, bead-free fibers. SPI/PEO blend solutions were electrospun at delivery rates between 0.5 to 1.2 ml/h, air gap distance between 10 - 20 cm, and accelerating voltage between 10 to 27 kV. For zein solutions, the optimized delivery rate was 0.5 ml/h, air gap distance was 15 cm, and accelerating voltage was 20 kV for 35% and 40% solutions and 25 kV for 45% solutions. As a synthetic material for comparison in cell culture studies, 20% (w/v) 90:10 poly(lactic-*co*-glycolic acid) (PLGA) was

electrospun at 0.5 ml/h, 15 kV and 15 cm. As a natural, animal-derived material for comparison, 8% (w/v) gelatin (Sigma) was electrospun at 0.8 ml/h, 12 kV and 20 cm. To capture the electrospun fibers, circular glass cover slips (Fisher), 15 mm in diameter, were attached to a rectangular aluminum collector. For microscopic analysis of individual fibers, 0.2 ml of solution was electrospun; as cell culture substrates, 1 ml was electrospun onto the cover slips, yielding scaffolds of approx. 20 µm thickness. For mechanical testing, organotypic skin equivalent co-culture experiments, and *in vivo* experiments, fibrous mats (~ 0.1 – 0.2 mm thickness) were electrospun and collected directly on the aluminum collector.

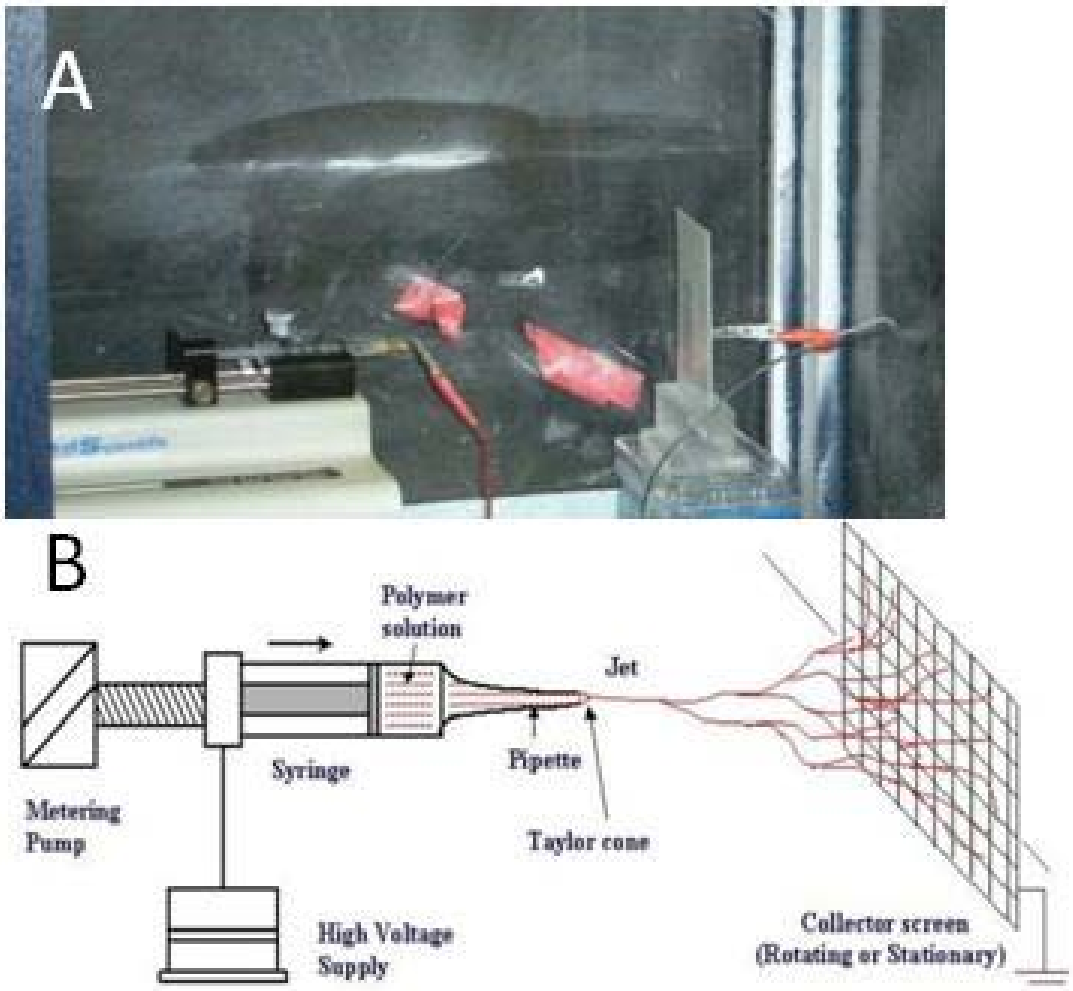

Figure 3.1. Electrospinning setup in our laboratory (a) and schematic (b) (from http://www.che.vt.edu/Wilkes/electrospinning/electrspinning.html).

3.2.2. Materials characterization

3.2.2.1. Measurement of fiber diameters: Glass cover slips coated with electrospun fibers were mounted onto metal stubs with carbon tape and sputter-coated for 30 s with platinum and palladium (Pt/Pd) prior to visualization in an environmental scanning electron microscope (ESEM,

XL-30 SEM-FEG) (FEI, Hillsboro, OR) at an accelerating voltage of 10 kV and spot size 3. For each sample at least 10 measurements per image were taken from 10 images of random areas. Fiber diameters were measured using University of Texas Health Science Center at San Antonio (UTHSCSA) ImageTool 3.0 software (n=100 for each sample).

Dry samples were mounted as spun. To investigate the degree of swelling with hydration, samples of SPI/PEO were immersed in sterile distilled deionized water, 1X phosphate buffered saline (PBS) solution without calcium and magnesium (Mediatech Inc., Herndon, VA), or Dulbecco's modified Eagle's medium (DMEM) (Mediatech) supplemented with 10% fetal bovine serum (FBS) (Atlanta Biologicals, Lawrenceville, GA) at 37^{o}C and 5% CO_2 for 3 h, 7 days and 14 days. Samples were washed with distilled deionized water and dehydrated before mounting for SEM. SPI/PEO samples were dehydrated first in 100% ethanol (EtOH) before critical point drying (CPD7501, SPI Supplies, West Chester, PA) to preserve structural morphology.

3.2.2.2. Surface analysis of electrospun scaffolds: Elemental analysis was performed using Oxford energy-dispersive X-ray microanalysis on a scanning electron microscope (Zeiss Supra 50VP, Carl Zeiss, AG, Germany) and SmartSEM™ software (Zeiss).

3.2.2.3. Mechanical testing: Mats were electrospun and cut into rectangular strips (approximately 5mm x 25mm x 0.1mm). Tensile tests were performed in triplicate for at least 3 independent samples using an Instron 5564 in dry and hydrated states. For testing hydrated samples with various concentrations of SPI, the mats were immersed in sterile DMEM + 10% FBS for 3 h to simulate a physiological condition where proteases would be present. For testing the effect of hydration on tensile properties over time, scaffolds electrospun from 7% SPI/0.05% PEO were immersed in DMEM + 10% FBS, 1X PBS, or water for 3 h (0 days), 7 days and 14 days at 37^{o}C and 5% CO_2. Samples were tested to breakage at a gauge length of 15 mm on a 10 N load cell. Crosshead speed was 1 mm/min for dry samples and 10 mm/min for wet samples as the higher speed was more appropriate to account for the higher ductility of wet samples.

3.2.2.4. *In vitro* degradation: SPI/PEO mats were electrospun and cut into rectangular pieces (approximately 10mm x 25mm x 0.1mm). Each piece was placed in a 60mm diameter petri dish and its dry weight was taken as a baseline. Pieces were then sterilized by UV exposure and divided into 4 groups with at least 3 specimens per group per time-point, to be hydrated in 3 ml distilled deionized water, DMEM, DMEM + 10% FBS, and DMEM/equine serum (ES) in a 1:1 ratio respectively. Samples were kept in a humidified incubator at 37°C and 5% CO_2; the hydration media were changed daily. At time-points of 1, 4, 7, 14, 21, 28, 35 and 42 days, the media were

removed, the specimens were washed twice with water to remove residual salts and placed in a vacuum oven at 50°C overnight for complete dehydration. Specimens were weighed again in their dishes and the percentage mass loss was calculated as:

% mass loss = 100*(original mass - final mass) / original mass

To confirm that SPI/PEO scaffolds could be degraded proteolytically, strips were immersed in 1 mg/ml collagenase (415 units/mg solid of collagen digestion activity; Sigma) dissolved in 1X PBS (Mediatech) for 1 h, 2 h and 4 h. Native SPI powder was subjected to the same conditions for comparison.

3.2.2.5. Characterization of *in vitro* degradation products: Supernatants from the degradation study were collected at time-points of 1, 4, 7, 14, 21, 28, 35 and 42 days and frozen at -20 ◦ C to be analyzed later using sodium dodecyl sulfate polyacrylamide gel electrophoresis (SDS-PAGE). After thawing, 15 µl of each supernatant was mixed with 15 µl of 2X Laemmli buffer (Bio-Rad, Temecula, CA) in a microcentrifuge tube and boiled for 5 min to denature the proteins. The mixtures were then allowed to cool for approximately 5 min before loading into each well of a 4–20% Mini-PROTEAN TGX Precast Gel (Bio-Rad). The proteins were run through the gel at a constant voltage of 100 V for 70 min. The gel was fixed for 20 min in 25% isopropanol and 10% acetic acid in 50 ml distilled deionized water, stained with Coomassie Brilliant Blue solution

overnight and destained in 10% acetic acid overnight before imaging on a Molecular Imager ChemiDoc XRS+ System (Bio-Rad).

3.2.2.6. Quantitation of protein in *in vitro* degradation products: Supernatants from the degradation study were analyzed using the bicinchoninic acid (BCA) assay (Pierce, Rockford, IL) for a 96-well plate according to the manufacturer's instructions. Calibration curves correlating absorbance at 562 nm to protein content were prepared using SPI and bovine serum albumin (BSA). A 10 µl aliquot of each supernatant was diluted with 10 µl of distilled deionized water in a 96-well plate before adding 150 µl of freshly prepared BCA reagent to each well. The plate was sealed and incubated at 37 ◦ C in a water bath for 20 min before reading the absorbance at 562 nm on a spectrophotometric plate reader (Biotek, Winooski, VT).

3.3. Results and Discussion

3.3.1. Fabrication of SPI/PEO scaffolds

3.3.1.1. Preparation of protein solutions: Of the solvents we investigated, sodium hydroxide (NaOH), ammonium hydroxide, and HFP dissolved SPI. Initially 0.1 N NaOH was selected and the concentrations of SPI and PEO were varied between a range of 5 – 12% (w/v) SPI and 0.05 - 2% (w/v) PEO. Beaded fibers were formed with 5% SPI, 1% PEO solutions (Figure 3.2a), due to

“capillary breakup of the electrospinning jets by surface tension” that occurs at low solution viscosities (Fong et al., 1999). While 10% and 12% SPI with 1% PEO both electrospun into smooth, bead-free fibers (Figure 3.2 b and c respectively), the 12% solutions tended to clog the needle. 10% SPI, 1% PEO in 0.1 N NaOH was determined to be the optimal solution.

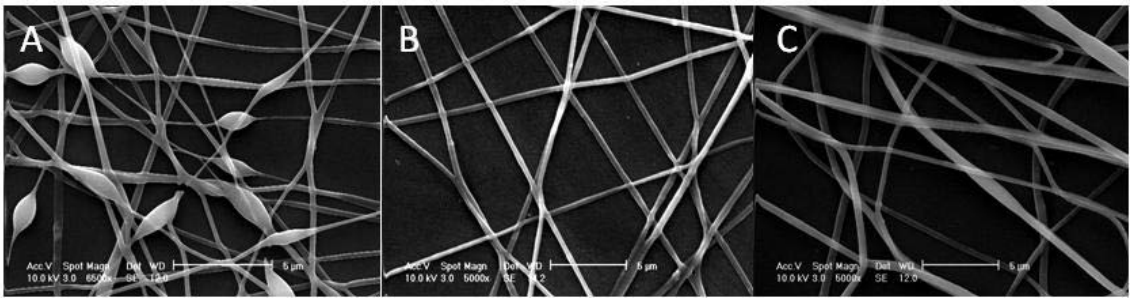

Figure 3.2. Scanning electron micrographs of electrospun SPI/PEO fibers with varying concentrations of SPI. (a) 5% SPI, 1% PEO; (b) 10% SPI, 1% PEO; (c) 12% SPI, 1% PEO electrospun from solutions dissolved in 0.1 N NaOH. Scale bars 5 µm.

However, this solvent system had several disadvantages. Firstly, solutions were unstable and the protein tended to degrade within days, such that beaded, broken fibers were formed or only electrospraying occurred. Also, even the smooth fibers were brittle and dissolved upon contact with any aqueous media unless they were chemically crosslinked, with 0.4% (w/v) 1-ethyl-3-[3-dimethylaminopropyl]carbodiimide hydrochloride (EDC) (Pierce, Rockford, IL). Since solutions in HFP tend to be stable indefinitely and fibers electrospun from SPI and PEO dissolved

in HFP in an initial trial were ductile to the touch, the parametric optimization of solute concentrations was repeated for HFP.

An important discovery made during this process was that SPI/PEO scaffolds formed by electrospinning solutions in HFP remained stable in aqueous media without any need for further cross-linking. This is a significant benefit as chemical crosslinkers and even “natural” crosslinkers such as genipin may confer a certain degree of cytotoxicity, and increase the stiffness of the scaffold, which may adversely affect cell culture and *in vivo* applications.

In HFP, 1% (w/v) PEO formed a gel. Therefore, the concentration was lowered to a range between 0.05 – 0.5%. Figure 3.3 shows some of the various concentrations tested. 5% SPI, 0.05% PEO electrospun into smooth fibers (Figure 3.3a), but higher concentrations of PEO yielded incompletely formed fibers in addition to regular fibers (Figure 3.3 b – d). It was therefore determined that 0.05% PEO was a maximal concentration required to form fibers, and further investigation would explore lower concentrations to find the minimal. Conversely, a maximal SPI concentration was desired in order to increase the amount of protein fibers produced from the same volume of solution.

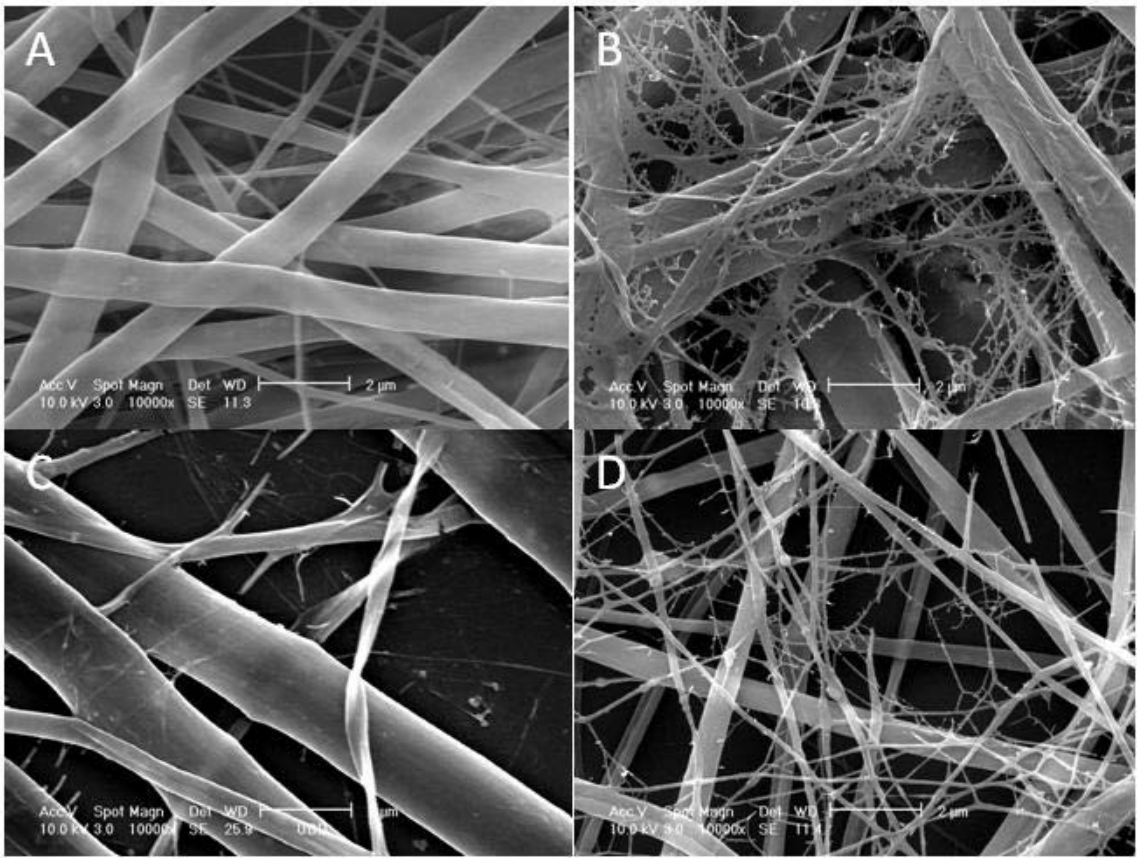

Figure 3.3. Scanning electron micrographs of electrospun SPI/PEO fibers with varying concentrations of PEO. a) 5% SPI, 0.05% PEO; b) 5% SPI, 0.1% PEO; c) 5% SPI, 0.5% PEO; d) 10% SPI, 0.1% PEO. Scale bars 2 µm.

Further parametric studies were performed with 5 – 8% SPI and 0.025 – 0.05% PEO. Above 8% SPI, the solution agglomerated at the needle tip during electrospinning. At every concentration of SPI tested, 0.025% PEO appeared to be too low to form consistently smooth fibers, as represented by Figure 3.4. Therefore, 0.05% PEO was also determined to be the minimum concentration required.

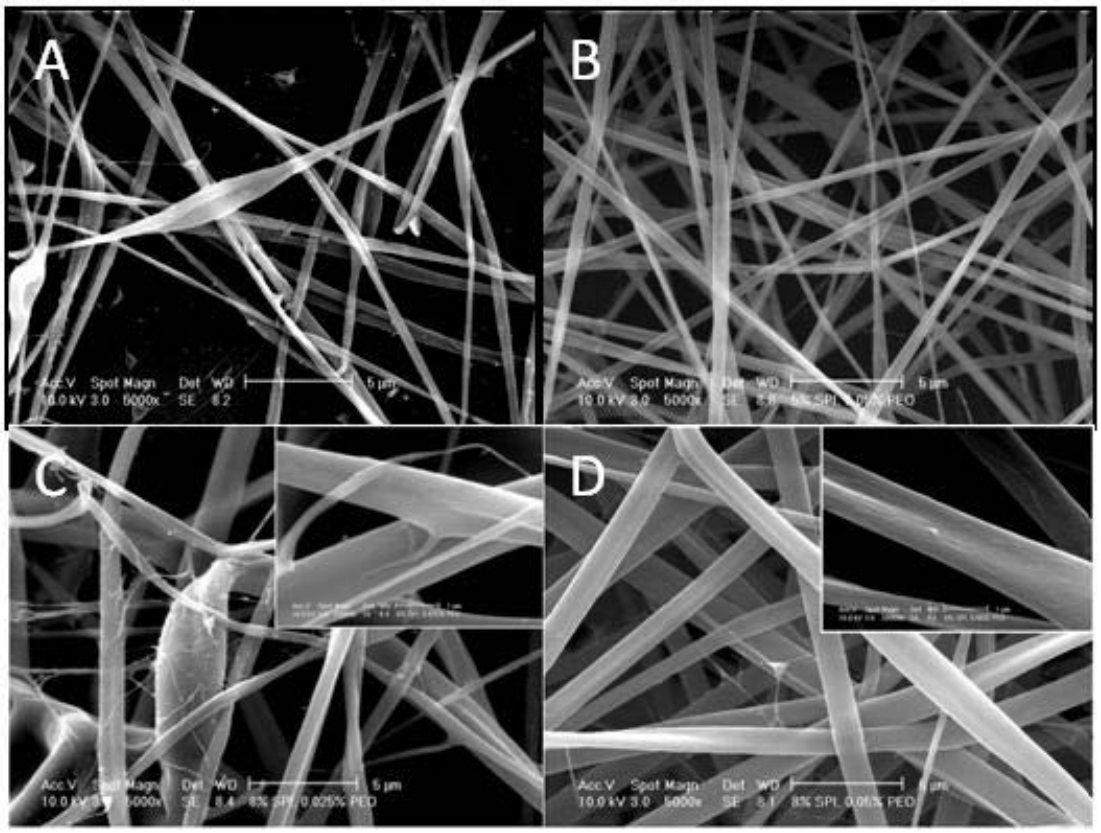

Figure 3.4. Representative images showing the dependence of consistent SPI/PEO fiber formation on a threshold amount of PEO. a) 5% SPI, 0.025% PEO; b) 5% SPI, 0.05% PEO; c) 8% SPI, 0.025% PEO (inset shows fine strands overlapping fibers); d) 8% SPI, 0.05% PEO (inset shows ribbon-like flat morphology). Scale bar 5 µm (insets 1 µm).

3.3.1.2. Electrospinning parameters: For each set of protein concentrations tested, electrospinning parameters were varied to determine which set yielded consistent, bead-free fibers. Increasing flow rate increases fiber diameter, while increasing air gap distance decreases fiber diameter. Increasing accelerating voltage may or may not increase fiber diameter (reviewed by Bhardwaj and Kundu, 2010). These key parameters can also make the difference between

smooth fibers and beaded fibers. The optimal parameters for 5 – 8% SPI, 0.05% PEO in HFP were flow rate 0.8 ml/h, voltage 15 kV, and air gap distance 12 cm.

3.3.2. Characterization of SPI/PEO scaffolds

3.3.2.1. Variation of fiber diameter with SPI concentration: Higher SPI concentration correlated to a larger size of fibers. Table 3.2 shows the fiber diameters obtained with SPI/PEO electrospun from NaOH solution. The increase in diameter is not proportionate to the increase in SPI concentration, which could be explained by taking into account the fact that the 12% SPI solution was much closer to gelation and therefore had a much higher resistance. After our completion of this work, Vega-Lugo and Lim (2008) independently published a report on similar work with similar results. Their optimized values were 15% SPI as it was the highest concentration they attained before the solution gelled, 0.8% PEO, and 0.5% TritonX-100 as a surfactant, dissolved in 1% NaOH. Their nanofibers ranged from approximately 200 – 260 nm in diameter. More recently, Fung et al. (2010) electrospun soy protein isolated from the soluble fraction of factory agrowaste of “okara” or soybean, using 1 N NaOH as a solvent and adding 5% (w/v) PEO. They attained continuous tubular nanofibers <500 nm in diameter. The main reason for the differences between their results and ours is most likely their addition of surfactant, as this would allow for reduced protein resistance resulting in a higher concentration of SPI being electrospinnable and

also smaller fiber diameters.

Table 3.2. Variation of fiber diameter with SPI concentration in solutions dissolved in 0.1 N NaOH (n = 30).

% SPI with 1% PEO	Fiber diameter (nm)
5	253 ± 69
10	296 ± 75
12	497 ± 101

Figure 3.5 shows increasing fiber diameter with SPI concentrations, with PEO concentration kept constant at either 0.025% or 0.05% for our HFP-dissolved solutions. Surprisingly, lower content of PEO did not correlate with smaller fiber diameters (Figure 3.5) compared to higher PEO content. This may be because the increased chain entanglements in solution with the higher PEO content (Shenoy et al., 2005) led to decreased protein aggregation, allowing for extrusion into finer fibers. Across the range of concentrations of SPI tested, SPI/PEO blend solutions yielded submicron to micron-sized fibers, with approximately 702 ± 201 nm width (heterogeneity 29%) at 5% SPI, 0.05% PEO and 1251 ± 306 nm width (heterogeneity 24%) at 8% SPI, 0.05% PEO. These values are much higher than the ~200 - 300 nm obtained from the solutions dissolved in NaOH. HFP is a volatile solvent, with much lower surface tension compared to NaOH, and this leads to rapid

evaporation when the polymer leaves the needle tip, collapsing to form fibers with flat, ribbon-like morphology (Koombhongse et al., 2001).

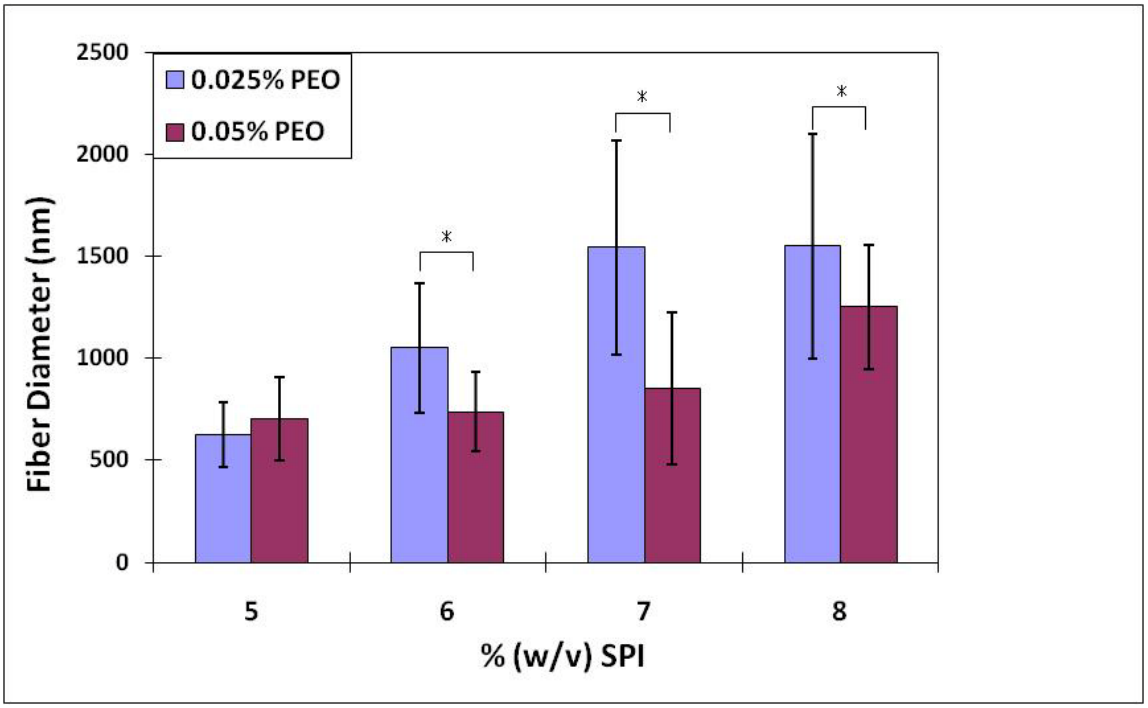

Figure 3.5. Variation of fiber diameter with relative SPI and PEO concentrations in HFP. While increasing the concentration of SPI increases fiber diameter, increasing the concentration of PEO from 0.025% to 0.05% resulted in decreased diameters for 6%, 7% and 8% SPI (n = 100, asterisks show statistical significance, $p<0.05$). Between percentages, all groups are statistically significantly different ($p<0.05$) except 7% vs. 8% SPI with 0.025% PEO and 5% vs. 6% SPI with 0.05% PEO.

3.3.2.2. Increase in fiber diameter with hydration: SPI/PEO fibers swelled upon hydration in water, PBS, and DMEM + 10% FBS. Figure 3.6 shows a whole scaffold hydrated in DMEM. Between 3 h and 7 days of hydration, only fibers in water swelled significantly more at 7 days, and only fibers in PBS swelled significantly more at 14 days of hydration compared to 3 h (Figure 3.7). This indicates that SPI/PEO fibers absorb fluids rapidly and remain stable in aqueous media, as also shown by their morphology after hydration over time (Figure 3.8).

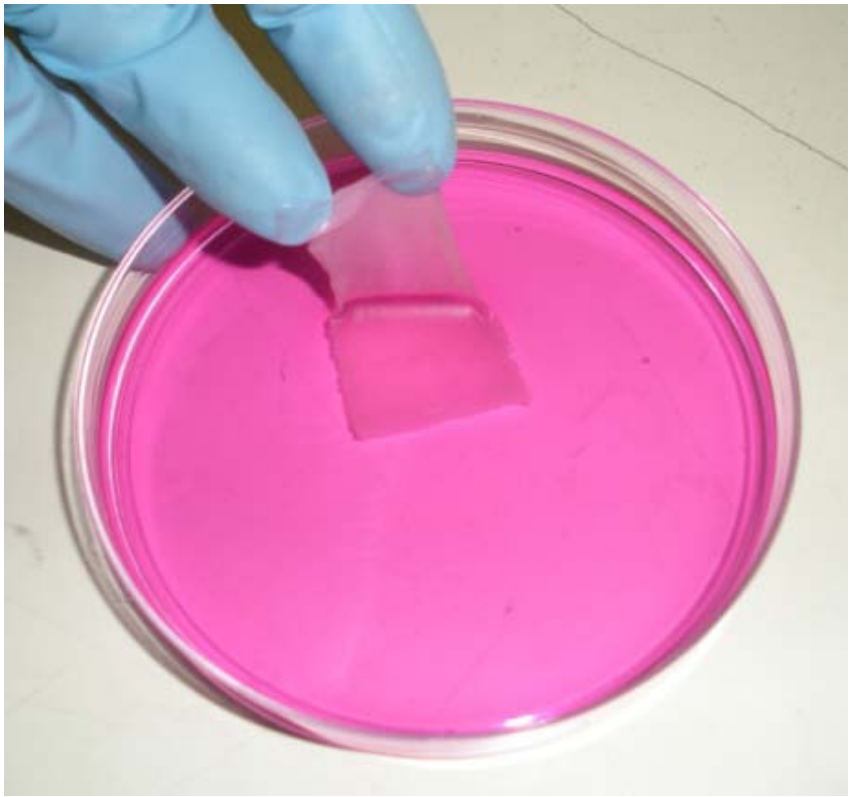

Figure 3.6. Electrospun SPI/PEO scaffold hydrated in DMEM.

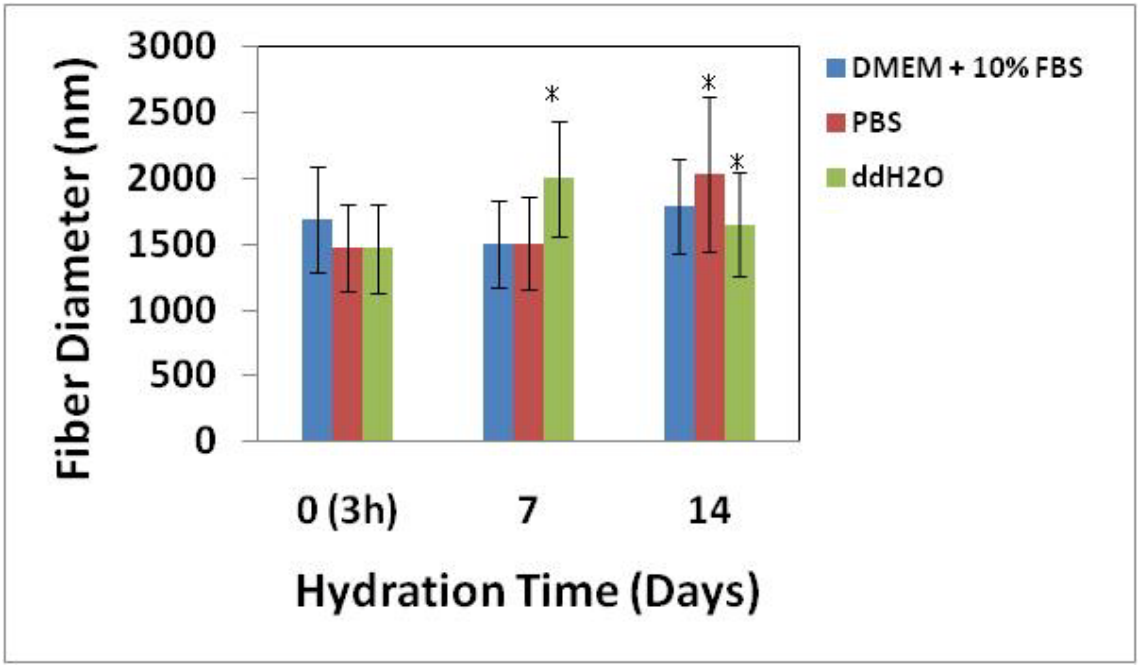

Figure 3.7. Variation of SPI/PEO fiber diameter with hydration time. Asterisks (*) indicate statistically significant ($p<0.05$) increase in swelling compared to day 0.

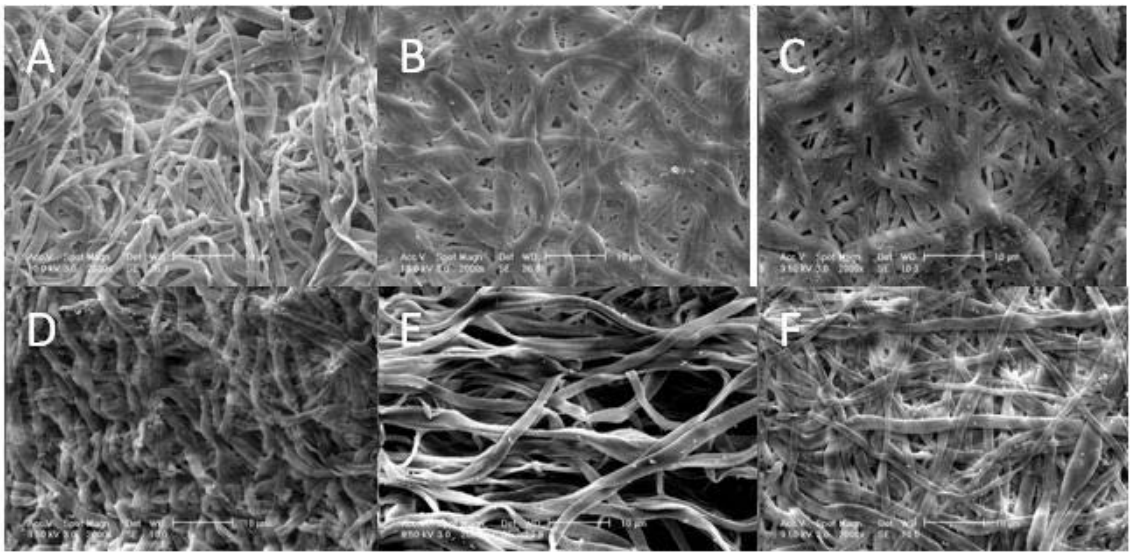

Figure 3.8. Scanning electron micrographs of hydrated 7% SPI/0.05% PEO scaffolds. Representative images of 7% SPI/0.05% PEO scaffolds after hydration for 3 hours in a) DMEM + 10% FBS; b) 1X PBS; c) water, and for 14 days in d) DMEM + 10% FBS; e) 1X PBS; f) water (scale bars 10 µm).

3.3.2.3. Elemental surface analysis of SPI/PEO scaffolds: The predominant elements detected on the surfaces of SPI/PEO scaffolds are shown in Table 3.3. Fluorine was detected on as-electrospun scaffolds (Table 3.3 and Figure 3.9), indicating residue from HFP that did not sufficiently evaporate during electrospinning. Molybdenum and sulfur were also sporadically present (Figure 3.9). After immersing scaffolds in 1X PBS without calcium and magnesium for 1 h, fluorine was no longer detectable (Table 3.3 and Figure 3.9). Therefore, concern about residual HFP that may be cytotoxic *in vitro* or *in vivo* may be addressed by washing scaffolds with sterile saline solution before use, as part of surgical preparation in the operating room. Magnesium, calcium and potassium also appeared to have been washed away by PBS.

Table 3.3. Percentages of elements detected on electrospun SPI/PEO scaffolds as spun and after immersion in PBS for 1 h.

	As spun				**PBS 1h**			
Element	Avg Weight %	St. Dev.	Avg Atomic %	St. Dev.	Avg Weight	St. Dev.	Avg Atomic %	St. Dev.
C K	63.00	3.77	69.62	3.69	65.06	6.76	70.05	6.08
N K	13.90	3.38	13.19	3.29	21.13	3.51	19.56	3.37
O K	17.16	2.28	14.23	1.83	11.29	4.34	9.19	3.68
F K	1.71	0.93	1.20	0.66				
Na K	1.21	0.22	0.70	0.13	1.16	0.15	0.66	0.09
Mg K	0.33	0.10	0.18	0.06				
P K	1.22	0.30	0.52	0.13	0.54	0.27	0.23	0.12
S K	0.48	0.27	0.20	0.11	0.69	0.05	0.28	0.02
K K	0.97	0.20	0.33	0.07				
Ca K	0.52	0.15	0.17	0.05				
Mo L	0.71		0.10					
Cl K					0.32	0.00	0.12	0.00
Totals	100				100			

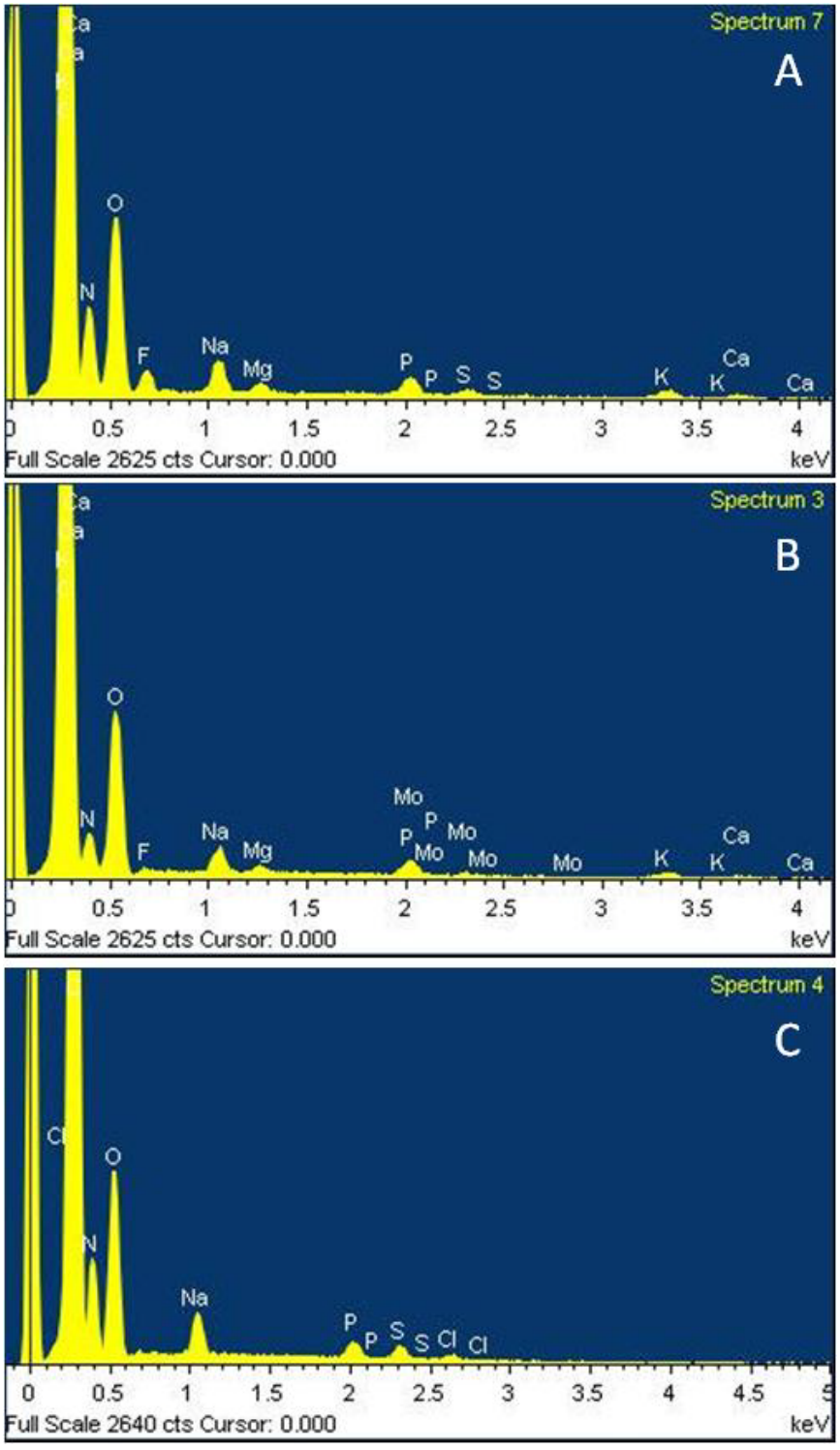

Figure 3.9. Energy-dispersive spectra of electrospun SPI/PEO scaffolds. Representative spectra of as-electrospun SPI/PEO scaffold surfaces (a and b), and after 1 h in PBS, with the fluorine peak absent (c).

3.3.2.4. Mechanical testing: SPI/PEO scaffolds were tensile tested to break. No significant difference was observed between mechanical properties of dry SPI/PEO scaffolds with variation in the protein concentrations investigated (Table 3.4). Hydrated samples had ultimate tensile strengths roughly one order of magnitude lower than dry samples (Figure 3.10a), with a strain at break one order of magnitude higher than dry samples (Figure 3.10b). Pig skin was also tested for comparison. Importantly, the strain at break values for hydrated SPI/PEO scaffolds (~83%) are in the same order of magnitude as the reported values for human skin, which is approximately 100% (Diridollou et al., 2000). The ultimate tensile strengths (UTS) of hydrated SPI/PEO scaffolds (~0.1 MPa) are roughly two orders of magnitude less than that reported for skin, approximately 7.7 MPa (Adekogbe and Ghanem, 2005). However, this may not be cause for concern if SPI/PEO scaffolds used as wound dressings are not stretched to the maximum in a treatment scenario.

Table 3.4. Ultimate tensile strength (UTS) and strain to break values for dry and hydrated (3 h in DMEM + 10% FBS) scaffolds with varying concentrations of SPI.

Scaffold	**Condition**	**UTS (MPa)**	**Strain to Break (%)**
5% SPI, 0.05% PEO	dry	1.06 ± 0.23	10.67 ± 3.11
	hydrated	0.06 ± 0.03	73.35 ± 26.98
6% SPI, 0.05% PEO	dry	0.90 ± 0.38	7.45 ± 2.92
	hydrated	0.07 ± 0.03	84.88 ± 27.67
7% SPI, 0.05% PEO	dry	0.91 ± 0.39	7.53 ± 1.29
	hydrated	0.10 ± 0.05	83.33 ± 21.18
8% SPI, 0.05% PEO	dry	0.95 ± 0.31	7.51 ± 1.99
	hydrated	0.11 ± 0.03	81.25 ± 22.47

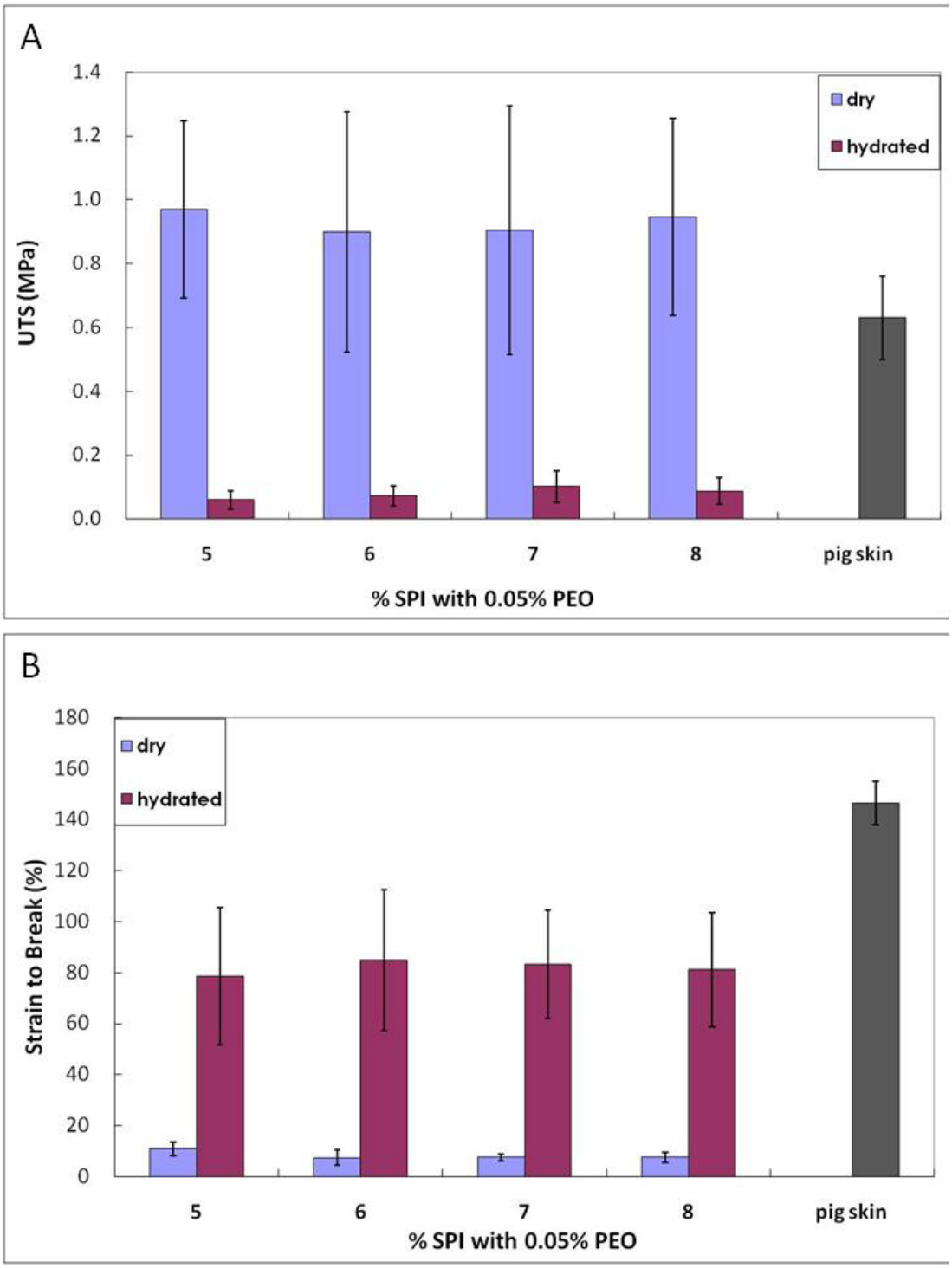

Figure 3.10. Variation of tensile properties of electrospun SPI/PEO scaffolds with SPI concentration. Ultimate tensile strength (a) and strain to break (b) of electrospun SPI/PEO scaffolds at different concentrations of SPI in dry and hydrated conditions.

7% SPI/0.05% PEO scaffolds were hydrated for 3 h (0 days), 7 days and 14 days in DMEM + 10% FBS, PBS and water to test the effects of hydration on tensile properties over time. Both UTS and strain at break were statistically significantly ($p<0.05$) lower at 7 days and 14 days compared to 3 h in DMEM + 10% FBS, while UTS was statistically significantly higher at 7 days and 14 days compared to 3 h in PBS and extremely statistically significantly ($p<0.01$) higher in water (Figure 3.11). Strain at break was statistically significantly lower at 7 days compared to 3 h in PBS and extremely statistically significantly higher in water (Figure 3.11b). These differences may be explained by PBS and DMEM both being osmotically balanced, while water not only causes osmotic pressure for the proteins in the scaffold but is also a poor solvent for SPI, which may cause aggregation of the hydrophobic units over time (Kuipers and Gruppen, 2008). This would result in both higher strength and ductility of the scaffolds as the aggregates are being stretched.

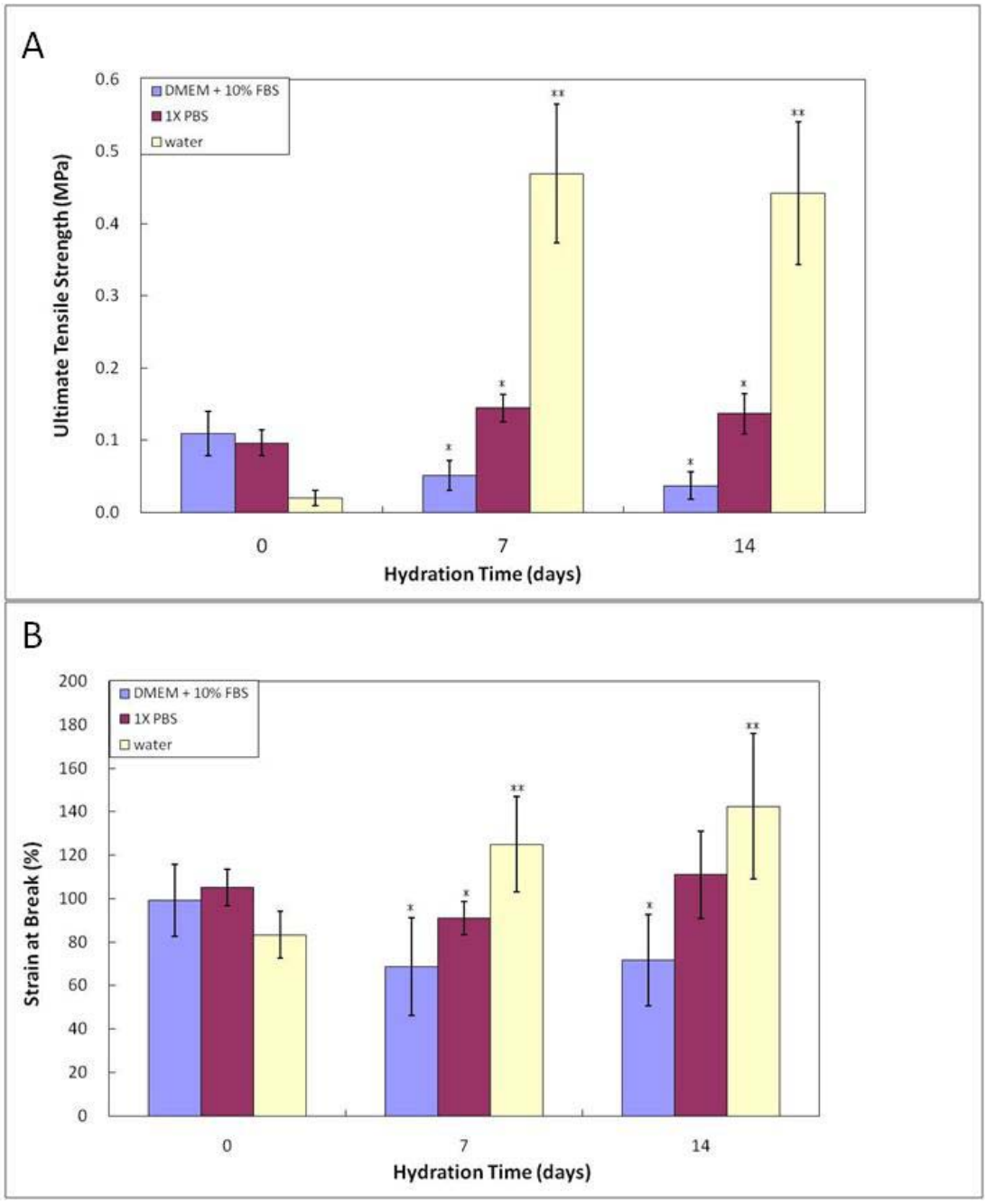

Figure 3.11. Variation of ultimate tensile strength (UTS) (a) and strain at break (b) with hydration time in various media. Asterisk (*) shows statistically significant difference ($p<0.05$) and double asterisk (**) shows extremely statistically significant difference ($p<0.01$) from day 0.

3.3.2.5. *In vitro* degradation: SPI/PEO scaffolds lost ~10% of their original mass in the 50/50 mix of DMEM and equine serum (ES), ~25% in DMEM with or without FBS, and ~40% in distilled deionized water within the first day of hydration (Figure 3.12). After that they remained stable for 42 days. Scaffolds may have degraded more in water due to hydrolysis coupled with osmotic imbalance, whereas the effect of hydrolysis in DMEM was reduced by the osmotic pressure balancing presence of salts. The presence of serum did not increase scaffold degradation in the case of both 10% and 50% serum in the buffer, indicating that certain factors present in serum may have inhibited the activity of serum proteases. The stability of these SPI/PEO scaffolds in the presence of serum may be attributed both to the protective effects of serum against proteolytic degradation, as well as to the intrinsic protease inhibitors in the structure of soy protein. The inhibitory effect of serum on serine proteases is a known phenomenon in the *in vitro* digestion of extracellular matrix (ECM) proteins in mammalian cells. For example, Wang and Zheng (2009) recently quantified the inhibition of FBS on trypsin digestion of bovine articular cartilage explants using ultrasound biomicroscopy.

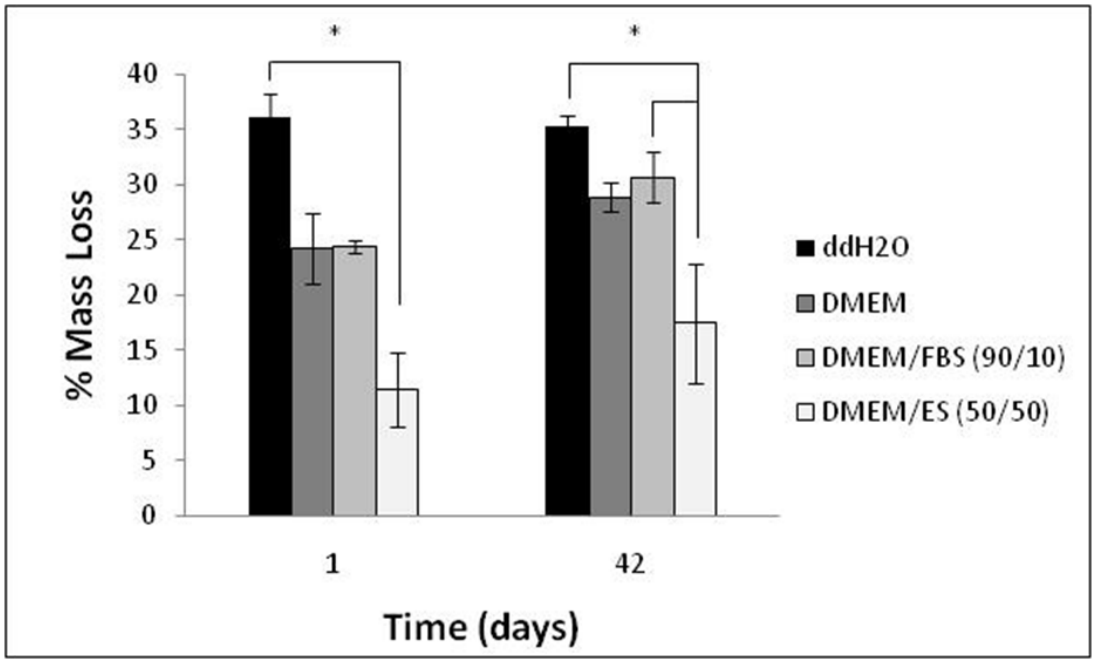

Figure 3.12. Variation of percentage mass loss of SPI/PEO scaffolds over time in water, DMEM, DMEM + 10% FBS and 50/50 DMEM/ES. Asterisk (*) indicates statistical significance ($p<0.05$). No statistically significant differences were observed between 42 days and 1 day for any of the conditions.

Vaz et al. (2003) tested the degradation of SPI extruded into thermoplastic pellets with and without crosslinking by glyoxal or heat treatment at 80 ◦ C for 24 h. To investigate non-enzymatic degradation, the authors immersed SPI pellets in isotonic saline solution for 0, 1, 3, 5, 7 and 14 days. While un-crosslinked pellets showed approximately 14% weight loss over 14 days, weight loss was reduced with increasing concentrations of glyoxal, and less than 2% weight loss occurred with heat-treated pellets over 14 days. They attributed the degradation of SPI materials to surface erosion, as also evidenced by a decrease in thickness of pellets with immersion time.

In our case, although our SPI/PEO scaffolds were not crosslinked, they may also have degraded only slightly and by surface erosion. It appears that an initial rapid surface erosion occurred within the first day of immersion, after which the scaffolds remained mostly stable. These results were also confirmed by characterization of the degradation products, as discussed in the next section.

3.3.2.6. Characterization of degradation products of SPI/PEO scaffolds: Supernatants of water, DMEM, DMEM + 10% FBS, or DMEM/ES in which SPI/PEO scaffolds were immersed were analyzed by SDS-PAGE. As controls, native SPI powder and electrospun SPI/PEO scaffold were dissolved in 0.1 N NaOH. Importantly, the characteristic bands of soy protein appeared in both these lanes (Figure 3.13, box), indicating that SPI retained its molecular structure even after the process of electrospinning. The strongest bands correspond to the 18 kDa basic (B) polypeptide of glycinin (the 11S fraction), the 31 kDa acidic (A) polypeptide of glycinin, and the 70 kDa α and α' subunits—which share a 90% homology—of β-conglycinin (the 7S fraction), respectively (Curciarello et al., 2008). A faint band also appears around 50 kDa that may correspond to the AB subunit of glycinin (Curciarello et al., 2008).

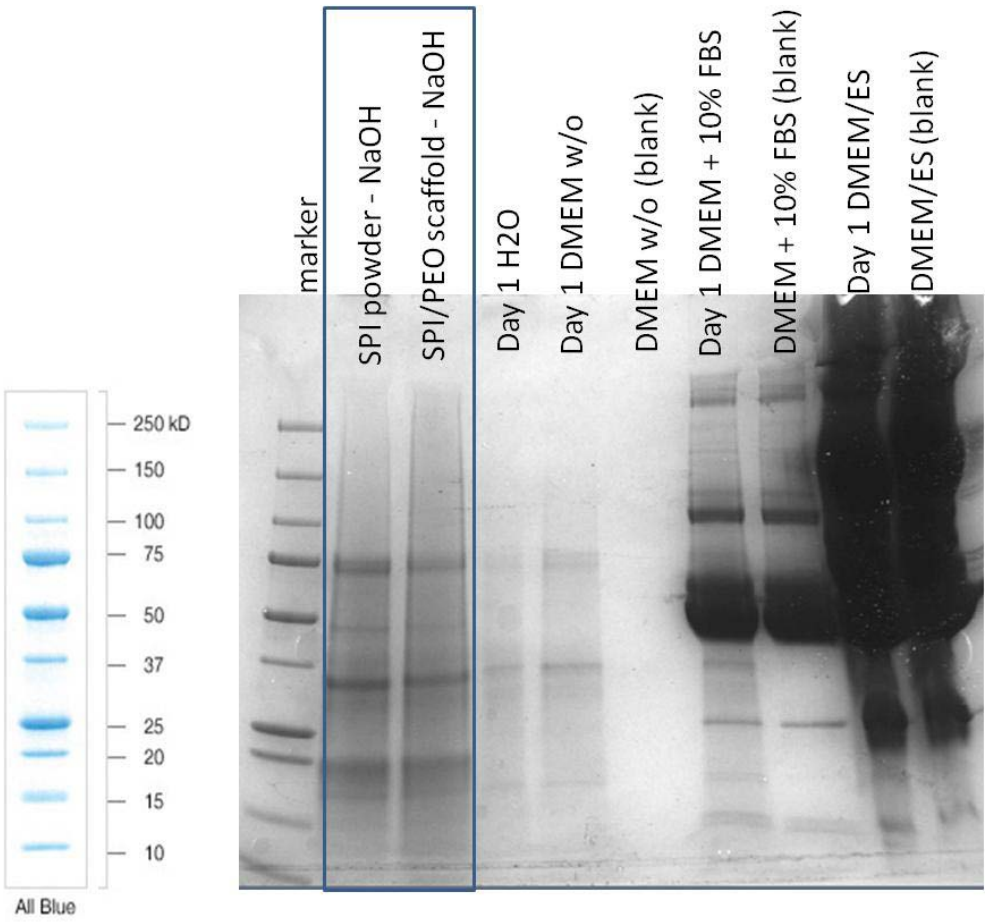

Figure 3.13. SDS-PAGE of supernatants from Day 1 of immersion of SPI/PEO scaffolds in water, DMEM, DMEM + 10% FBS and DMEM/ES. Boxed lanes show characteristic bands of soy protein after dissolving SPI powder and electrospun SPI/PEO scaffold in 0.1 N NaOH.

Figure 3.13 shows the protein bands of supernatants at day 1. Fewer characteristic bands of soy protein appeared in any of the supernatant lanes compared to the controls, but the same soy protein bands appeared in all the supernatant lanes that could be seen clearly, and were absent from the lanes with the media alone. DMEM/ES lanes were too smeared to read any bands due to protein overload from serum. This suggests incomplete degradation from surface erosion on

day 1. Vaz et al. (2003) also performed SDS-PAGE analysis on degradation products of soy pellets from immersion supernatants, and showed the same characteristic bands on days 0, 3, and 14 of continuous immersion. In our case, media were changed daily, and no SPI products could be detected in the supernatants after day 1, as represented by bicinchoninic acid (BCA) assay of water supernatants (Figure 3.14). According to the standard curve of SPI (Figure 3.14a), 0 mg protein corresponded to an absorbance at 562 nm of 0.0785. Therefore, negligible or no protein was detectable at any of the time points after day 1 of immersion (Figure 3.14b).

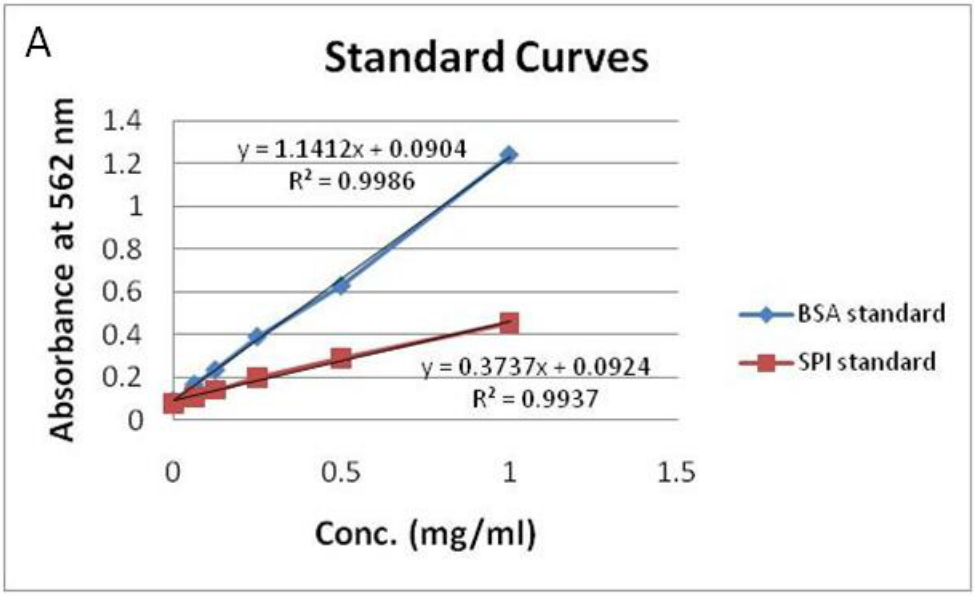

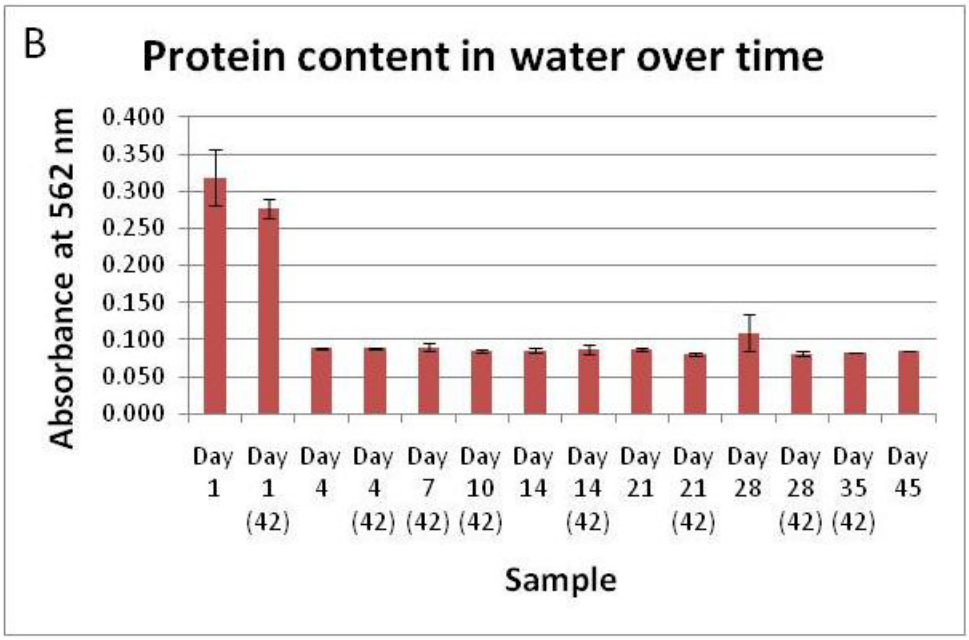

Figure 3.14. BCA assay for protein content in the supernatants from the degradation study. a) Standard curves using bovine albumin serum (BSA) and SPI. b) Protein content in water supernatants over time with immersion of electrospun SPI/PEO scaffolds. The (42) in parentheses indicate the same sample used at each of the different time points, kept for a period of 42 days.

Although these SPI/PEO scaffolds are stable in aqueous media and in the presence of serum, they are not completely resistant to proteolysis. Soy protein has specific sites where it can be cleaved enzymatically. Shutov et al. (1996) identified four cleavage points in the α-chain A2 of glycinin (the 11S fraction) as well as in the α'-chain of β-conglycinin (the 7S fraction). The C-terminal domain in 7S and N-terminal domain in 11S globulin subunits, as well as hydrophilic inserts within the chains, are susceptible to proteolytic attack (Shutov et al., 1996).

Collagenase, which is present in skin wounds, cleaves collagen after the Gly residue in the sequence of Gly~[Ile/Leu]-[Ala/Leu] (Xiao et al., 2010). In our experiments, SPI/PEO scaffolds were susceptible to degradation by 1 mg/ml collagenase, but only 2 bands of soy protein were detected by SDS-PAGE (Figure 3.15a). These appear to correspond to the subunits of intact β-conglycinin, with 70 kDa α and 50 kDa β subunits (Figure 3.15b, Shutov et al., 1996; Oliveira et al., 2002).

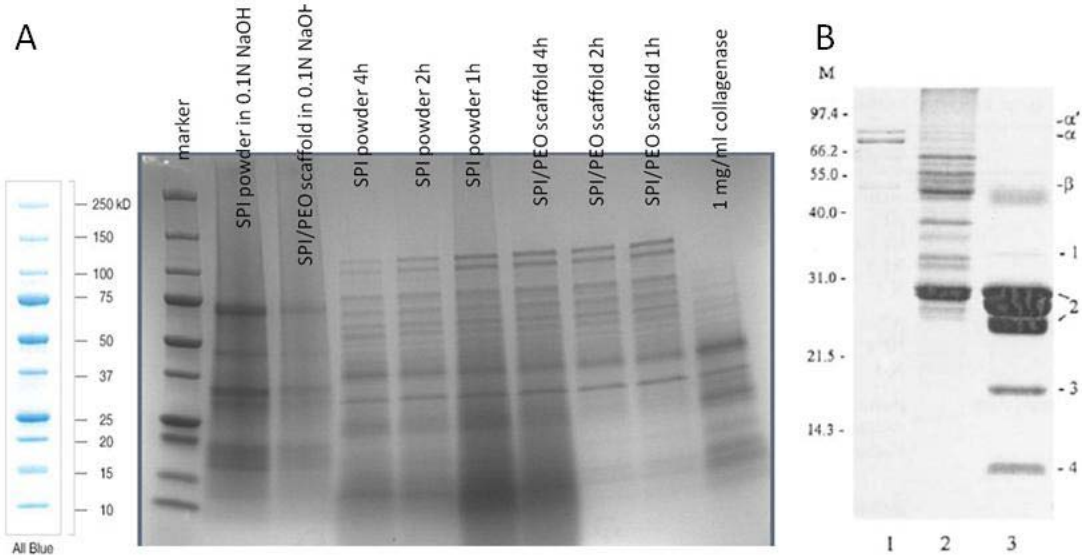

Figure 3.15. SDS-PAGE of proteolytically digested soy protein. a) SDS-PAGE of soy protein powder and scaffold digested by 1 mg/ml collagenase at 1h, 2h and 4h. b) Lane 1: intact β-conglycinin; Lane 2: 3-min trypsin hydrolysate; lane 3: 2h trypsin hydrolysate, with 1:600 mass ratio of trypsin to protein substrate (image taken from Shutov et al., 1996).

The hydrolytic stability of electrospun SPI/PEO scaffolds in aqueous environments, complemented by the ability to be degraded by proteolytic cleavage, is an encouraging property for a scaffold intended to promote skin wound repair. Although our focus is on using SPI/PEO scaffolds alone, these discoveries raise the possibility of investigating them as potential carriers for slow release bioactive components.

3.4. Conclusions

We developed a system for the production of electrospun submicron fibrous scaffolds based on soy protein isolate (SPI) with a minimal addition of PEO, using HFP as a solvent. Our system provides several advantages over our previous system and those reported by others (Vega-Lugo and Lim, 2008; Fung et al., 2010) who have independently electrospun soy protein using NaOH as a solvent. Namely, the solutions remain stable indefinitely, the fibers are more ductile to handle, the amount of PEO required is approximately 2 orders of magnitude less, and most importantly, fibers remain stable for over 7 weeks in aqueous media without any further crosslinking treatment. Tensile properties of hydrated SPI/PEO scaffolds are comparable to those reported for human skin, and degradation in aqueous media appears to occur by surface erosion within the first day of hydration, perhaps by removing protein debris that is not fully entangled within the fibers. SPI/PEO scaffolds retain the molecular structure of native SPI as evidenced by identical protein band patterns in SDS-PAGE. Taken together, these results present electrospun SPI/PEO scaffolds as a promising potential product for skin wound healing applications from a material standpoint. Further investigation based on biological characterizations is detailed in the next chapters.

Chapter 4. *In Vitro* Biocompatibility of Electrospun SPI/PEO Scaffolds

4.1. Introduction

After developing an electrospun SPI/PEO scaffold with desirable physical and mechanical properties, we aimed to determine its suitability in biomedical applications by investigating its biocompatibility *in vitro*. Typically, scaffolds are tested in culture with the cell type of the organ the scaffold is intended for in its design. Since our intended application is skin regeneration, we used primary human dermal fibroblasts for cell culture studies. We investigated the attachment, spreading and proliferation of these fibroblasts on electrospun SPI/PEO and other substrates including zein, gelatin as a natural animal-derived protein for comparison, and PLGA as a well-characterized (Li et al., 2006; Blackwood et al., 2008) synthetic material for comparison. We also developed the first skin equivalent based on electrospun SPI/PEO.

4.2. Materials and Methods

4.2.1 *In vitro* biocompatibility

4.2.1.1. Cell culture: Primary human dermal fibroblasts (HDF) from neonatal foreskin (Clonetics, San Diego, CA) were cultured in T-75 culture flasks in DMEM with 4.5 g/L glucose supplemented with 10% FBS and 50 I.U./ml penicillin, 50 μg/ml streptomycin (complete medium, from Mediatech) and used at passages 18 to 20. Flasks were kept in humidified incubators at 37 ^{o}C and

5% CO_2; the culture medium was changed twice per week. At confluence, cells were detached from flasks by incubating in 0.25% trypsin/2.21 mM EDTA (Mediatech) for 5 min. Complete medium was added to allow the FBS to terminate the enzymatic action of trypsin. The cell suspension was centrifuged for 10 min at 800 rpm and the pellet was resuspended in fresh complete medium prior to counting the cells and seeding them onto scaffolds.

4.2.1.2. Seeding of fibroblasts onto scaffolds: Scaffolds were sterilized by immersion in a 1:10 dilution of antibiotic-antimycotic solution (ABAM, from Mediatech) in 1X PBS for 48 h, followed by immersion in a 1:50 dilution of ABAM for 24 h. Scaffolds were then washed thrice with 1X PBS without calcium and magnesium to remove traces of ABAM before transferring to 24-well plates using sterile forceps inside a laminar flow hood and securing with Viton O-rings (Cole-Parmer, Vernon Hills, IL) (Li et al., 2006; Han et al., 2011).

Fibroblasts were seeded at a density of 30,000 cells per well in 200 µl volumes onto scaffolds in triplicate in a 24-well plate. For each type of scaffold, one was kept with no cells as a blank, i.e. to compensate for any effect of scaffold material on the alamarBlue™ readings (see below, Section 4.2.1.3). Soy protein scaffolds were prepared from 5%, 6%, 7% and 8% SPI, each with 0.05% PEO; zein scaffolds were prepared at 35%, 40% and 45% (w/v) zein. Cells were also seeded

in triplicate onto scaffolds electrospun from 20% poly(lactic-*co*-glycolic acid) (PLGA) and 8% gelatin as synthetic and natural control materials respectively, and onto glass cover slips and directly into the well, as standard controls.

4.2.1.3. alamarBlue™ assay: Prior to seeding cells onto scaffolds electrospun onto 15 mm diameter glass coverslips and placed inside 24-well plates, fluorescence spectrophotometric reading was calibrated against cells grown at a range of densities from 1,000 – 500,000 cells per well on tissue culture polystyrene (TCPS) inside a 24-well plate to determine the appropriate seeding density for the experiment. This was determined to be 30,000 cells per well.

Cell proliferation was determined using the alamarBlue™ assay, as previously described (Nikolaychik et al., 1996; Li et al., 2005, 2006; Guo et al., 2007; Han et al., 2011). After allowing the cells to attach to the scaffolds for 1 h, complete medium with 10% (v/v) alamarBlue™ (BD Bioscience, Franklin Lakes, NJ) was added to each well to a total volume of 0.5 ml. Plates were incubated at 37℃, 5% CO_2 for 3 h before 200 µl supernatant from each well was transferred in duplicate to a 96-well plate. alamarBlue™ fluorescence was read on a Cytofluor fluorescence microplate reader (Perseptive Biosystems, Framingham, MA) (excitation λ=530 nm and emission λ= 580 nm). Medium was removed from the 24-well plate and replaced with fresh medium. On

days 2, 4, 6 and 8 of culture, 10% (v/v) alamarBlue™ was added to each well and incubated for 3 h before taking the fluorescence readings. Values were averaged for each condition and the corresponding blanks subtracted from the averages.

4.2.1.4. Visualization of cell morphology on scaffolds: The morphology of cells on the scaffolds was assessed by fluorescence microscopy and SEM, as previously described (Li et al., 2005, 2006; Han et al., 2011). For fluorescence microscopy, the specimens were fixed in 3.7% paraformaldehyde (Fisher) for 10 minutes, washed three times with 1X PBS, and stained with 4 μg/ml Hoechst 33258 (BBZ, bisBenzimide from Sigma) and 2 μg/ml TRITC-conjugated rhodamine phalloidin (phalloidin tetramethyl-rhodamine B isothiocyanate, from Sigma) in 1X PBS with 0.2% Triton-X100 (Sigma) for 15 min for staining nuclei and F-actin cytoskeleton, respectively. Samples were visualized in a Leica DMRX upright microscope equipped with the appropriate fluorescence filters. Digital images were acquired with a Leica DC 300FX camera. For SEM visualization, the samples were fixed with 2.5% glutaraldehyde in PBS for 1 h at 4 ℃, washed three times with 1X PBS, and dehydrated in a gradient of ethanol at 15%, 30%, 50%, 75%, 85%, 90%, 95% and 100%, as previously described (Li et al., 2005, 2006). Dehydrated samples were critical point dried and mounted onto stubs for SEM visualization.

4.2.2. Skin equivalent organotypic co-culture of fibroblasts and keratinocytes

4.2.2.1. Cell culture: Primary human dermal fibroblasts were cultured as described earlier. Primary human epidermal keratinocytes (NHEK) from neonatal foreskin (a generous gift from Dr. David Moscatello at the Coriell Institute, Camden, NJ) were cultured in progenitor cell targeted (PCT) medium (Millipore, Billerica, MA) in cell culture flasks coated with 0.67 μg/cm^2 collagen type IV from human placenta (Sigma). Keratinocyte cultures were weaned to defined keratinocyte serum-free medium (D-KSFM, Invitrogen, Carlsbad, CA) by switching to 75:25 PCT medium:D-KSFM, then 50:50, then 25:75 respectively with each medium change before switching completely to D-KSFM. D-KSFM included supplements of bovine pituitary extract (BPE) and epidermal growth factor (EGF). Upon confluence, keratinocytes were detached by first washing with 1X PBS and incubating with Versene (Invitrogen) for 3 min before incubating with a 1:5 dilution of trypsin/EDTA for 5 – 10 min at 37^{o}C and 5% CO_2. The trypsin was inactivated by adding an equal volume of 1 mg/ml soybean trypsin inhibitor (Amresco, Solon, OH). The suspension was centrifuged for 10 min at 800 rpm. Keratinocytes were used between passages 4 – 6.

4.2.2.2. Skin equivalent co-culture: Scaffolds electrospun from solutions of 7% SPI, 0.05% PEO in HFP were cut into rectangular pieces approximately 25 mm x 30 mm and sterilized using serial

dilutions of ABAM as described earlier. Scaffolds were then placed onto 3.0 µm cell culture inserts (BD Bioscience) in 6-well deep well plates (BD). Co-culture of fibroblasts and keratinocytes was performed following the protocol of Gangatirkar et al. (2007) with a few modifications adapted from the literature for electrospun scaffolds (Boehnke et al., 2007; Powell et al., 2008). Briefly, dermal fibroblasts were seeded onto SPI/PEO scaffolds at a density of 5 x 10^4 cells/cm^2 and kept submerged in DMEM + 10% FBS for 2 days. Epidermal keratinocytes were then seeded onto the fibroblast-populated scaffold at a density of 1 x 10^5 cells/cm^2 and kept submerged in a mixture of DMEM:Ham's F-12 medium with the appropriate supplements (per 500 ml, the following were added: 9.75 ml $NaHCO_3$, 0.4 ml hydrocortisone (500 µg/ml), 1 ml ITT (2.5 mg/ml insulin, 2.5 mg/ml transferrin, 1 x 10^{-8} M tri-iodothyronine), 1 ml EOP (50 mM ethanolamine, 50 mM phosphorylethanolamine), 1 ml adenine (90 mM), 1 ml selenium (2.65 nM), 0.25 ml gentamicin (50 mg/ml) and 0.25 ml amphotericin B, 1 ml $CaCl_2$ (0.94 M), 1.5 ml FBS, 1 ml progesterone (1 µM)) for 1 week during its epidermalization phase before lifting the culture onto an air-liquid interface on a transwell. The culture was kept at the air-liquid interface for a further 2 weeks while it cornified and was maintained in this mature state. Modifications included a shortened pre-cultivation time of the dermal component before seeding the keratinocytes, based on thorough observations by Boehnke et al. (2007) that pre-cultivation of dermal fibroblasts in a fleecy, non-woven hyaluronic acid-based scaffold Hyalograft® for 7 days

did not result in better stratification of mature epidermis than pre-cultivation in the same scaffold for just 2 days.

4.2.2.3. Histological observation of skin equivalents: At days 7 and 14 of co-culture, scaffolds were cut into strips and fixed in 10% buffered formalin (Fisher) before embedding in paraffin blocks. Samples were cut into sections 4 – 7 µm thick using a Leica RM2255 microtome (Leica Microsystems GmbH, Wetzlar, Germany) and collected onto glass coverslips coated with poly-L-lysine (Sigma). These sections were rehydrated in a gradient of xylene (EMD Chemicals, Gibbstown, NJ) and ethanol (EMD) and stained with hematoxylin (EMD) and eosin (EMD). Stained sections were visualized using a Leica DMRX upright microscope and digital images were acquired with a Leica DC 300FX camera.

4.3. Results and Discussion

4.3.1. Electrospun SPI/PEO scaffolds support the attachment, growth and proliferation of primary human dermal fibroblasts

4.3.1.1. Proliferation of primary human dermal fibroblasts on electrospun SPI/PEO and other substrates: Primary human dermal fibroblasts were seeded onto electrospun SPI/PEO and zein scaffolds and cultured for 8 days until confluence. For comparison, the same cells were also

seeded on electrospun gelatin and PLGA scaffolds, as well as glass and tissue culture treated polystyrene (TCPS) surfaces as non-electrospun, standard controls. Fibroblasts cultured on various substrates proliferated steadily over 8 days to confluence. As shown in Figure 4.1, cells on all substrates showed approximately 2- to 5.5-fold alamarBlue™ fluorescence by day 4 compared to day 0, and approximately 3- to 7.5-fold by day 8 compared to day 0. While cells on all substrates followed a similar trend of increasing alamarBlue™ fluorescence indicative of proliferation over the 8 days in culture, the cells on the scaffolds tested demonstrated a trend towards higher normalized fluorescence values than the “gold standard”, TCPS. The somewhat higher AB fluorescence of cells on the electrospun scaffolds might indicate that the 3-D structure and porosity of the scaffolds might favor the formation of multilayered cell assemblies.

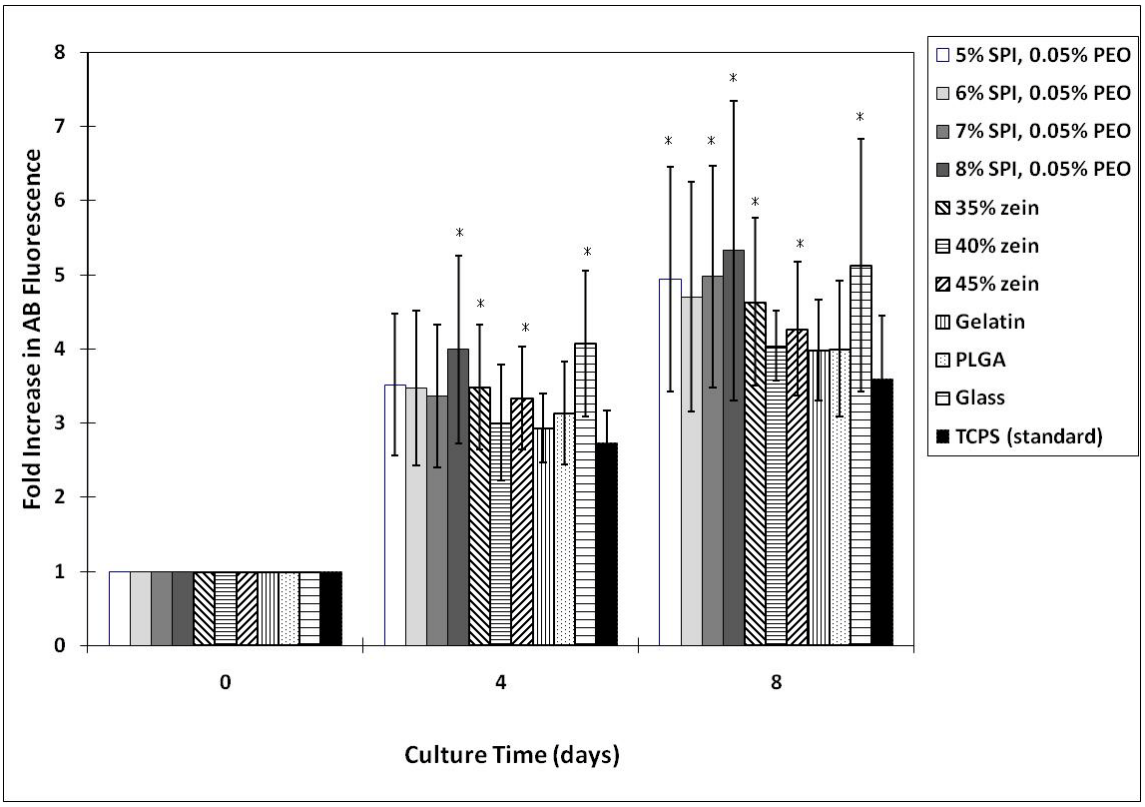

Figure 4.1. Increase in alamarBlue™ fluorescence with time normalized to fluorescence readings on day 0. Asterisks indicate statistically significant ($p<0.05$) increase compared to TCPS for each timepoint (n = 3).

4.3.1.2. Fibroblasts exhibit cytotypic morphology and spreading behavior on electrospun SPI/PEO: At confluence, fluorescent staining for filamentous actin (F-actin) cytoskeleton revealed similar cytotypic elongated "fibroblast-like" morphologies on all scaffolds (Figure 4.2). No differences were seen in the morphology of cells cultured on scaffolds electrospun from different concentrations of SPI/PEO (Fig. 4.2 a, b) and zein (Fig. 4.2c), or between the two "green" materials. Inspection of the cultures by SEM showed that the cells fully spread over the scaffolds,

expressed lamellipodia and secreted their native extracellular matrix (Figure 4.3).

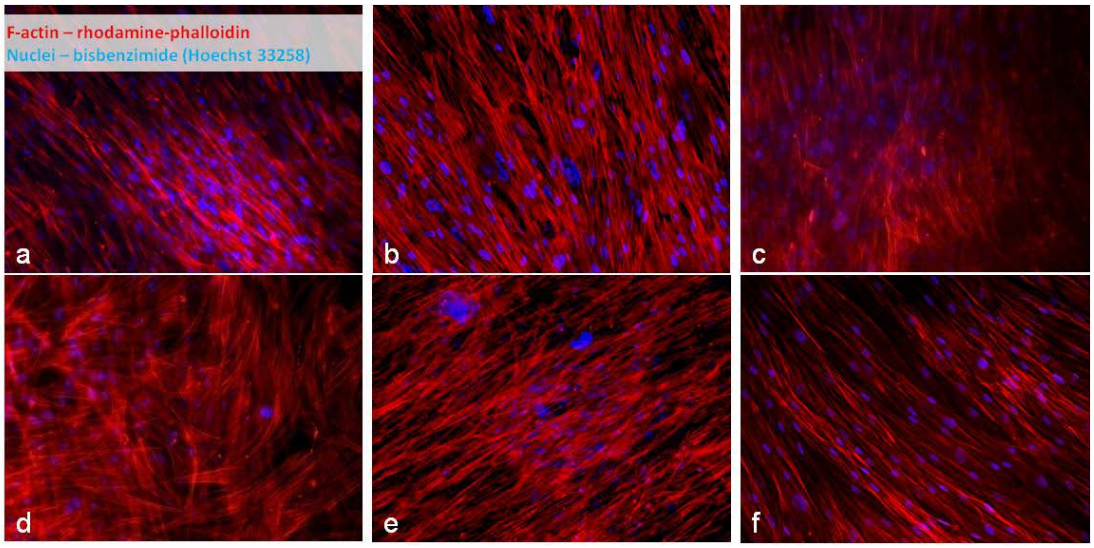

Figure 4.2. Human dermal fibroblasts grew to confluence on Day 8 of culture on various scaffolds. a) 5% SPI, 0.05% PEO; b) 8% SPI, 0.05% PEO; c) 40% zein; d) gelatin; e) PLGA; f) glass. (Nuclei, blue; F-actin cytoskeleton, red; original magnifications 200x).

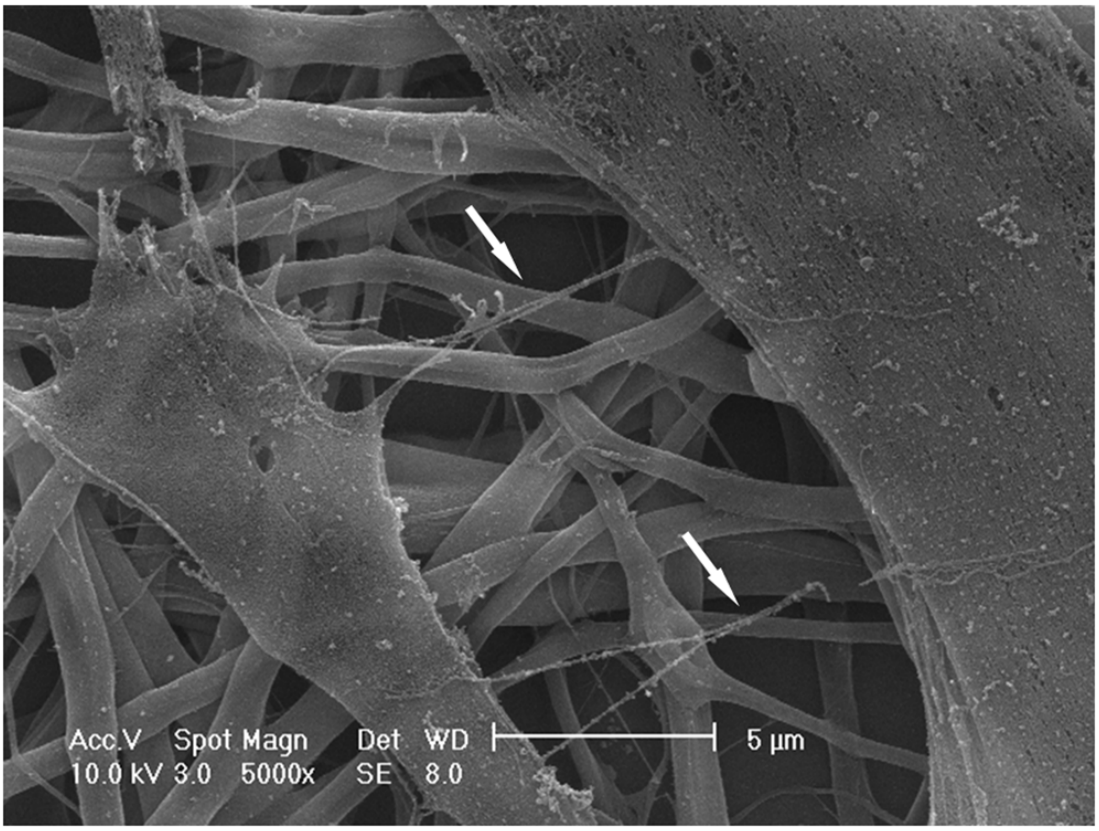

Figure 4.3. Scanning electron micrograph of primary human dermal fibroblasts cultured on electrospun SPI/PEO on Day 8. Fibers are intact and fibroblasts have secreted native extracellular matrix (arrows) on the scaffold. Scale bar 5 µm.

The biocompatibility of SPI fibers, formed by wet spinning, has recently been demonstrated by Reddy and Yang (2009) from the University of Nebraska using NIH-3T3 mouse fibroblasts. Their fibers ranged from 50 to 150 µm in diameter, thus many cells spread over a single fiber, and proliferated until confluence. As a biomaterial, the effects of SPI as a biofilm were investigated on normal human fibroblasts and keratinocytes separately (Curt et al., 2009). Both cell types showed cytotypic morphology and proliferation, although fibroblasts were more affected than

keratinocytes by the formaldehyde used to cross-link the films, with reduced proliferation as formaldehyde concentration increased from 1% to 3%. SPI biofilms promoted the up-regulation of interleukin-6 (IL-6) and IL-8 mRNA expression in fibroblasts and tumor necrosis factor alpha (TNFα) mRNA expression in keratinocytes after 4 days of culture.

Yang's group at the University of Nebraska also electrospun zein nanofibers and cross-linked them using citric acid in order to enhance their water stability (Jiang et al., 2010). They demonstrated the cytocompatibility of these scaffolds with NIH-3T3 cells. They also observed that cross-linked zein scaffolds promoted up to 7-fold greater cell attachment and approximately 4- to 7-fold greater cell proliferation than uncross-linked electrospun zein scaffolds. This difference in cell behavior was attributed to the greater stiffness of the cross-linked scaffolds, as will be discussed in more detail.

Lowery et al. (2010) used electrospun poly(ε-caprolactone) (PCL) fibrous mats of varying fiber diameters and pore sizes to elucidate a balance between cellular infiltration and ECM deposition between fibers. In general, with bead-free continuous fibers, pore size increases linearly with fiber diameter. In their study, pore sizes were varied from approximately 1 to 40 μm while fiber diameters were kept within a similar range of nanometers, 2 μm or 8 μm. By co-electrospinning

PCL with PEO of different molecular weights and then removing the PEO by immersing the scaffolds in water for 7 days, they were able to reduce pore sizes by 50 to 80% while shrinking the fiber diameters only by 10 to 25%. Although larger pores and larger fibers encouraged greater proliferation of primary human dermal fibroblasts, ECM deposition by these cells was delayed on scaffolds with large pores, compared to almost immediate on scaffolds with pore sizes less than 15 µm. This reflects their preference for infiltration rather than growing on the surface of scaffolds with large gaps between fibers.

Fibroblasts are a suitable cell type for scaffold biocompatibility studies not only because they are the main dermal cell type in our case, but also because they are robust and therefore not as sensitive to general culture conditions when the scaffold is the variable of interest. van Aalst et al. (2008) electrospun primary human dermal fibroblasts and human adipose-derived stem cells with a solution of polyvinyl alcohol (PVA) to incorporate the cells into the nanofibers, and found that both cell types retained their viability (approximately 30 – 65% for fibroblasts and 22% for stem cells). The PVA nanofibers were then solubilized and the cells cultured until confluence. However, while fibroblasts were able to proliferate, the adult stem cells were not. As a control group, the same cells were electrosprayed rather than electrospun to account for the effects of mechanical stress and burst force alone. Fibroblasts also did not proliferate under this condition.

In a study by Milleret et al. (2009) investigating the cyto- and hemocompatibility of Degrapol fibers, mouse embryonic fibroblasts (NIH-3T3) or human umbilical vein endothelial cells (HUVECs) were cultured on Degrapol® fleeces (mats) and their proliferation compared to that of the same cells cultured on PLGA or Degrapol fleeces that were pre-adsorbed with fibronectin or collagen I. After 8 days, NIH-3T3 cultured on Degrapol proliferated less than those on PLGA, comparably to those on Degrapol pre-adsorbed with collagen I, and more than those on Degrapol pre-adsorbed with fibronectin. However, NIH-3T3 showed the highest proliferation when cultured on glass. HUVECs, on the other hand, did not proliferate on Degrapol and barely proliferated on PLGA, but responded similarly well to fibronectin- or collagen-adsorbed surfaces and glass. This again illustrates how fibroblasts adhere to foreign substrates more readily than certain other cell types.

Scaffold or substrate stiffness has been shown to moderate fibroblast proliferation (Hadjipanayi et al., 2009; Jiang et al., 2010) in 2-D culture, with fibroblasts proliferating more on stiffer matrices that induce them to produce greater contractile forces corresponding to wound healing by granulation tissue. Cells growing on stiffer substrates produce more actin stress fibers and spread more than they do on softer substrates. We see this when comparing the morphology of

fibroblasts on gelatin (Figure 4.2d) compared to glass (Figure 4.2f). Fibroblasts show the most pronounced actin fibers and stretching, as well as aligning to each other, on glass. On gelatin, the softest of the substrates compared, fibroblast alignment appears the least directional.

Fernández et al. (2006) modeled the spreading fibroblast (using NIH-3T3s in deformation experiments) as a nonlinear gel, with viscoelastic behavior. They show that regardless of whether the cell is generating force due to actin filament contraction or experiencing force due to external stretching, the viscoelastic moduli of cells are solely dependent on this force and not on changes in length during stretching. In addition, fibroblasts exhibit “stress stiffening” and may reorganize their cytoskeleton, rearranging connection points inside the cytoskeletal network. Solon et al. (2007) interpret that cells do not have a pre-defined stiffness, as they will alter their internal stiffness depending on the stiffness of their substrate, thus regulating their morphology and motility. Cells also tend to migrate from areas of lesser stiffness to areas of greater stiffness, a phenomenon known as durotaxis, as modeled by Lazopoulos and Stamenović (2008) for two-dimensional cultures. Here, actin stress fibers are represented as pre-stressed elastic line elements, that transmit tension to the substrate via focal adhesions. Stress fibers stiffen with increasing tension. Since stiffness is inversely proportional to strain, assuming pre-stress is constant, then at the boundary between a softer substrate and a stiffer substrate, a fibroblast

will receive feedback from its lamellipodia that the strain in the part of the cell that is on the stiffer substrate is smaller than the strain in the part that is on the softer substrate. Thus, the total potential energy of the stress fiber is less than it originally was when the whole cell was on the softer substrate, and stability criteria dictate that the system is at equilibrium when total potential energy is at a global minimum. This shift in potential energy continues as the cell migrates (perceiving greater stability as a greater area of the cell senses decreased strain), until eventually the whole cell has moved to the stiffer substrate (Lazopoulos and Stamenović, 2008).

In our case, substrates are assumed not to confer any directional strain, and fibroblasts are seen to align mostly to each other (Figure 4.2). This is coherent with the work of Bischofs and Schwarz (2003), who explain the observation that "cells orient themselves in the direction of maximal stiffness of the environment" with the theory that cells optimize their interaction with their environment for force pattern that minimizes the work required from the cell in order to achieve a certain force at the contact. Considering the extracellular environment as isotropic and linearly elastic, they propose that since the cell probes its environment using many contacts simultaneously (Figure 4.4, Bischofs and Schwarz, 2003), if stiffness at certain contacts in one direction is larger than at the other contacts, the cell will orient in that direction in order to minimize the work required to generate the same force at each contact.

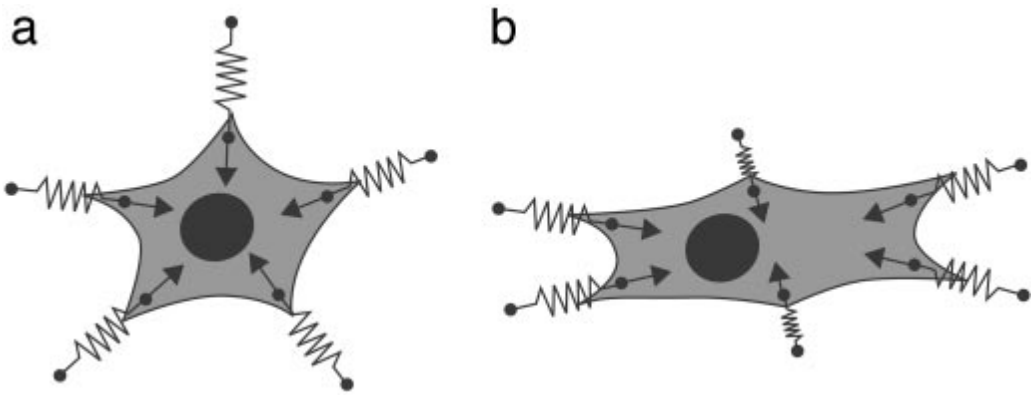

Figure 4.4. Model of an adherent cell spreading on an isotropic (a) and an anisotropic (b) substrate. The cell-substrate contacts are represented by linearly elastic springs with different spring constants. From Bischofs and Schwarz (2003).

As in our case, and with electrospun scaffolds with random fibers in general, alignment cues are not characteristic of the scaffold but rather generated by the cells themselves. Bischofs and Schwarz (2003) also address the observation that cells align to each other by attributing it to how “the mechanical activity of one cell triggers the activity of the other cell, thereby forming a positive feedback loop”. When a single cell orients itself to a fiber underneath it, it develops a traction that then serves as a cue to adjacent cells that may not have adhered as tightly, creating anisotropic strain fields in an otherwise isotropic topography. We see morphological evidence of this as well, with fibroblasts probing in different directions when cultured on an electrospun SPI/PEO scaffold on Day 2 (Figure 4.5a), aligning to each other as they form cell-cell contacts and becoming uniformly aligned by confluence at Day 8 (Figure 4.5b).

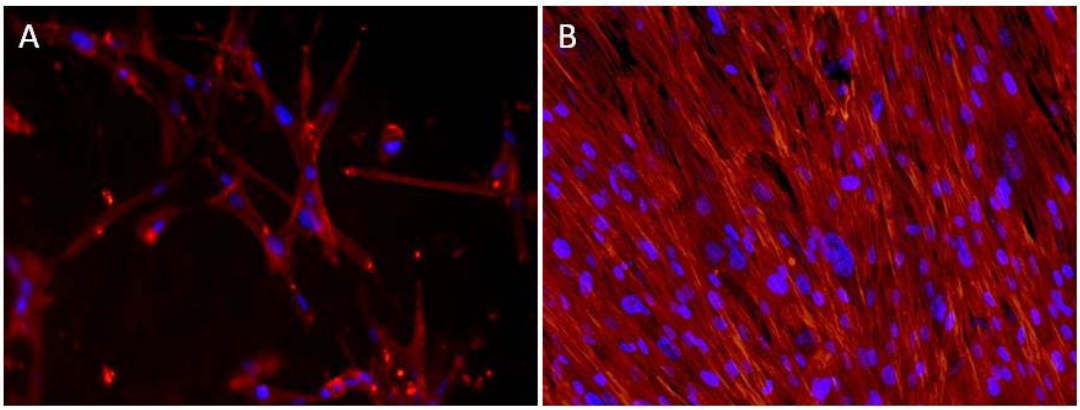

Figure 4.5. Primary human dermal fibroblasts cultured on electrospun SPI/PEO scaffold on Day 2 (a) and Day 8 (b). At Day 2, fibroblasts have not defined their alignment and are still probing in random directions. By confluence at Day 8, they have aligned fully to each other. (Nuclei, blue; F-actin cytoskeleton, red. Original magnifications 200x.)

By contrast to 2-D, in 3-D culture, cells have been shown to proliferate better in less stiff matrices. Bott et al. (2010) cultured human dermal fibroblasts in collagen or poly(ethylene glycol) (PEG) hydrogels with elastic shear moduli (G') varying from approximately 240 to 1200 Pa, and saw DNA fold change to be approximately 6-fold vs. 2-fold respectively. In 3-D, cells face physical barriers in every direction, which prevent migration. In PEG gels that were designed to be cleavable by matrix metalloproteases (MMPs), proliferation was much higher (~6-fold vs. 3-fold) in gels with G' = 241 Pa, less so (~3-fold vs. 2-fold) in gels with G' = 637 Pa, and similar in gels with G' = 1201 Pa. This highlights the role of MMPs in matrix remodeling, discussed further in Chapter 5, but also the limit of their influence on cell proliferation in high stiffness 3-D matrices.

4.3.2. Electrospun SPI/PEO scaffolds support the histotypic co-culture of primary human dermal fibroblasts and primary human epidermal keratinocytes

Following the protocol of Gangatirkar et al. (2007) for skin equivalent co-culture with modifications to shorten the pre-cultivation time of the dermal component based on observations by Boehnke et al. (2007), we developed a skin equivalent based on electrospun SPI/PEO scaffolds (Figure 4.6). These constructs remained stable for up to 28 days in culture at an air-liquid interface.

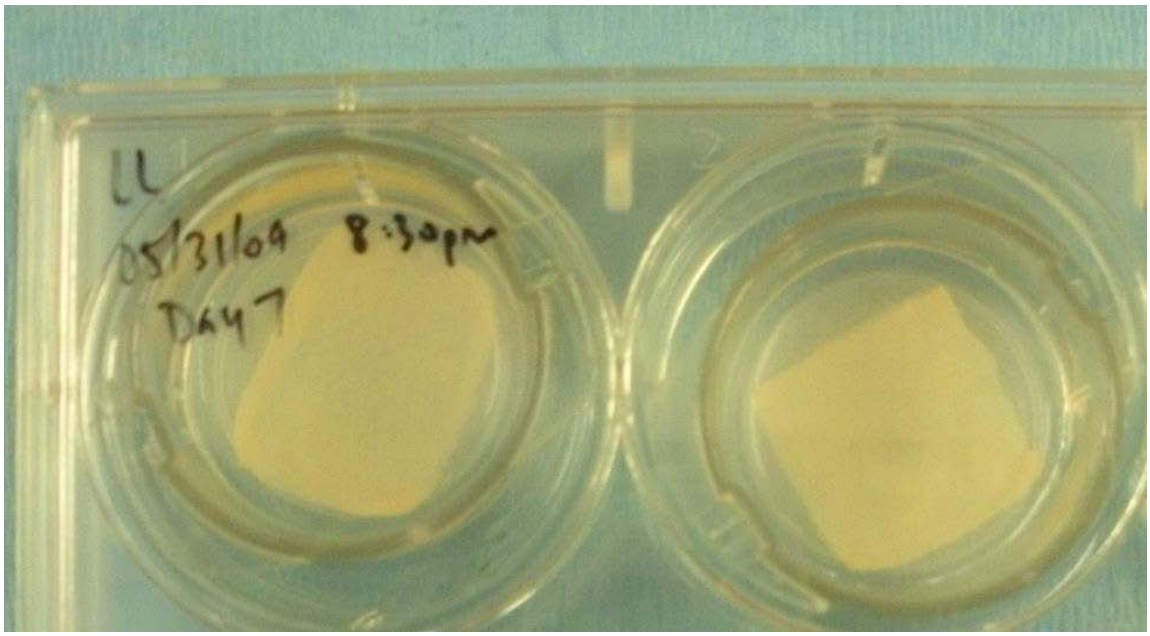

Figure 4.6. Electrospun SPI/PEO scaffold-based skin equivalents at Day 7 of fibroblast/keratinocyte co-culture. Samples shown are being fixed in 10% formalin in a 6-well plate prior to embedding for histological analysis.

At Day 7 of co-culture, cells are covering the surface of the SPI/PEO scaffold and stratification can be seen, although cell types are indistinguishable by routine histology with hematoxylin and eosin staining (Figure 4.7a). By Day 14, the layers are more discernible (Figure 4.7b). The cells remain on the surface of the scaffold without infiltrating. Although in-depth characterization of the fibroblasts and keratinocytes in this construct is beyond the scope of this thesis, we have shown that our SPI/PEO scaffold is suitable as a base for skin equivalent co-culture. This carries implications for future wound healing applications as well as for new *in vitro* skin equivalent models.

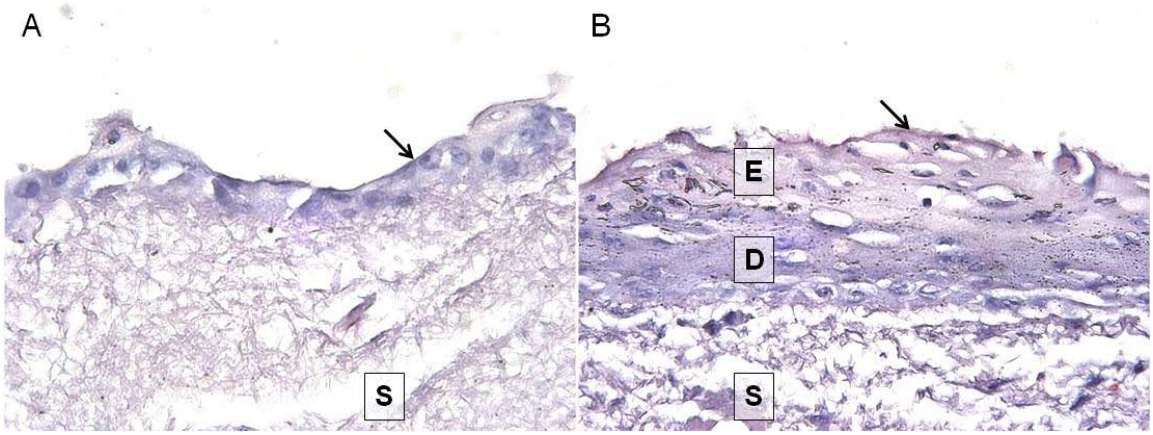

Figure 4.7. Tissue engineered skin equivalent based on the SPI/PEO scaffold. Human dermal fibroblasts (D) and epidermal keratinocytes (E) were co-cultured on multi-layered electrospun SPI/PEO scaffolds (S), following the procedure of Gangatirkar et al., 2007. The epidermal stratification at the air-liquid interface is clearly visible (arrows) on Day 7 (a) and Day 14 (b). H&E stained histological section, original magnifications 200x.

The original model for organotypic skin co-culture consisted of a collagen gel embedded with fibroblasts, allowed to contract (Bell et al., 1979) and then seeded with epidermal cells that differentiate and keratinize on the dermal construct (Bell et al., 1981). These grafts were cultured from rat cells *ex vivo* and re-implanted into the rat donors, and shown to incorporate well, inhibit wound contraction and become well vascularized in the host. Bell et al. determined that the pre-contraction of the dermal construct was a pre-requisite to graft acceptance. They founded Organogenesis Inc., Canton, MA in 1985 to market this technology as Apligraf®, which was approved by the Food and Drug Administration (FDA) for the treatment of venous ulcers in 2000.

The collagen gel model, while useful, had many limitations such as poor mechanical stability and early degeneration, and the tendency to contract made the dimensions harder to control. To better mimic the structure of native ECM and provide more matching mechanical properties to the tissue, fibrous materials were later also used to create skin equivalents.

Stark et al. (2006) cultured skin equivalents using nonwoven esterified hyaluronic acid fibers (Hyalograft-3D) by first creating a dermal construct with human dermal fibroblasts in fibrin gel seeded into the fleece, then seeding keratinocytes onto the dermal construct after one week

and then exposing the surface to an air-liquid interface one day later. They found that these skin equivalent co-cultures achieved many characteristics of tissue homeostasis, specifically maturation of the dermal component including basement membrane (BM) structures, polarization of BM components, and enhanced deposition of collagen VII in the BM by 3 weeks. Faster epidermal regeneration and better organized epidermal architecture, with polarization of keratinocytes at 2 and 3 weeks of culture, was observed on fibrous dermal constructs compared to collagen gel dermal constructs. The uppermost, cornified keratinocyte layer, the *stratum corneum*, continued to thicken over 12 weeks. Expression of the differentiation-specific keratin marker K10 indicated that it was still differentiating as well as proliferating. Tissue homeostasis was also evidenced by the co-expression of keratins K10 and K1, both early differentiation markers, and the downregulation of K16 over time, since K16 is expressed during skin wound regeneration but not in healthy epidermis.

While the structure of the dermal equivalent appears to impact the “organotypic” success of the co-culture, the material does not seem to be a key factor in the organization of the cellular components in a scaffold-based skin equivalent. Sun et al. (2005) used electrospun polystyrene (PS) to demonstrate that even without biochemical cues, cells could organize themselves according to their organotypic assembly. They co-cultured fibroblasts, keratinocytes and

endothelial cells together in one single suspension onto electrospun PS fibers of approximately 10 μm width—the diameter of a single cell—and exposed the surface to an air-liquid interface 18 h after seeding. By 2 weeks, the endothelial cells and fibroblasts had infiltrated the fibers, while the keratinocytes formed a thick top layer. This spatial assembly was attributed to the air-liquid interface.

Fibroblasts, by virtue of regulating keratinocyte proliferation and migration, as well as secretion of the ECM required for skin regeneration, appear to dictate the outcome of the skin equivalent. Boehnke et al. (2007) attempted to quantify the minimum amount of fibroblasts required to form a continuous, stable skin equivalent, as well as the optimal time between fibroblast and keratinocyte seeding. Using Hyalograft-3D as the scaffold base, they investigated fibroblast seeding densities of $5 \times 10^3/cm^2$, $5 \times 10^4/cm^2$ and the "standard" $2 \times 10^5/cm^2$ for 3×10^5 keratinocytes/cm^2. Skin equivalents attempted with no fibroblasts showed "poorly differentiated atrophic epithelium". The lowest amount of fibroblasts investigated, 5×10^3 cells/cm^2, allowed for a well-developed epithelium as well as expression of collagen VII and integrin β4 marking a dermo-epidermal junction—however, these features did not as fully resemble the *in vivo* structure as they did when 5×10^4 fibroblasts/cm^2 was used. They determined 5×10^4 fibroblasts/cm^2 to be optimal, yielding tissue quality equal to that formed with the higher

density. These skin equivalents were stable for at least 12 weeks in culture, with no shrinkage observed.

In terms of precultivation time for dermal equivalents, 2 days was found to be as effective as the standard 7 days for epidermal regeneration and differentiation as marked by expression of keratins K1 and K10, distribution of collagen IV and linear deposition of collagen VII in the BM. Surprisingly, a 14-day precultivation period yielded underdevelopment in both epidermal and dermal components, which was attributed to proteolytic degradation by fibroblasts in the absence of epithelial-mesenchymal interactions with keratinocytes (Boehnke et al., 2007).

Rnjak et al. (2009) investigated the interactions of primary human dermal fibroblasts with electrospun tropoelastin scaffolds, specifically the effects of fiber diameter and consequently spaces between fibers on fibroblast attachment, spreading, proliferation and infiltration. The cross-linked fibers varied from 3.4 ± 0.8 μm for denser scaffolds to 3.6 ± 0.8 μm and 5.5 ± 1.6 μm for more “open-weave” scaffolds, and correspondingly, fibroblasts infiltrated more through the scaffolds as fiber diameter and inter-fiber spacing increased.

In our case, fibroblasts did not infiltrate the SPI/PEO scaffolds, but spread across the surface and

deposited their own ECM (Figure 4.3). Although this is not undesirable for *in vitro* skin equivalents, it may be beneficial for this or other applications to have cells evenly distributed throughout the scaffold to provide signaling factors. To achieve this for electrospun scaffolds, Yang et al. (2009) developed a novel approach using layer-by-layer deposition of electrospun fibers and cells. PCL/collagen nanofibers with average diameter 454.5 ± 84.9 nm were electrospun onto the grounded surface of cell culture medium in a vertical setup, and human dermal fibroblasts were seeded onto this layer of nanofibers. The next layer was then electrospun directly onto the cell layer after draining the medium, and fibroblasts deposited again. This process was repeated until the desired constructs were formed—10 layers of alternating fibroblasts and fibers for a dermal equivalent or 18 layers of fibroblasts and fibers plus 2 layers of keratinocytes and fibers for a full skin equivalent. Encouragingly, they also used HFP as their solvent and showed that even with electrospinning directly into the medium, no significant cytotoxicity was found even when the medium was collected and tested specifically for such.

As fibroblasts attached and elongated along the separate layers, the constructs became more compact and layers became visually indistinguishable by 7 days of culture. The dermal constructs also continued to contract over 14 days, more than 40%, while bilayer constructs contracted

approximately 20% between days 3 and 7 but no further between days 7 and 14. For the bilayer construct, the keratinocyte layers were also seeded onto the fibroblast layers without precultivation of the latter (Yang et al., 2009).

4.4 Conclusions

We have shown that electrospun SPI/PEO scaffolds support the attachment, spreading and proliferation of human dermal fibroblasts comparably to other natural and synthetic electrospun materials. Fibroblasts appeared to receive directional cues from each other rather than from the scaffold, as evidenced by aligning to each other on a randomly oriented scaffold. Fibroblasts did not infiltrate the scaffold, but spread over the surface and deposited their native ECM. Not only has the SPI/PEO scaffold been shown to be biocompatible with fibroblasts, it also supports the co-culture of fibroblasts with epidermal keratinocytes in a histotypic skin equivalent model. The next chapter investigates some of the possible mechanistic interactions of the fibroblasts with the SPI/PEO scaffold.

Chapter 5. Interactions of Human Dermal Fibroblasts with SPI Substrates

5.1. Introduction

Mammalian cells attach to natural substrates (e.g. extracellular matrix proteins) mainly via a class of transmembrane receptors called integrins (Ingber, 1991; Assoian and Klein, 2008). Specifically, human dermal fibroblasts use α2β1 to bind collagens, αvβ3 and αvβ5 for vitronectin, and at least αvβ1, α4β1, α5β1, and αvβ3 for fibronectin; αvβ3 also binds fibrinogen (Noszczyk et al., 2002). These integrin-ligand interactions play a key role in contraction during wound healing (Sethi et al., 2002). In human wound explants, α2, αv and β1 were upregulated early (6 – 7 days) after dermal injury, in the area of dermal scar formation (Noszczyk et al., 2002). Integrin α1β1, involved in negative feedback regulation of collagen synthesis, has been shown to be more highly expressed in fibroblasts explanted from keloids and hypertrophic scars than normal human skin (Szulgit et al., 2002).

Although cell-matrix interactions have been well characterized in different cell types with their native ECM components, little is known about how human or animal cells interact with foreign materials. Initial adhesion appears to depend on electrostatic interactions and wettability of the surfaces (van der Valk et al., 1983). In order to elucidate possible roles of integrins in adhesion to foreign substrates, several studies have been done by blocking specific integrin subunits and

measuring the reduction in number of adhered cells. The adhesion of human osteoblasts to PLGA copolymers 2 h after plating was reduced by approximately 70% when β1 and α5β1 complexes were selectively blocked (Di Toro et al., 2004). By contrast, adhesion was reduced by only approximately 30% when integrin αv was blocked. Even the same materials with different surface treatments can induce differential integrin receptor expression by cells. Human nasal chondrocytes were shown to preferentially express αvβ3 vitronectin (VN) and α5β1 fibronectin (FN) receptors on gas plasma treated films of high molecular weight (1000 g/mol) PEG with 70/30 poly(ethylene glycol)-terephthalate/poly(butylene terephthalate) (PEGT/PBT), compared to the same films without gas plasma treatment (Woodfield et al., 2006). Likewise, a lower molecular weight PEG (300 g/mol) with 55/45 PEGT/PBT also promoted greater cell adhesion and expression of αvβ3 and α5β1 both with and without gas plasma treatment.

Siebers et al. (2008) investigated the effect of blocking β1 and β3 integrins on primary rat osteoblast-like cells from bone marrow, cultured on calcium phosphate (CaP)-coated and non coated titanium (Ti). On non coated Ti, pre-treatment with anti-integrin β1 antibodies did not affect initial attachment. However, pre-treatment with anti-integrin β3 resulted in approximately 30% decrease in adhesion after 30 and 60 min ($p<0.05$). On CaP coated substrates, blocking β1 did have an effect, decreasing attachment by approx. 30% after 30 min ($p<0.05$), and 20-30%

after 60 and 240 min and after 1 day ($p<0.05$). Blocking β3 decreased attachment by approx. 40-50% after 30 min ($p<0.01$), 60 and 240 min ($p<0.05$), 1 day ($p<0.01$), and 3 days ($p<0.05$). Interestingly, on both substrates, pre-treatment with either anti-integrin β1 or anti-integrin β3 increased mRNA expression of integrin β1. Conversely, pre-treatment with either antibody resulted in decreased mRNA expression of integrin β3 in one run and increased expression in another run after 3 days of culture on non coated Ti substrates. On CaP coated substrates, pre-treatment with either antibody decreased the mRNA expression of integrin β3. Taken together, the attachment of osteoblast-like cells onto CaP coated substrates was attributed to β1 integrin (Siebers et al., 2008).

The study by Siebers et al. (2008), like ours, was done in serum-free medium. However, Chastain et al. (2006) have shown that the initial adhesion of mesenchymal stem cells to synthetic polymers poly(caprolactone) (PCL) and poly(lactic-co-glycolic acid) (PLGA) are differentially mediated by the ECM proteins vitronectin and type I collagen respectively, derived from the serum in the cell culture medium. This supports the hypothesis that cells attach to tissue engineered scaffolds by binding to the proteins that have adsorbed onto the surfaces from the serum. Since these ECM proteins can differentially adsorb onto different substrates, the adhesion of cells will also vary by substrate as an indirect effect of this.

Based on the hypothesis that initial adhesion of human dermal fibroblasts to SPI/PEO substrates is at least partially mediated by integrins and/or other specific cell adhesion molecules, we profiled the expression of genes related to human extracellular matrix (ECM) and adhesion molecules using targeted PCR arrays from SABiosciences (now QIAGEN), when fibroblasts were cultured on SPI or collagen I substrates. We then targeted the expression of individual genes shown to be upregulated or highly expressed on these substrates.

5.2. Materials and Methods

5.2.1. Real-time reverse transcriptase polymerase chain reaction (RT-PCR) analysis of fibroblast-scaffold interactions

In preliminary experiments, individual integrins were targeted based on the body of available literature describing the subunits associated with human dermal fibroblast adhesion in the context of adhesion to ECM, or wound healing, as mentioned in Section 5.1.

5.2.1.1. Substrates for initial PCR experiments: Solutions of SPI/PEO were prepared as for electrospinning and diluted in HFP to a final concentration of 0.1% (w/v) SPI with 0.001% (w/v) PEO. Glass coverslips, 15 mm in diameter, were coated with this diluted solution by dropwise

pipetting and allowing the solvent to evaporate in a fume hood overnight. These substrates were then sterilized by UV exposure for 30 min, transferred into a 24-well plate and immersed in 500 µl of 1X PBS without calcium and magnesium to equilibrate pH. For comparison, 0.1% PLGA, human dermal fibronectin, collagen type I from rat tail, and bovine gelatin substrates were also used. PLGA substrates were prepared in the same way as SPI substrates. For fibronectin (Sigma), collagen (BD Bioscience) and gelatin (Sigma) substrates, 200 µl of a 10 µg/ml solution of each of these natural proteins was pipetted dropwise into triplicate wells of the same 24-well plate and allowed to bind for at least 30 min in a humidified incubator at 37°C and 5% CO_2. All wells were aspirated and washed twice with 1X PBS prior to cell seeding.

5.2.1.2. RNA isolation for initial PCR experiments: Primary human dermal fibroblasts were seeded onto coated substrates in triplicate wells at a density of approximately 20,000 cells per well in serum-free DMEM. Cells were also seeded onto uncoated glass coverslips and TCPS (bare wells) as controls. At 1 h post-seeding, the medium was removed and the cells were washed twice with ice-cold 1X PBS with calcium and magnesium and lysed with TRIzol LS reagent (Invitrogen) for RNA isolation using the phenol-chloroform method. Briefly, 0.2 ml of chloroform per 1 ml of TRIzol was added to separate the aqueous and organic phases of the mixture. 0.5 ml of isopropyl alcohol per 1 ml of TRIzol was then added to the aqueous phase to precipitate the

RNA. RNA was purified by centrifuging through RNase-free spin filters (Mo Bio, Carlsbad, CA) and washing with 70% ethanol (200 proof, Spectrum, New Brunswick, NJ) twice before removing excess ethanol residue by further centrifugation and reconstituting in nuclease-free water (Ambion, Austin, TX).

5.2.1.3. RNA quantification: RNA concentration was determined using a NanoDrop ND-1000 spectrophotometer (Thermo Scientific, West Palm Beach, FL) spectrophotometer and ND-1000v3.2.1 software. 2 µl of reconstituted RNA was pipetted onto the Nanodrop and measured. Nuclease-free water was used as a blank. RNA samples with a ratio of absorbance at 260 nm to absorbance at 280 nm (260/280 ratio) between 1.7 and 2.0, indicating absence of genomic contamination, were deemed sufficiently pure to use in experiments.

5.2.1.4. cDNA synthesis: Complementary DNA (cDNA) was synthesized from purified RNA using the High Capacity cDNA Reverse Transcription Kit (Applied Biosystems, Carlsbad, CA). Mixtures of RNA and cocktail in 0.2 ml thin-walled microcentrifuge tubes (Ambion) were subjected to a thermal denaturation and annealing process of 94°C for 5 min followed by 25 cycles of 94°C for 30s, 55°C for 30s, and 72°C for 30s, ending with 72°C for 7 min and cooling to 4°C. Thermal cycling was performed in a GeneAmp® PCR System 9700 (Applied Biosystems).

5.2.1.5. PCR: PCR was performed on a StepOne™ Real-Time PCR System (Applied Biosystems) using the TaqMan® Fast Universal PCR Master Mix (Applied Biosystems) and inventoried TaqMan® primers for human integrins α1 (Hs00235030_m1; NCBI reference sequence NM_181501.1), α2 (Hs00158127_m1; NM_002203.3), α5 (Hs01547673_m1; NM_002205.2), αv (Hs00233808_m1; NM_002210.3), β1 (Hs00236976_m1; NM_002211.3) and β3 (Hs00183924_m1; NM_014288.3) (Applied Biosystems). Human peptidyl-prolyl cis-trans isomerase A (PPIA) (Hs99999904_m1; NM_021130.3) was used as the endogenous control. Samples were subjected to a "fast" thermal cycle of 95 ◦ C for 20 s followed by 40 cycles of 95 ◦ C for 1s and then 60 ◦ C for 20 s. Results were generated with StepOne software v2.0. Gene expression values for each substrate were normalized to values for glass (as controls for SPI- and PLGA-coated glass substrates) or TCPS (as controls for natural proteins coated on bare wells).

5.2.1.6. Substrates for PCR array analysis: Solutions of SPI/PEO were prepared as for electrospinning and then diluted in HFP to a final concentration of 0.1% (w/v) SPI with 0.001% (w/v) PEO for the purposes of coating. Glass cover slips, 15 mm in diameter, were coated with this diluted solution by drop-wise pipetting and allowing the solvent to evaporate in a fume hood overnight. These substrates were then sterilized by UV exposure for 30 min, transferred

into a 24-well plate and immersed in 500 µl of 1X PBS to equilibrate pH. For collagen substrates, 200 µl of a 10 µg/ml solution of collagen type I from rat tail (BD Bioscience) was pipetted drop-wise into each well of the same 24-well plate containing sterile glass cover slips and allowed to bind for 30 min in a humidified incubator at 37°C and 5% CO_2. All wells were aspirated and washed twice with 1X PBS prior to cell seeding.

5.2.1.7. RNA isolation for PCR array analysis: Primary human dermal fibroblasts were seeded onto coated substrates in triplicate wells of 24-well plates at a density of approximately 150,000 cells per well in serum-free DMEM. At 2 h and 24 h post-seeding, respectively, the medium was removed and the cells were washed and lysed for RNA isolation using the QIAGEN RNeasy Mini Kit (QIAGEN, Valencia, CA), as per the manufacturer's instructions.

5.2.1.8. RNA quantification and determination of purity: RNA concentration and purity were quantified using a NanoDrop ND-1000 spectrophotometer as described earlier in Section 5.2.1.3. As a further check for the absence of genomic or other contamination, denaturing agarose gel electrophoresis was performed and the gel was imaged on a Kodak imaging system (Eastman Kodak Company, Rochester, NY) to confirm intact RNA by ethidium bromide staining (not shown) of bands at 18S and 28S ribosomal RNA but absence of a third, lower band that would indicate

organic contamination or possibly “small RNAs”.

5.2.1.9. Focused PCR arrays for human extracellular matrix (ECM) and adhesion molecules: One microgram of high-quality RNA obtained as above was used to synthesize complementary DNA (cDNA) using the RT² Nano PreAMP cDNA Synthesis Kit (SABiosciences, Frederick, MD); cDNA was diluted, added to the RT² SYBR® Green qPCR Master Mix (SABiosciences) according to manufacturer’s instructions, and loaded into each well of a 96-well PCR array plate targeting human extracellular matrix and cellular adhesion molecules (PAHS-013, SABiosciences). PCR was performed on a Stratagene MX3000P (Agilent Technologies, La Jolla, CA) using a thermal cycle program of 95 ºC for 10 min followed by 45 cycles of (95 ºC, 15 s; 60 ºC, 60 s). The data were analyzed using RT^2 Profiler PCR Array Data Analysis software (SABiosciences) and MultiExperiment Viewer software (MeV v4.5, Dana-Farber Cancer Institute, Boston, MA) (Saeed et al., 2006).

5.2.1.10. Validation of PCR array data: To validate the microarray data, we assessed differential gene expression of select target mRNA species using quantitative real time PCR. Fibroblasts were cultured, as above, on glass cover slips coated with SPI, PLGA, collagen type I solutions and on uncoated glass cover slips for 2 h and 24 h. At each time point, the cells were lysed with TRIzol

(Invitrogen) and RNA was isolated by the phenol-chloroform method as described earlier in Section 5.2.1.2. cDNA was synthesized using the High Capacity cDNA Reverse Transcription Kit (Applied Biosystems) and PCR was performed on a Stratagene MX3000P (Agilent) using the TaqMan® Fast Universal PCR Master Mix (Applied Biosystems) and inventoried TaqMan® primers (Applied Biosystems) with FAM reporter dye for the following human genes: matrix metallopeptidase 10 (MMP-10) (Hs00233987_m1; NCBI reference sequence NM_002425.1), MMP-1 (Hs00899660_g1; NM_001145938.1), integrin alpha-1 (ITGA2) (Hs00158127_m1; NM_002203.3), collagen type VII alpha 1 (COL7A1) (Hs01574741_g1; NM_000094.3) and laminin beta-3 (LAMB3) (Hs00165078_m1; NM_001017402.1) (Applied Biosystems). These genes were chosen, as they were identified as highly upregulated using the PCR arrays. Gene expression was normalized to that of peptidylprolyl isomerase A (PPIA) (Hs99999904_m1; NM_021130.3) as invariant housekeeping gene.

5.2.1.11 Statistical analysis

All experiments were repeated at least three times in triplicate. Data are expressed as mean ± standard deviation, where applicable. One-way analysis of variance (ANOVA) was used to determine statistical significance ($p<0.05$). The Holm-Sidak method for post hoc testing was employed using SigmaStat software (Systat Software, Chicago, IL).

5.3. Results and Discussion

5.3.1. Homogeneity of protein substrate coating: Our coating methods produce homogeneous coatings of SPI (Fig. 5.1a) and collagen I (Fig. 5.1b) on glass coverslips, as confirmed by fluorescence microscopy of eosin staining. Thus, the substrates are suitable for studies involving cell surface receptor binding to substrates.

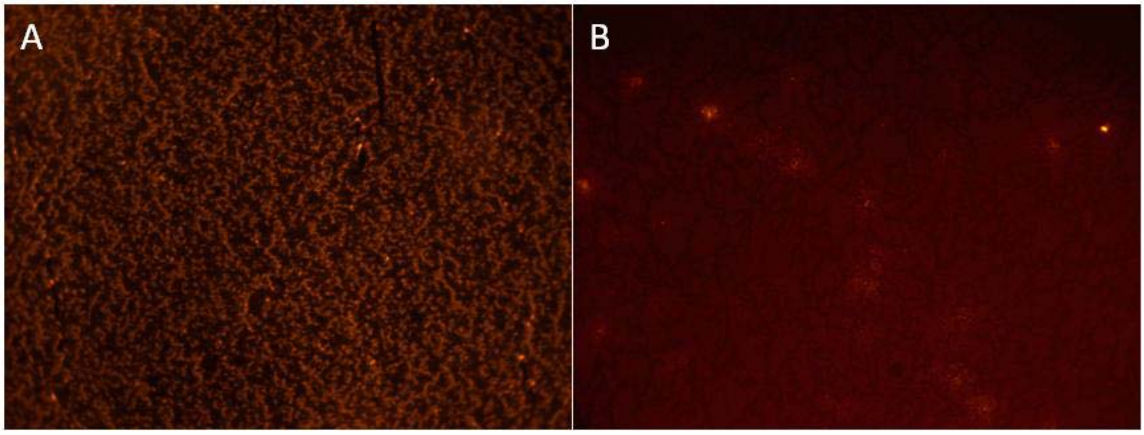

Figure 5.1. Homogeneity of protein coatings. Eosin staining of (a) SPI and (b) collagen type I coatings on glass coverslips, showing homogeneity of protein distribution. Original magnifications 200x.

5.3.2. Preliminary targeting of integrin mRNA expressed by primary human dermal fibroblasts cultured on SPI or collagen I substrates:

Surprisingly, integrin mRNA expression was not more highly expressed by fibroblasts after 1h attachment on ECM proteins than on SPI or PLGA. It had been expected that α2 would be most highly expressed on collagen I and α5 most highly expressed on fibronectin, with β1 showing

high expression on ECM proteins and β3 possibly showing higher expression on fibronectin than on other substrates. However, none of these results were seen—rather, no significant differences were seen in the expression of any of the targeted integrins across all substrates tested (Figure 5.2). Standard deviations were larger for integrin α1 than for other integrins on all substrates. Of note, integrin gene expression was similar on the foreign substrates SPI and PLGA as on the ECM proteins. Although these preliminary results were encouraging in that they suggest SPI may elicit a similar initial adhesion response from fibroblasts as native matrix proteins, a more comprehensive set of data was required in order to draw any conclusions.

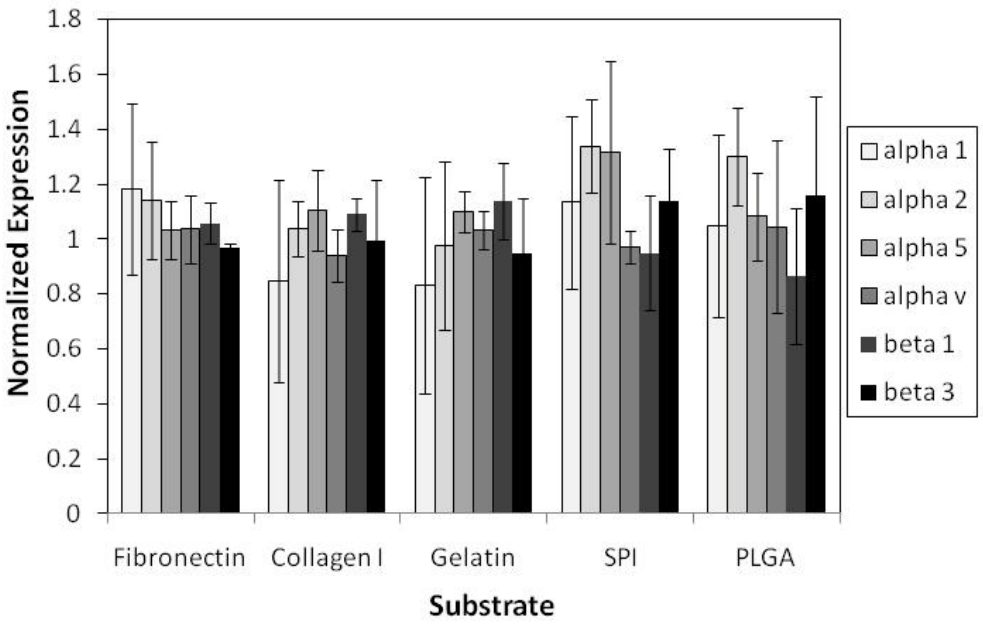

Figure 5.2**.** Expression of mRNA of various integrins by human dermal fibroblasts on different substrates after 1 h attachment.

5.3.3. Differential expression of human ECM and adhesion related genes by fibroblasts on SPI and collagen type I substrates after 2 h and 24 h attachment:

Primary human dermal fibroblasts were seeded onto glass cover slips that had been coated with either SPI or collagen type I solutions, and allowed to attach for 2 h or 24 h. The early time point of 2 h was used in order to allow for a more stable expression level of mRNA after the cells had equilibrated to their microenvironment. We then evaluated differential expression of mRNA species for a number of integrins, ECM proteins and matrix metalloproteinases (MMPs) using a targeted PCR array (SA Biosciences). The comprehensive list of genes and their functional categories is shown in the Appendix. Overall, we found minimal qualitative differences between the various substrates, i.e., in no case did we find any gene that was upregulated on SPI to be downregulated on collagen or vice versa; the differences were rather quantitative in nature. As expected there was significant upregulation of a number of ECM-related genes (Table 5.1) on SPI and collagen type I after 24 h compared to the same substrates at 2 h. For both these substrates, upregulation of matrix metalloproteinase 10 (MMP-10) was the highest, followed by MMP-1, integrin α2, collagen type VII alpha 1, and laminin β3.

Table 5.1. Time-dependent upregulation of select genes upregulated in primary human dermal fibroblasts cultured on SPI and collagen type I substrates. Data are presented as the ratio of fold upregulation at 24h vs. 2h of culture on the two substrates.

Gene Symbol	Description	PCR arrays		PCR validation	
		Fold Regulation (p-value)		Fold Regulation (p-value)	
		SPI	Col I	SPI	Col I
MMP10	Matrix metallopeptidase 10 (stromelysin 2)	1152.7255 (0.0232)	471.4083 (0.0525)	554.4832 (0.0131)	996.1905 (0.011)
MMP1	Matrix metallopeptidase 1 (interstitial collagenase)	53.7242 (0.0068)	36.7796 (0.039)	236.6591 (0.0078)	196.2660 (0.0533)
ITGA2	Integrin, alpha 2 (CD49B, alpha 2 subunit of VLA-2 receptor)	16.8052 (0.001)	12.5606 (0.0245)	30.0821 (0.0046)	81.1177 (0.0071)
COL7A1	Collagen, type VII, alpha 1	6.6231 (0.0008)	6.0106 (0.0085)	7.0902 (0.0222)	8.2344 (0.0897)
LAMB3	Laminin, beta 3	6.4718 (0.0002)	7.0494 (0.0078)	6.5375 (0.1086)	5.6016 (0.055)

To validate the PCR array data we also performed quantitative real time PCR for select genes and compared their expression in fibroblasts seeded at similar densities on the same substrates (SPI and collagen I) for 2 and 24 h. As seen in Table 5.1, RT-PCR analysis yielded qualitatively similar patterns as the gene arrays, albeit somewhat lower absolute values for the expression and upregulation of ECM related genes after 24 h, with, respectively, MMP-10 again showing the highest levels (~ 500- to 1000-fold), collagen VII alpha 1 and laminin beta 3 showing the lowest levels (~5- to 8-fold) and little difference between cells plated on the various substrates. In addition to SPI and collagen, PLGA (also coated on glass) and bare glass coverslips were also

investigated for comparison. Figure 5.3 shows similar ranges of values and trends across all substrates, corroborating our PCR array profiling data.

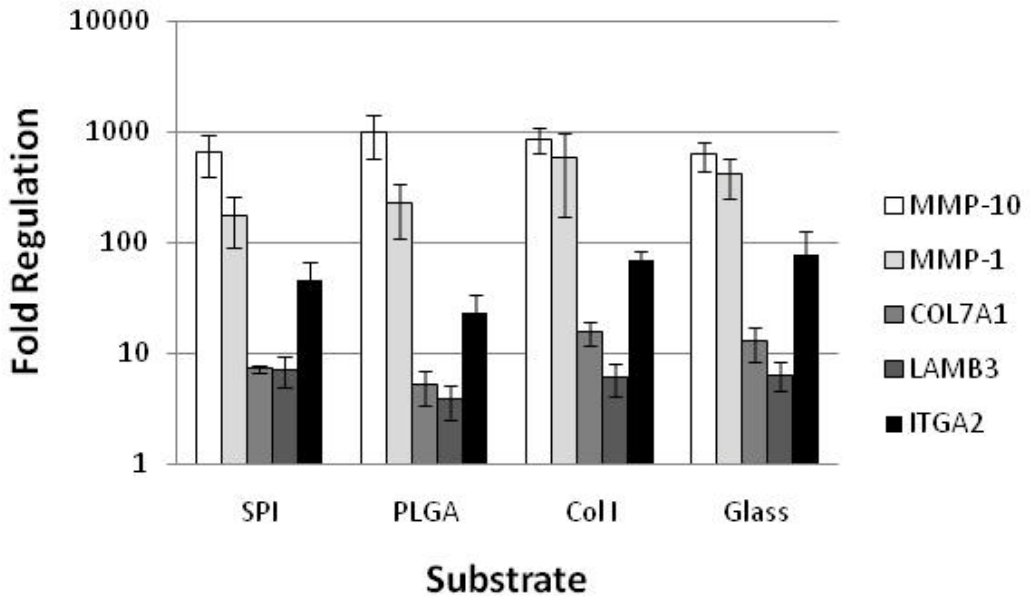

Figure 5.3. Differential upregulation of targeted genes expressed by fibroblasts on various substrates after 24h compared to 2h of attachment. Similar trends are seen across all substrates.

Other genes that were identified by the PCR arrays to be upregulated include MMP-3, -7, -8, -9, -13 and -14. Of the TIMPs, only TIMP-1 was highly expressed and slightly upregulated (2.44- and 2.38-fold on SPI and collagen, respectively). Integrin subunit β3 was also upregulated (3.57-fold on SPI and 2.47-fold on collagen), although its usually corresponding subunit αv was neither upregulated nor downregulated. Integrin subunit α4 was downregulated 3.2- and 4.11-fold on

SPI and collagen respectively. This subunit is not associated with dermal fibroblasts or wound healing.

The combined upregulation of MMP-1 and -10 together with MMP-7 has previously been associated with intestinal wound healing as expressed by migrating enterocytes in ischemic colitis-associated ulcers (Salmela et al., 2004). Dermal fibroblasts also up-regulate MMP-10 as well as MMP-1, -3, -8 and MT5-MMP (membrane-type MMP-24) in response to stratifin, a protein molecule secreted by differentiated keratinocytes that may play a role in preventing hyperproliferative disorders by mediating MMP expression profile in wound healing (Medina et al., 2007). Expression of MMP-1 and -3 in human periodontal ligament cells is also stimulated by basic fibroblast growth factor (bFGF), suggesting that these MMPs are involved in the ECM degradation required to initiate mineralization in periodontal regeneration (Hakki et al., 2009). In the absence of stimuli from other cell types, cell-cell contact between human dermal fibroblasts *in vitro* activates an inflammatory response that leads to non-apoptotic programmed cell death, correlating with a high upregulation of MMP-10 (106-fold, as compared to non-contact activated fibroblasts, Sirén et al., 2006). In our case, a similar mechanism may have been responsible for the high upregulation of MMP-10 on different kinds of substrates, since this was also observed when cells were cultured on PLGA and uncoated glass for 2 h and 24 h.

MMP-1 is commonly associated with skin wound healing as well as cancer, and is often expressed by normal fibroblasts *in vitro* (Pardo and Selman, 2005). *In vivo*, normal MMP-1 expression is approximately 8-fold higher in old (>80 years old) compared to young (21 – 30 years old) dermis, and this correlated with the fragmented collagen matrix of the aged dermis (Fisher et al., 2009). *In vitro*, culture of dermal fibroblasts with medium conditioned by bone marrow-derived fibrocytes "reprogrammed" by the deprivation of transforming growth factor beta (TGF-β) significantly increased MMP-1 expression and reduced type I collagen expression, showing an anti-fibrotic response that may increase the tissue remodeling capacity of these fibroblasts (Medina and Ghahary, 2010).

In the presence of keratinocytes, in organotypic skin equivalent coculture, fibroblasts appear to regulate certain genes in a manner to prevent fibrosis. At 2 days of air-liquid interface coculture in a 3-D collagen gel, these genes were significantly regulated by keratinocytes: urokinase-type plasminogen activator (uPA), MMP-1, and MMP-3 were up-regulated in fibroblasts, while connective tissue growth factor (CTGF), collagen I, collagen III, fibronectin, plasminogen activator inhibitor-1 (PAI-1), tissue inhibitor of matrix metalloprotease-2 (TIMP-2), TIMP-3, and alpha smooth muscle actin (α-SMA) were down-regulated (Koskela et al., 2010). These changes reflect

anti-fibrosis and suppression of myofibroblast differentiation. The authors chose 2 days as their analysis time point because it had been previously shown that the “more significant changes in gene expression occurred after 2–4 days compared with 6 days of air-exposure culturing, which reflects an altered keratinocyte activity and/or fibroblast susceptibility with time.” Gene regulation was also more pronounced in collagen gel cocultured fibroblasts than in cultures on plastic, which the authors attributed to the mechanical stresses conferred by the stiffer substrates diminishing the effect of keratinocytes.

From our data it appears that the response of fibroblasts does not differ between substrates upon initial adhesion at the early time point at 2 h, when interactions between cells and substrates are largely dependent on electrostatic parameters (van der Valk et al., 1983) or after equilibrating with the environment at the later time point of 24 h. The high upregulation of MMPs suggests active breakdown of substrate protein, followed by the expression of native ECM components collagen type VII and laminin β3, as well as natural receptors for ECM, especially the collagen receptor integrin α2. Integrin α2β1, a predominant collagen receptor, is also more highly expressed in aged dermis compared to young dermis, and its activation may be the cause of the increased expression of MMP-1 (Fisher et al., 2009). Integrin α subunits are more specialized than β subunits, as one β subunit can combine with one or several different α

subunits (Noszczyk et al., 2002). Integrins α2β1 and α1β1 play opposite roles in collagen regulation—when α2β1 binds to its ligand collagen I, the synthesis of collagen is further upregulated; conversely, α1β1 is a feedback inhibitor of collagen synthesis (Szulgit et al., 2002). It should be noted that integrin α2β1 is often associated with MMP-1 expression, and has a contrasting role to integrin α1β1 in the activation of human hepatic stellate cells from quiescence to myofibroblast-like cells (Znoyko et al., 2006). Integrin α2β1 upregulates and integrin α1β1 downregulates MMP-1 mRNA expression and MMP1 promoter activity, and the stimulation of α2β1 or the inhibition of α1 both promoted the development of well-developed multicellular networks (Znoyko et al., 2006). In the context of early dermal wound healing, fibroblasts transiently express mainly α2 and αv subunits associated with upregulation of the β1 subunit (Noszczyk et al., 2002).

In addition to the aggressive proteolytic activity, the moderate upregulation of collagen type VII suggests the concomitant occurrence of the constructive side of the remodeling process. Collagen type VII is a necessary component of the anchoring fibrils at the dermal-epidermal junction, and in disorders where it is absent, such as dystrophic epidermolysis bullosa (DEB), it has been shown in mouse models to be restored by the delivery of allogenic fibroblasts (Woodley et al., 2007; Wong et al., 2008). In a full-thickness mouse wound model, normal

human dermal fibroblasts, which express collagen VII, or human fibroblasts genetically modified to overexpress collagen VII were injected intravenously 8-10 h after wound infliction. Both cell types homed to the wound site and integrated into the newly formed basement membrane zone, but no human collagen VII was seen in unwounded skin or the skin of unwounded mice who received the same treatment (Woodley et al., 2007). Wong et al. (2008) took this further, into human subjects with recessive DEB, and found that allogeneic fibroblasts injected intradermally could promote sustained increase in collagen VII at the dermal-epidermal junction, although apparently due to increased expression in the patients' own *COL7A1* gene.

In vitro, cultured human dermal fibroblasts have been shown to upregulate collagen VII in response to TGF-β1, PDGF, IL-1β, and TNF-α but not TGF-α (Amano et al., 2007). Collagen VII synthesis did not vary with the age of cell donors, ranging from newborn to 91 years old.

Taken together, the gene array and the RT-PCR data show good quantitative and qualitative agreement, suggesting that fibroblasts seeded onto SPI will deposit and remodel their own ECM substrates in a manner similar to that on other established substrates, such as collagen and PLGA. These data from our *in vitro* studies suggest that SPI is a useful biomaterial that will induce a cellular tissue remodeling response similar to that of native ECM proteins.

It must be stressed that even though fibroblasts showed a very similar response on SPI, collagen I, PLGA and glass surfaces, they do not indiscriminately attach to and grow on any and all substrates. This was demonstrated by Machida-Sano et al. (2009) with human dermal fibroblasts on alginate films with either ferric ions or calcium ions incorporated (Fe-alginate and Ca-alginate respectively). In serum-free conditions, adhesion was low, ~35% on Fe-alginate and ~25% on Ca-alginate respectively after 4 h. With the addition of 10% FBS, Fe-alginate demonstrated ~100% adhesion with spreading, while Ca-alginate barely improved, with a similar level of adhesion as without serum and no spread cells. This difference was attributed to the 10.35-fold greater ability of Fe-alginate to adsorb serum proteins, including fibronectin and vitronectin, which correlates with its greater hydrophobicity.

The direct correlation between hydrophilicity and the inhibition of adhesion of human dermal fibroblasts was demonstrated by Groth et al. (2002). Acrylonitrile was copolymerized with 5%, 20% or 30% (w/w) of hydrophilic N-vinylpyrrolidone (NVP) to form membranes. Fibroblasts attached and spread well on the 5% NVP membranes, but were significantly inhibited on 20% and 30% NVP, and cells tended to grow in islands.

In further support of the role of integrins in cellular attachment to foreign substrates, several studies have shown inhibition of attachment when integrins were blocked. The ability of hTERT-BJ1 human foreskin fibroblast cells to adhere onto nanopatterned topography as well as flat surfaces of polycarbonate was reduced when the cells were blocked with anti-integrin α1 antibody (Curtis et al., 2006). The number of attached cells after 2h was reduced by over 50% on both nanopatterned and flat surfaces after blocking integrin α1. Wood et al. (2008) showed that inhibiting β1 integrin on hTERT-BJ1 cells actually increased their ability to "nanoimprint", or conform to the shapes of nanopatterned silicon substrates after 12 h. Inhibiting β3 integrin had the opposite effect, reducing their ability to nanoimprint. The potential role of β3 integrin in the binding of cells to nanopatterned substrates was also investigated by Walter et al. (2006), who revealed a correlation between the density of integrin ligands on nanopatterned gold substrates and the adhesion force of the integrin-substrate bond during the first 10 min of adhesion in rat embryonic fibroblasts. Each gold nanoparticle functionalized with the cyclic RGD peptide c(-RGDfK-) could bind a single αvβ3 integrin. They found the force required to detach an integrin using magnetic tweezers to decrease non-linearly with increasing distance between ligands (Walter et al., 2006).

Integrin αvβ3 may also be crucial for rigidity sensing of fibronectin substrates by fibroblasts through the complex it forms with a receptor-like protein tyrosine phosphatase, RPTPα, at the leading edge early in spreading. Mouse fibroblasts were plated for 15 h on soft (0.03% bis/8% acrylamide) or rigid (0.4% bis/8% acrylamide) substrates coated with fibronectin. It was observed that in normal fibroblasts, spread area was much greater on the rigid surface (~2800 μm^2) than on the soft surface (~800 μm^2). However, in RPTPα$^{-/-}$ fibroblasts, both substrates promoted a similar spread area (~1500 μm^2). When normal fibroblasts were incubated with monoclonal antibody against αvβ3, cells also showed no difference in spread area on both substrates (Jiang et al., 2006).

At the single-integrin level, α2β1 binding with collagen-coated atomically flat substrates has been shown to mediate adhesion during the first 60 s of contact for Chinese hamster ovary (CHO) cells (Taubenberger et al., 2007). Wild-type CHO cells do not express integrin α2, but can be transfected with human α2 to determine its isolated effect on adhesion. The force required to break a α2β1-collagen bond was measured to be 47 ± 13 pN. However, after 60 s, the force required to rupture a cell-collagen bond is greater than that measured at the single-integrin level, suggesting cooperativity between integrin receptors. The cells enter into an “activated” adhesion state, and over a period of up to 600 s, the force required to detach a transfected cell increased

nonlinearly from several hundred piconewtons to ~20 nN. Taubenberger et al. identified three stages of adhesion formation—initiation, reinforcement, and maturation. During initiation (< 60 s), detachment forces increased slowly to about 3 nN; during reinforcement (60-180 s), they increased rapidly by to about 10 nN, after which during maturation (> 180 s), forces increase slowly by another 2-3 nN.

Cai et al. (2009) blocked the β1 integrin on the surface of porcine esophageal fibroblasts (PEFs) and showed that adhesion to fibronectin was inhibited during the first 90 minutes, resulting in less spreading. However, this difference diminishes by 120 minutes and by 240 minutes, the spreading was very similar between β1-blocked and non-blocked cells. This initial effect may be realized through focal adhesion formation and actin cytoskeleton remodeling. Blocking β1 integrin increased the lag time between cell deposition and focal adhesion formation by 30 min from 30 min for unblocked cells to 60 min. Although spreading equilibrates with time, the maximum adhesion strength achieved by the cells over the 240 min does not, with the strengths of non-blocked and β1-blocked cells being 52.8 and 34.4 Pa, respectively.

Zlatanov et al. (2005) measured the migration velocity of clusters of β1 integrins in human dermal fibroblasts, as identified by fluorescent anti-integrin antibodies. They compared

hydrophilic (clean glass) and hydrophobic (octadecyl-silanized; i.e., ODS) surfaces, both coated with fibronectin, and found that the wettability of the glass still had a significant impact on β1 integrin activity. They identified 3 populations of integrins with different speeds (82.76% immobilized, 13.08% fast, and 4.16% slow) on hydrophilic glass and only 2 populations (83.36% immobilized and 16.64% fast) on hydrophobic ODS. Surprisingly, the percentage of immobilized cells on both substrates was similar (approx. 83%).

Hannafin et al. (2006) cultured canine fibroblasts derived from anterior cruciate ligament (ACL) and medial collateral ligament (MCL) on TCPS, type I collagen, elastin, laminin and fibronectin and quantified their expression of integrins β1, β3 and α5 using flow cytometry. Conditions varied from static to 2h or 22h of 5% uniaxial cyclic strain daily for 3 days. Up-regulation of subunits with cyclic strain was seen to be substrate-dependent (summarized in Table 5.2). No significant differences were seen between 2 h and 22 h.

Substrate	ACL			MCL		
	α5	β1	β3	α5	β1	β3
Collagen I	33%	33%		39%	54%	
Laminin	32%	44%	52%	32%	37%	48%
Fibronectin	36%	45%		34%	40%	
Elastin						
TCPS						

Table 5.2. Summary of substrate-dependent increase in integrin subunit expression of canine ACL and MCL fibroblasts after 2 h of cyclic strain daily for 3 days, compared to static controls (data from Hannafin et al., 2006).

Taken together, these studies suggest that cellular responses to their microenvironment, whether native or foreign, are mediated at least partially by integrins and these changes can be measured at the single-integrin level. As such, effect on integrin expression may be another factor to take into consideration when tailoring scaffold material properties to its application.

5.4. Conclusions

We have investigated cell surface interactions of human dermal fibroblasts with SPI compared to other substrates including collagen I, PLGA and glass, and found qualitatively similar up-regulation of certain genes related to cell adhesion across these substrates. The highest up-regulated gene was MMP-10, followed by MMP-1, suggesting aggressive proteolytic activity toward remodeling the immediate matrix microenvironment. The lesser, but still significant, up-regulation of integrins and ECM proteins points to the constructive aspect of the remodeling process. Our results suggest that SPI as a biomaterial promotes a favorable initial cellular response, similar to other well-characterized biomaterials.

Chapter 6. *In Vivo* Evaluation of SPI/PEO Scaffolds Using a Full-thickness Excision Wound Model

6.1. Introduction

So far, no *in vitro* or computational model exists that can replicate the complex and dynamic wound environment at the organism level. Thus an *in vivo* model is required to evaluate the efficacy of new scaffolds, as well as identify any systemic effects such as inflammatory response. The rat is a widely used animal model for skin wound healing (Birch et al., 2005; Weingarten et al., 2006, 2008; García-Esteo et al., 2007; Garcia et al., 2008). Weingarten et al. used the established streptozotocin (STZ)-induced diabetic rat model to validate near infrared (NIR) and diffuse reflectance spectroscopy (DRS) as reliable non-invasive optical technologies to measure the healing of diabetic wounds over time. Garcia et al. (2008) used full-thickness skin wounds in male Sprague-Dawley rats to test the efficacy of collagen gel scaffolds on wound healing, based on analysis of parameters such as wound closure, epithelialization, angiogenesis, inflammatory response and scarring.

Rat skin and human skin have in common an epidermis, dermis, basement membrane, and hair follicles. However, unlike humans, rats have loose skin that does not adhere to underlying structures, lack apocrine and eccrine glands, and do not form keloid or hypertrophic scars

(Dorsett-Martin and Wysocki, 2008). In a full-thickness wound model, both the epidermis and dermis are removed to the panniculus carnosus. A fibrin clot is formed from the base, followed by invasion by granulation tissue. Epithelialization occurs from the margins, with migration along the interface between the granulation tissue and the clot (Dorsett-Martin and Wysocki, 2008).

We evaluated our electrospun SPI/PEO scaffolds with an established protocol based on these well-described models and our surgical and technological expertise at Drexel University in collaboration with surgeons at Drexel University College of Medicine. Hairless rats are chosen because hair interferes with the study of wound healing as shaving can further inflame and infect the wounds (Papazoglou et al., 2008). Male rats are preferred to avoid any hormonal fluctuations that are known to affect wound healing (Birch et al., 2005), as estrogen deficiency is associated with impaired cutaneous healing and also because the thicker skin of male rats allows for less healing by contraction than in females (Dorsett-Martin and Wysocki, 2008). As further rationale, in humans, elderly males are more pre-disposed to chronic ulceration and heal acute skin wounds more slowly (Gilliver et al., 2009).

Previously, our collaborators developed a fast, portable, non-invasive and reliable diagnostic device for the measurement of wound healing based on near infrared (NIR) spectroscopy and

diffuse reflectance spectroscopy (Papazoglou et al., 2005, 2008; Weingarten et al., 2006, 2008, 2010). Briefly, NIR optical measurements were first validated to correlate with wound area reduction over time and could distinguish between diabetic and non-diabetic wounds in a rat model. More recently, a portable frequency domain diffuse optical tomography instrument that noninvasively measures the optical properties, i.e. amplitude and phase shift of light, of tissue at depths of several millimeters was implemented (Weingarten et al., 2008) and can assess oxy- and deoxy-hemoglobin and water in the wound. NIR absorption coefficients correlated with blood vessel ingrowth (confirmed by lectin staining) over time and DRS scattering data correlated with collagen concentration (confirmed by Gomori's trichrome staining) in the wounds, in both diabetic and control rats.

We first confirmed that electrospun SPI/PEO scaffolds do not interfere with optical measurements, when probed against an optical phantom. This has significant implications in our favor in that the scaffold will not need to be removed from the wound in our animal model when measurements are taken to determine wound healing over time.

We hypothesized that electrospun SPI/PEO scaffolds will promote an enhanced wound healing response in an adult rat model compared to control treatment, as assessed by accelerated

wound closure and re-epithelialization, and/or reduced scarring. In our study, we investigated the efficacy of SPI/PEO scaffolds in promoting wound healing, and identified improvements to the rat model.

6.2. Materials and Methods

6.2.1. Animal model: Hairless Sprague-Dawley rats (CD Hairless, Charles River Laboratories, Wilmington, MA) aged approximately 11 weeks were chosen as the animal model for full-thickness skin excision wounding due to their docility and the absence of the need for shaving fur, which causes local irritation.

6.2.2. Surgery: According to our protocol approved by the Institutional Animal Care and Use Committee (IACUC) of Drexel University (#18284), animals were anesthetized using 2% isoflurane gas and square full-thickness excision wounds of approximately 2 cm x 2 cm were created on the dorsum. In the initial pilot study to optimize wound location, only one wound was inflicted on each animal, and animals were randomized to either treatment with SPI/PEO scaffold or with Tegaderm™ (3M, Minneapolis, MN) polyurethane dressing as a control. Ten rats were used in this study and one died during anesthesia, so 6 rats (3 male, 3 female) were treated with SPI/PEO and 3 rats (1 male, 2 female) were treated with Tegaderm™. In the second pilot

study, 10 rats (all male) each received 2 wounds symmetric along the dorsal midline, and one side was treated with SPI/PEO scaffold and secured with Tegaderm™ while the other side received Tegaderm™ alone (Figure 6.1). SPI/PEO scaffolds were sterilized by exposure to UV for 30 minutes on each side before application to wounds.

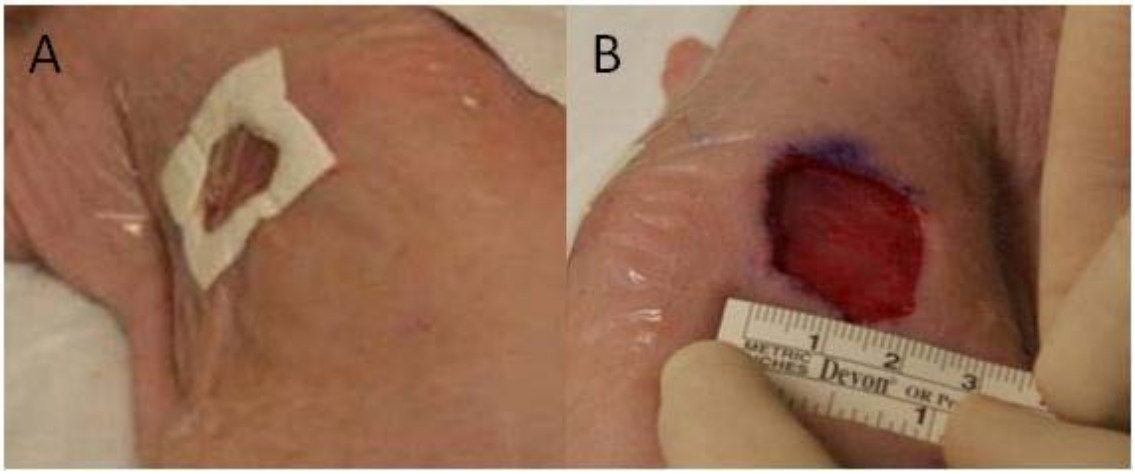

Figure 6.1. Full-thickness skin excision model in the rat. Wounds were treated with SPI/PEO scaffold on one side (a) and Tegaderm™ dressing on the other side (b, image shows wound before application of Tegaderm™).

6.2.3. Measurement of wound healing parameters: Digital photographs were taken of the wounds next to a ruler 2 to 3 times per week and the images were analyzed using University of Texas Health Science Center at San Antonio (UTHSCSA) ImageTool 3.0 software. Pixels were converted to metric units to determine wound area at each time-point. Wound closure was

assessed by calculating the area relative to the original wound area:

% wound closure = 100 × (wound area at day 0 – wound area at day N)/wound area at day 0.

Functional near infrared (fNIR) spectroscopy was also used to quantify wound healing according to methods described by Weingarten et al. (2006, 2008), correlating optical absorption to oxyhemoglobin content. It was first determined that the SPI/PEO scaffold, when hydrated, was optically transparent to the fNIR sensors. Thus, the scaffold would not interfere with wound measurements. The sensor was calibrated on an optical phantom before each set of measurements (Figure 6.2). The sensor was placed at the wound center as well as the edge for measurement, and unwounded skin on the flank was used as a control site. Rats were fully conscious during all measurements.

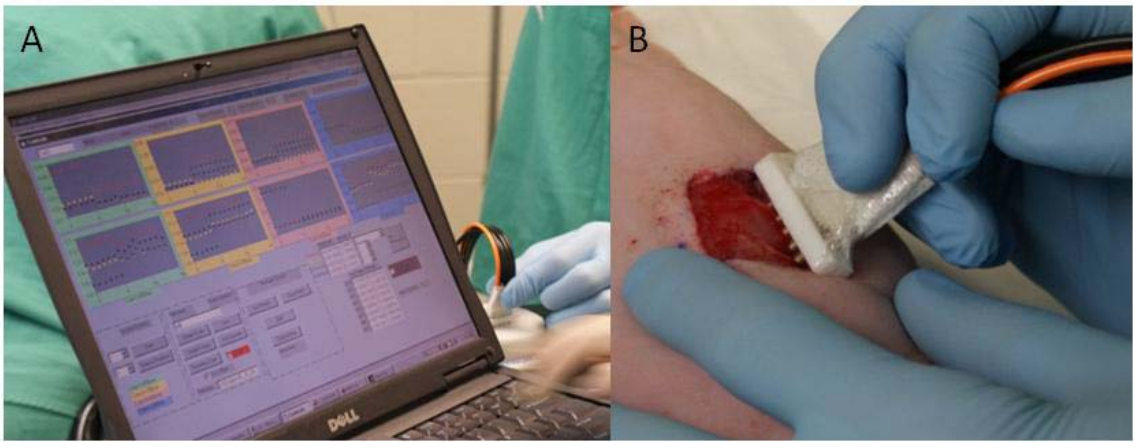

Figure 6.2. Calibration of fNIR sensor on an optical phantom (a) and measurement of a wound edge (b).

6.2.4. Histology: At day 31 post-operatively, 5 animals from each group were sacrificed and biopsies were taken of the wound sites for histological analysis. Samples were embedded in paraffin following a dehydration gradient of ethanol (EMD) and xylene (EMD) and cut into sections mounted on glass slides coated with poly-L-lysine (Sigma). Sections were rehydrated and stained with hematoxylin and eosin as well as Gomori's trichrome (Sigma) to identify interstitial collagen. Stained sections were visualized using a Leica DMRX upright microscope and digital images were acquired with a Leica DC 300FX camera.

6.2.5. Statistical analysis: Using power analysis we determined that with 5 animals per group we would be able to assess a 20% improvement of treatment over control even with 15% variability. Statistical significance in the difference between wound closure of control vs. experimental groups was determined by two-tailed, unpaired Student's t-test ($p < 0.05$ taken as significant). Data are expressed as mean ± standard deviation, where applicable.

6.3. Results and Discussion

6.3.1. SPI/PEO scaffolds promote quantitatively similar wound healing response as standard control

Wound closure was slightly, but not statistically significantly, faster in the SPI/PEO treatment group than the control group (Figure 6.3). The largest difference between groups was detected at postoperative day 2, when wounds were 71.5% ± 15.4% and 80.0% ± 6.9% of original wound area for SPI/PEO treated and control groups, respectively. Wounds were completely healed by postoperative day 18, although the neodermis continued to be replaced by thicker scar tissue up to the end of our study at day 31. This trend correlates with the model proposed by Cross et al. (1995) based on general observations of untreated full-thickness excision wounds in the rat, where wound healing occurs in 3 phases: a lag phase lasting approx. 2 days, followed by a sharp decrease in wound area during the contraction phase until approx. day 12, ending with the consolidation phase (Figure 6.4, Cross et al., 1995).

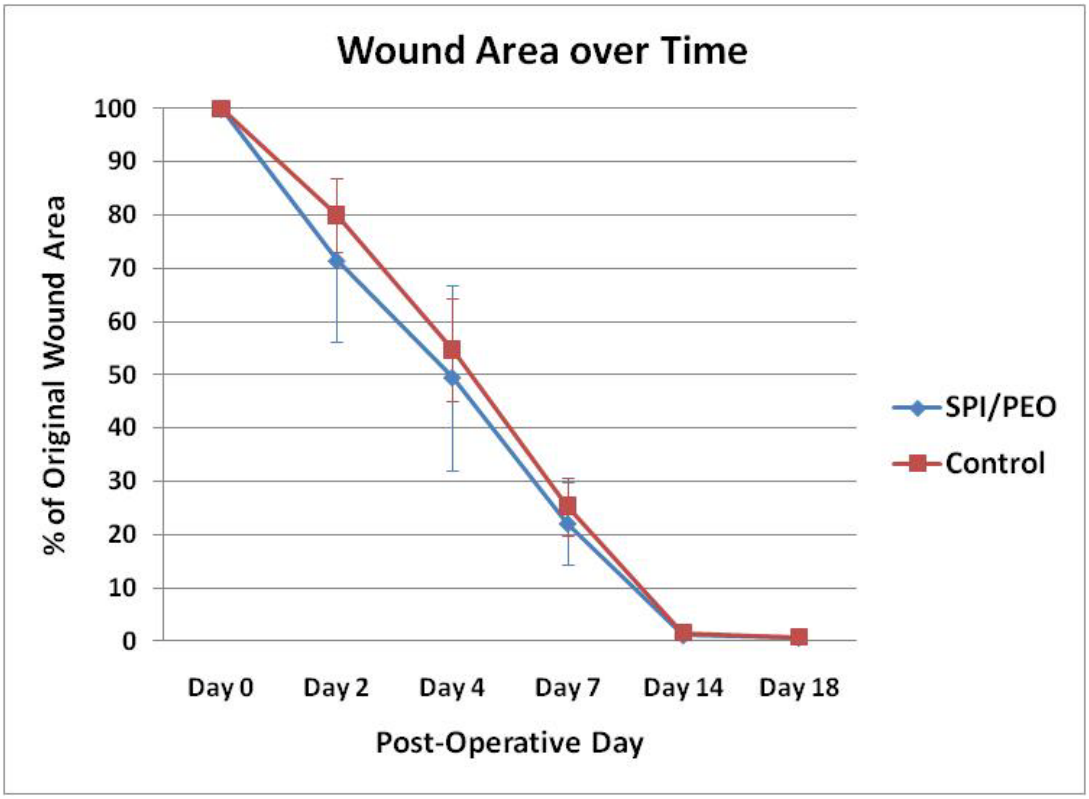

Figure 6.3. Wound area as percentage of original wound area over time. The SPI-PEO treated wounds healed slightly, but not significantly, faster than control treated wounds, especially on day 2. Wounds were closed by day 18. Data normalized from n = 15 SPI-PEO and n = 14 control.

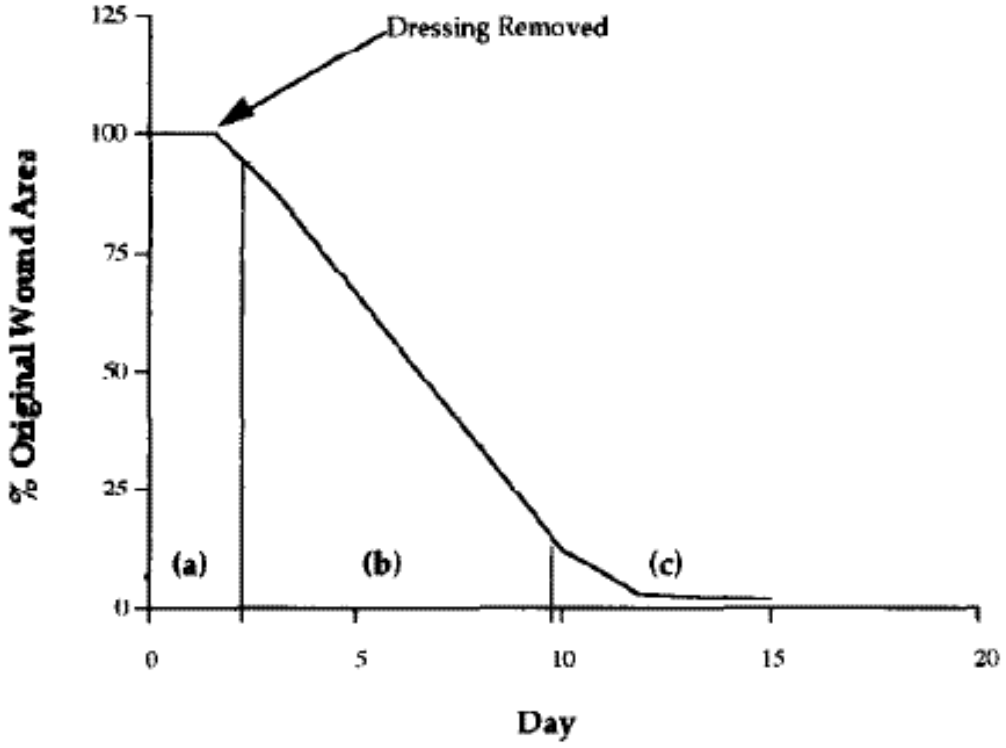

Figure 6.4. Healing of full-thickness wounds in the rat model. The timeline is divided into three phases, with an initial lag phase during the first 2 days (a), followed by a contraction phase until approximately day 10 (b), ending with the consolidation phase until approximately day 15 (c). Figure taken from Cross et al., 1995.

NIR measurements at wound and control sites corroborated our interpretation that the SPI/PEO promotes only slight quantitative improvement in wound healing over control. Figure 6.5 shows the variation of absorption at wavelength 685 nm over the healing period. This is in the range of wavelengths at which hemoglobin is a major chromophore. Wounds have a higher concentration of oxygenated blood than unwounded tissue, due to increased vascularization as part of the early healing process. Thus, healing wounds will show a downward slope of NIR absorption over

time as wound inflammation and angiogenesis decrease with remodeling, while non-healing wounds may show a constant or even upward slope (Weingarten et al., 2010). Our normalized data show a very similar trend between treatment and control groups, with no statistically significant difference.

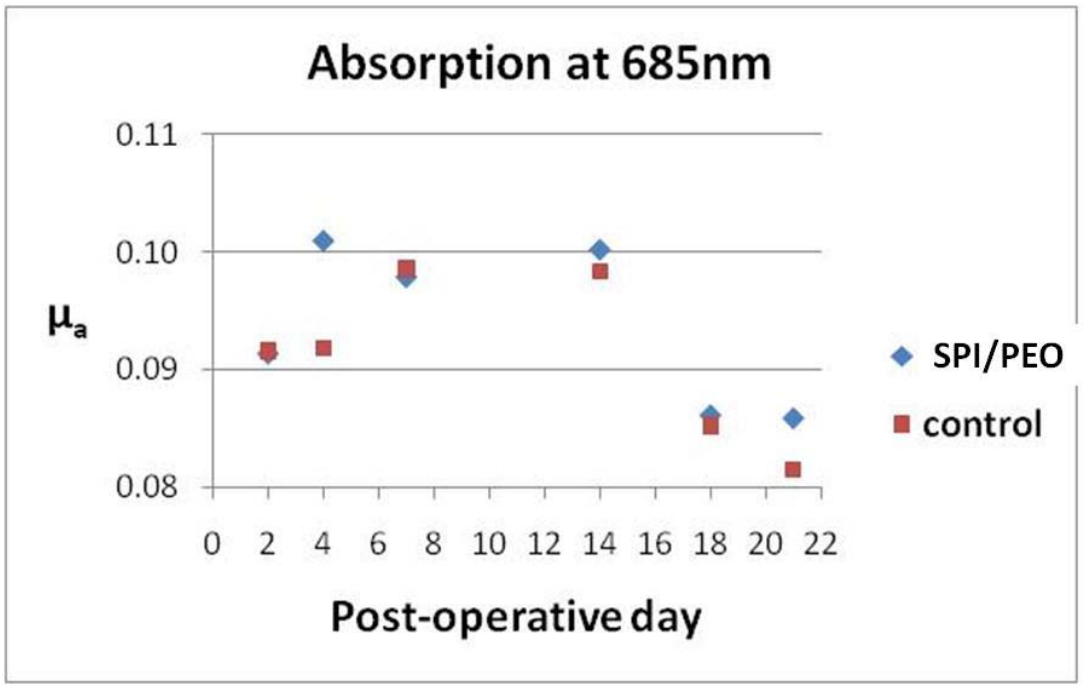

Figure 6.5. Variation of fNIR absorption at 685nm at the wound site with time.

6.3.2. Qualitative benefits of SPI/PEO scaffold over Tegaderm™ (control)

Although quantitatively, the SPI-PEO scaffold performs very similarly to the control, qualitative differences could be seen with the naked eye. By nature of the submicron-scale fibrous structure,

the SPI-PEO scaffold absorbed wound fluids and integrated itself with the wound, serving as a "breathable" interface between the raw wound and the external environment. The wicking action of the scaffold prevented excessive oozing of inflammatory wound exudates, which was still occurring on day 2 in control wounds (Figure 6.6).

The SPI/PEO scaffold thus functions initially as a permanent scaffold, rather than as a removable wound dressing. However, by day 7 it is detached naturally as part of the encrustation. To translate this phenomenon to a clinical setting, where wounds are surgically "cleaned" approximately weekly by debridement of necrotic tissue, the SPI/PEO scaffold or any remainder thereof would presumably be removed in this procedure and replaced with a new scaffold, and this process would be repeated until the wound is healed to a point where a scaffold is no longer necessary.

Figure 6.6. Macroscopic progression of wound healing in a single rat.

The qualitative differences between SPI/PEO treated and control groups may be attributed to fundamental differences in the properties of our electrospun SPI/PEO scaffold and Tegaderm™ (Table 6.1). Tegaderm™, used in standard wound care practice, is designed to be an occlusive dressing to keep wounds moist and sterile, by providing a barrier to pathogens and other external stressors while preventing moisture loss. It may be changed daily or as often as required, adheres to the area of unwounded skin surrounding the wound, and does not promote any cellular interaction. By contrast, our SPI/PEO scaffold is intended as a permanent scaffold that incorporates directly into the wound, in order to provide structural and molecular cues to the cells active in each stage of wound healing. The integration of SPI/PEO scaffold into the wound creates a dual effect of promoting cellular interaction and absorbing excess exudates, which may aid in accelerating homeostasis.

The mechanical properties of Tegaderm™, measured using the same methods as described in Chapter 3, Section 3.2.2.3, also differ significantly from those of electrospun SPI/PEO. The ultimate tensile strength (UTS) of Tegaderm™ is over two orders of magnitude greater than that of electrospun SPI/PEO, while the strain to break is approx. 2.5-fold greater (Table 6.1). While neither device closely matches the tensile properties of human skin, with UTS ~7.7 MPa (Adekogbe and Ghanem, 2005) and strain to break ~100% (Diridollou et al., 2000), the SPI/PEO

scaffold resembles human skin much more closely.

Table 6.1. Comparison of properties of SPI/PEO scaffold with Tegaderm™.

Property	**SPI/PEO**	**Tegaderm™**
Type of device	Permanent scaffold	Temporary dressing
Function	Promote healing response through cellular interaction; absorb excess fluid	Barrier to external environment
Material	Natural; plant-derived (soy protein)	Synthetic (polyurethane)
Structure	Fibrous/porous	Membrane
Permeability	Breathable	Occlusive
Mechanical properties†	UTS: 0.10 ± 0.05 MPa Strain at break: 83.3 ± 21.2 %	UTS: 38.4 ± 3.0 MPa Strain at break: 203.7 ± 28.6%
Biodegradability	Biodegradable	Not biodegradable
Interface with wound	Absorbent	Adhesive
Bioactivity	Potentially bioactive	Inert

UTS, ultimate tensile strength

†For SPI/PEO, values are given for hydrated conditions.

Histologically, by the end of study at day 31 no differences could be seen between SPI/PEO treated and control groups (Figure 6.7). Wounds are fully re-epithelialized and underlying dermal tissue is well vascularized. From this we can simply conclude that in the long term, wounds treated with SPI/PEO scaffold reach a tissue structure similar to those of wounds treated with Tegaderm™.

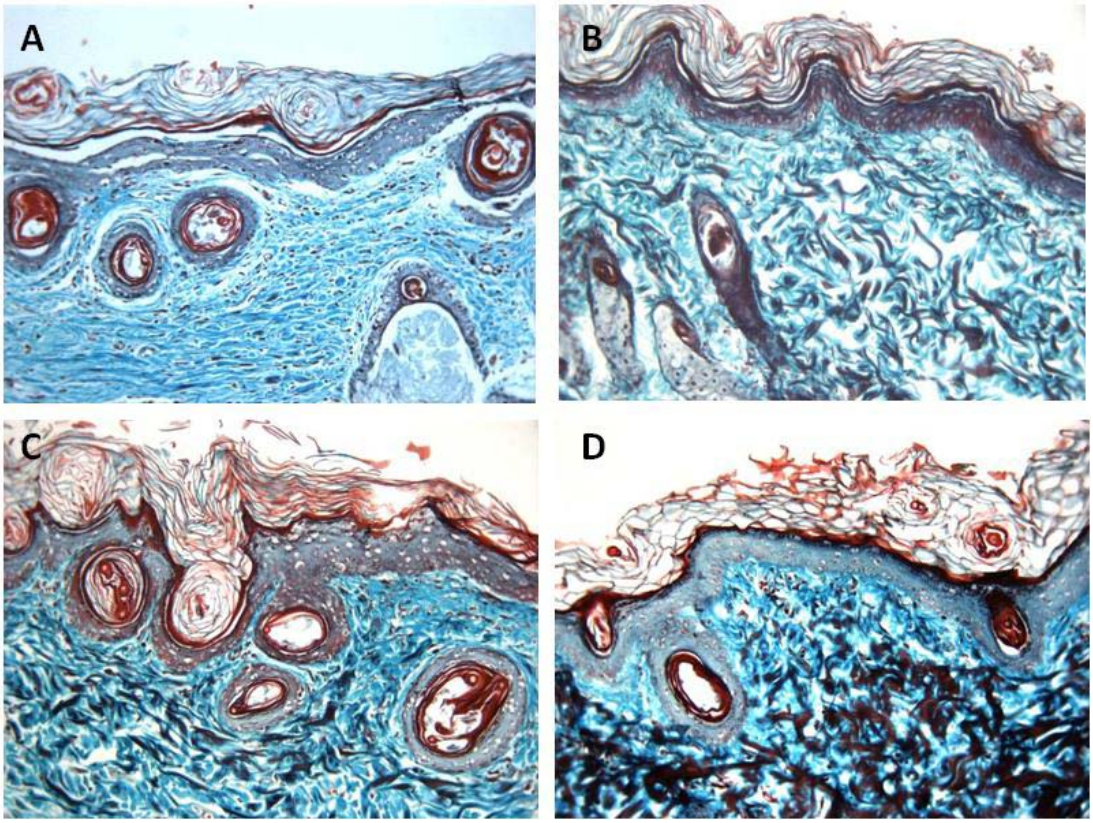

Figure 6.7. Histological sections at post-operative day 31. a) wound treated with SPI/PEO scaffold; b) unwounded area from the same SPI-PEO treated animal; c) wound treated with control, Tegaderm™; d) unwounded area from the same control treated animal. 5µm sections stained with hematoxylin and Gomori's trichrome (Nuclei: Black; Normal muscle myofibrils: Green-blue with distinct A and I bands; Intermyofibrillar muscle membranes and keratin: Red; Interstitial collagen: Green). Original magnifications 200x.

6.3.3. Improvements to our wound healing model

Several studies have used full-thickness excision wounds in a rat model to test electrospun and other scaffolds. For example, Waldeck et al. (2007) used a single ~1 x 1 cm^2 full-thickness wound on the dorsum of each approx. 3-month-old female Sprague-Dawley rat to compare unmodified gelatin interpenetrating networks (IPN) with RGD-modified IPN with keratinocyte growth factor

(RGD-IPN+KGF) and control, conventional dressing. IPN solutions were applied as a liquid and photopolymerized using UV *in situ.* At 2 days, 1 week, 2 weeks and 3 weeks, wounds were excised and histological sections were examined for inflammation, angiogenesis and capsule thickness. IPN inhibited wound contraction compared to the unrestricted control, since the wounds only had physical space to contract when the material degraded. In addition, RGD-IPN+KGF filled the wound and increased cellular growth compared to unmodified IPN and control, also decreasing wound closure by contraction. Initially, at 2 days, RGD-IPN+KGF induced the greatest neutrophil numbers, indicating a high inflammatory response; however, neutrophil numbers decreased significantly over 3 weeks of healing.

In our initial pilot study, we observed that female rats had thinner skin and thus accelerated contraction compared to male rats, in line with reports by Cross et al. (1995), although we did not compare these parameters between genders and the number of rats was not large enough to draw any significant conclusions. The thicker skin of male rats may be more resistant to underlying fibroblast contractile forces, allowing for a greater role of epithelialization in healing. We also found male rats to be generally more docile and easier to handle by virtue of their larger size, and continued further studies with only male rats.

Rats heal mainly by wound contraction, decreasing the healing time compared to animals that heal more by re-epithelialization, and this causes difficulties in assessing the efficacy of a treatment over a longer time frame (Dorsett-Martin and Wysocki, 2008). Aged rats are a model for delayed wound healing (Cross et al., 1995), and we investigated our SPI/PEO scaffold in an "old" male rat (approx. 7 months) following the same procedure (see Section 6.2.2) as for the younger rats, with two wounds, one on either side of the dorsal midline.

Only two aged rats were available from Charles River Laboratories when we requested them over a period of months, and one died during anesthesia before the operation. Therefore, only one rat was available for our experiment. All procedures were performed by Kimberly Wasko, CVT, RLAT.

Similar to the results from the pilot study with younger rats, healing by wound closure was closely similar in the two wounds in the old rat (Figure 6.8). Between days 1 and 14, the control wound appears to heal faster. This may be due to the presence of the scaffold creating a physical resistance to wound closure by contraction in the SPI/PEO treated wound.

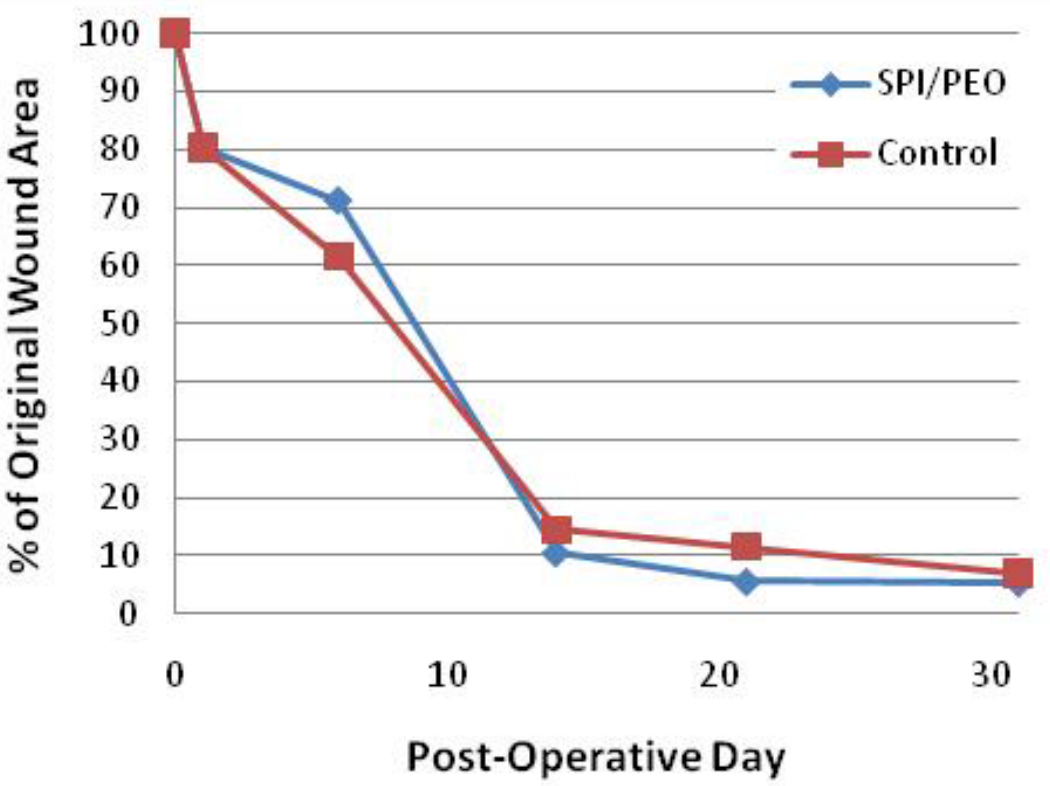

Figure 6.8. Wound area as percentage of original wound area over time for an aged rat. Healing trends are closely similar between the SPI/PEO treated and control wounds, with no statistically significant differences at any time point. Day 31 measurements were taken of the remaining scar.

Macroscopically, SPI/PEO treated and control wounds healed in a similar fashion, much like in the study with younger rats (Figure 6.9). Complete wound closure was not reached until after day 21, delayed compared to days 14-18 in younger rats. Although one rat is not enough to draw any conclusions, we have seen that the SPI/PEO scaffold promotes similar healing as Tegaderm™ in both young and aged models.

Due to the difficulty in obtaining aged rats, as vendors do not usually have them available, we investigated a model of physically impaired wound healing, by using an acrylic ring to splint open the wound. This model has been reported in the literature as an effective method to prevent contraction in rodents, allowing for healing completely by granulation tissue formation and re-epithelialization (Galiano et al., 2004; Shinzawa et al., 2007), and has even been termed "humanized" (Wong et al., 2010) as human wounds, like porcine wounds, heal primarily by re-epithelialization rather than by contraction. The same model has also been used in the miniature Bama pig for the same purpose (Ma et al., 2007). This type of "manipulated" wound is recommended where differences in healing between species, e.g. rat and human, are due to anatomical characteristics such as the presence of the panniculus carnosus in rodents, which separates the dermis from the sub-dermal tissue, resulting in a large amount of contraction when a section of full-thickness skin is removed (Lindblad, 2008). The physical barrier imposed by the ring allows for granulation tissue to form, more closely simulating the human condition.

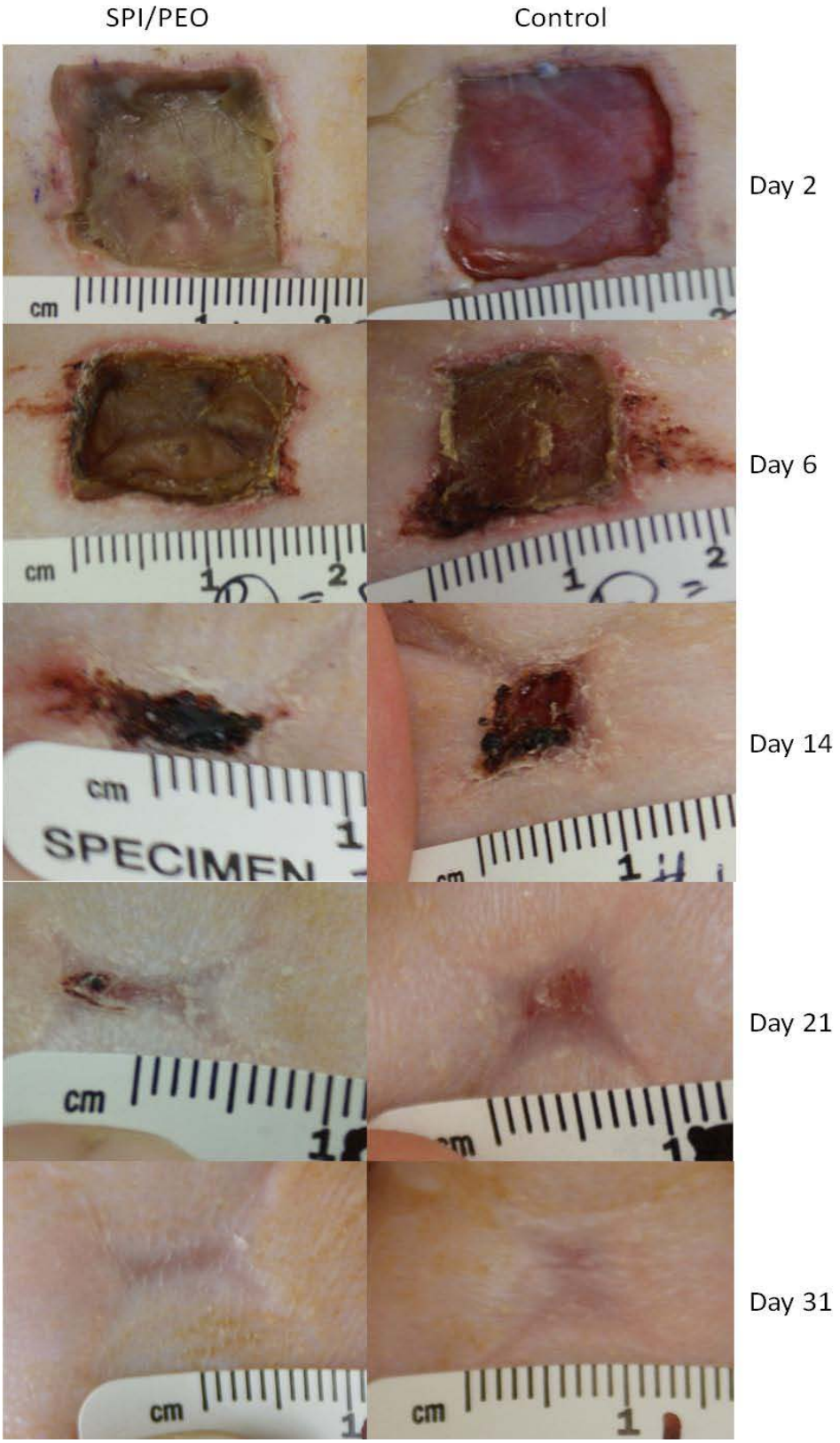

Figure 6.9. Macroscopic progression of wound healing in an aged rat.

Galiano et al. (2004) quantified the delay in wound healing imposed by the circular splint in a mouse model. Full-thickness excisions were made on the dorsum of healthy and diabetic mice. In both cases, splinted wounds healed more slowly than unsplinted wounds (12.7 days ± 0.96 vs. 7.81 ± 0.78 in healthy mice and 22.6 days ± 1.44 vs. 12.4 ± 0.96 in diabetic mice, respectively). Granulation tissue continued to form until wounds were completely re-epithelialized.

In order to increase granulation in the healing wound, Shinzawa et al. (2007) inhibited contraction in their full-thickness wound model using two 30mm-diameter wounds on the back of each male Sprague-Dawley rat. An acrylic ring of the same diameter was placed in each wound. Granulation tissue was seen to proliferate up to day 14, followed by fibrosis instead of epithelialization. Neovasculature could be seen at day 7 and the number of vessels was greatest on day 14, decreasing afterwards with increasing vessel thickness during the observation period up to day 28.

Wong et al. (2010) followed a similar procedure to investigate the efficacy of a pullulan-collagen hydrogel on dermal wound healing in a mouse model. Excisional wounds were splinted and treated with either the hydrogel or simply Tegaderm™ alone. Hydrogel-treated wounds closed significantly faster than non-treated wounds, being 86.4% ± 1.6% vs. 91.7% ± 1.0% of original

wound area on day 3 and 59.4% ± 3.6% vs. 73.2% ± 2.5% on day 5, respectively. Granulation tissue formation was significantly greater in hydrogel-treated wounds on day 3, but this difference was no longer significant by day 5.

In our proof-of-concept experiment for this model, two wounds 20 mm in diameter were made bilaterally along the dorsal midline (Figure 6.10). Wounds were splinted with an acrylic ring and treated with either electrospun SPI/PEO scaffold or Tegaderm™. By day 15, the SPI/PEO scaffold was still present in the wound as it was not contracted and therefore did not detach (Fig. 6.10c). In the control wound, granulation tissue had formed but the wound had not re-epithelialized, and was still “raw” (Fig. 6.10d).

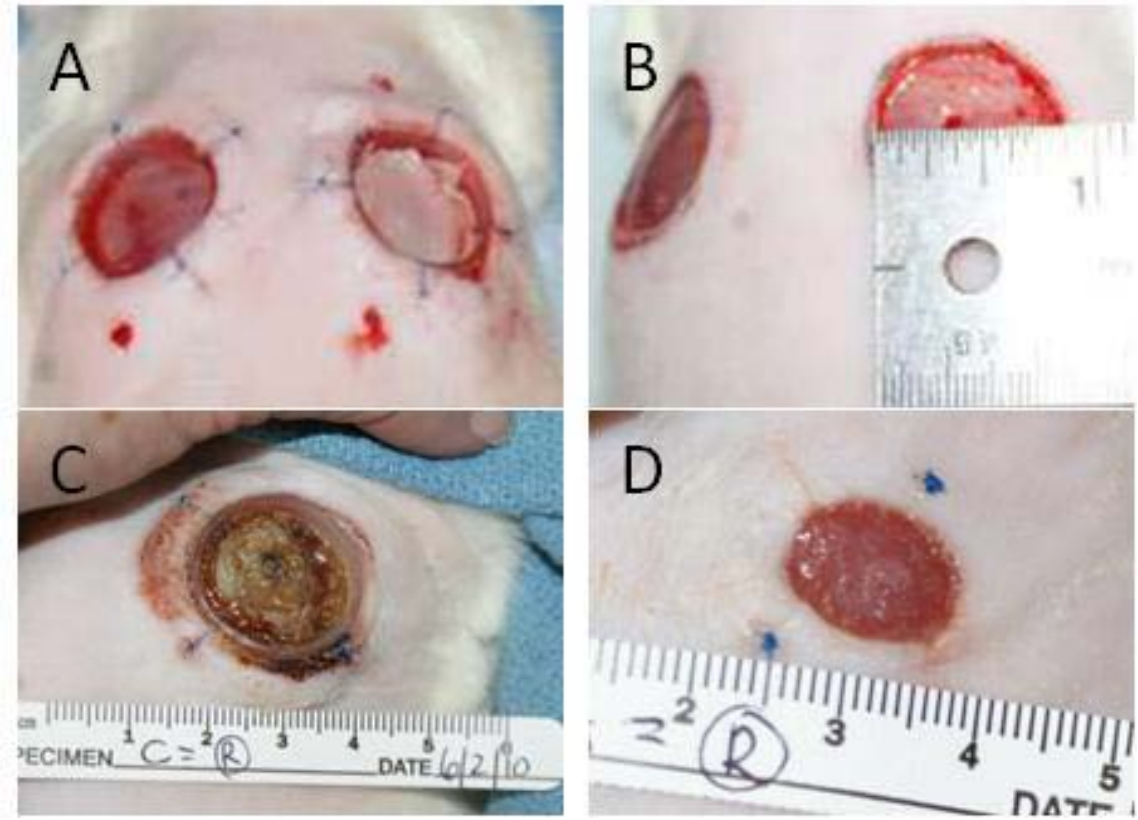

Figure 6.10. Splinted wound model in a hairless rat. a) Wounds were treated with SPI/PEO scaffold (right) or left untreated (left). b) Wounds measure approx. 20 mm in diameter (approx. 0.8 inches on the scale). c) SPI/PEO treated wound on day 15. d) Control wound on day 15.

These preliminary experiments have demonstrated that electrospun SPI/PEO scaffold invokes a similar wound healing response as Tegaderm™, or standard wound care, in the rat model. Further experiments may be able to identify benefits that manifest during the early stages of wound healing, such as during the acute inflammatory phase during the first 2 days post-wounding (Birch et al., 2005). Derrick et al. (2008) analyzed gene expression of wound tissue at day 2 post-wounding of 17-22 week-old male Zucker diabetic fatty (ZDF) rats. Each rat

received a 3cm-diameter full-thickness wound on the dorsum. In this model of impaired healing, rats received one of three treatments: vacuum-assisted closure, gauze under suction, or moist wound healing (control group). The control group was similar to ours, with the wound simply covered with Tegaderm™. Genes involved in pathways associated with inflammation mediated by cytokine and chemokine signaling, integrin signaling, B-cell activation, interleukin signaling, platelet-derived growth factor (PDGF) signaling, cytoskeletal regulation by Rho guanosine triphosphatase (Rho GTPase) and angiogenesis were significantly over-represented in all three groups.

It will be valuable to study more carefully the immune response induced by soy protein scaffolds at early time points, as soy protein contains immunogenic components. Soybean β-conglycinin includes a tridecapeptide sequence (MITLAIPVNKPGR) termed soymetide, which stimulates phagocytosis of human neutrophils (Tsuruki et al., 2003). Although very little research has been done on soymetides and interest has been in effects of their oral ingestion, they may be relevant as direct stimuli to cells in wounds if they are released.

Soy protein also contains major anti-inflammatory components. Lunasin, the 5 kDa, 43-amino acid peptide known for its anti-cancer activity based on its cell-binding RGD motif, also inhibits

inflammation by suppressing the NF-κB pathway in RAW 264.7 macrophages *in vitro*, completely inhibiting IL-6 production and significantly inhibiting IL-1β production with an IC_{50} of 13 μM (de Mejia and Dia, 2009). Lunasin also inhibits the production of reactive oxygen species (ROS) and the release of tumor necrosis factor alpha (TNF-α) as well as IL-6 in RAW 264.7 macrophages (Hernández-Ledesma et al., 2009).

Valsecchi et al. (2010) showed the *in vivo* anti-inflammatory properties of the soy isoflavone genistein, by treating diabetic mice with subcutaneous injections of 3 or 6 mg/kg of genistein daily for 3 weeks. After 3 weeks, the sciatic nerves were assayed for IL-1β, IL-6 and TNF-α levels. The production of these cytokines was elevated in diabetic mice, but was reverted to the normal level of non-diabetic controls with treatment with 3 or 6 mg/kg genistein. In the sciatic nerves as well as the brain and liver, a 50% higher level of ROS was seen in diabetic mice, but this was also reverted to non-diabetic levels by 3 mg/kg genistein. This study shows that while genistein does not affect the condition of chronic hyperglycemia in diabetes, it is effective in attenuating the inflammatory and oxidative state (Valsecchi et al., 2010).

It is also important to assess wound vascularization in more detail, since angiogenesis is a critical part of the early wound healing process. Histological staining shows blood vessels

macroscopically. Quantitative methods include analysis of vascular endothelial growth factor (VEGF) expression levels (e.g. Scherer et al., 2009; Wong et al., 2010), and immunohistochemical staining of angiogenesis markers such as platelet endothelial cell adhesion molecule 1 (PECAM-1) (Scherer et al., 2009) or lectin, a sugar that binds to endothelial cells and thus can reveal overall vascular structure (Papazoglou et al., 2008). Blood vessel density can be calculated from fluorescent micrographs by counting the number of vessels visualized in each high powered field of interest.

Investigation of how the electrospun SPI/PEO scaffold affects the early wound healing events of inflammation and vascularization will help us to understand some of the potential mechanisms of interaction between the scaffold and the cellular wound environment, and identify potential benefits of the scaffold in early wound healing.

6.4. Conclusions

We have demonstrated in preliminary pilot studies that electrospun SPI/PEO scaffolds are fully biocompatible and promote a similar wound healing response as the standard of care *in vivo* in a rat model. SPI/PEO scaffolds provide qualitative benefits of absorbing wound exudates and integrating easily into the wound defect. As such, they merit further investigation as a potential

new treatment modality, especially by assessing inflammation and angiogenesis during the early stage of wound healing.

It is widely acknowledged that there is no real “chronic” wound model to mimic the non-healing wounds that humans suffer. Therefore, at least to simulate aspects of the chronic wound environment, a model that limits contraction and allows for re-epithelialization would be more suitable. We have demonstrated this in a proof of concept using the splinted wound model. Larger animal models such as the pig, where feasible, may also provide a more valuable platform to evaluate the efficacy of electrospun SPI/PEO scaffolds.

Chapter 7. Conclusions and Recommendations for Future Work

7.1. Conclusions

The work in this thesis aimed to fulfill 3 specific aims as laid out in Chapter 2:

1) Fabricate a novel soy protein-based electrospun fibrous scaffold and characterize its mechanical properties, degradation behavior and *in vitro* biocompatibility.

2) Identify initial adhesion mechanisms of human dermal fibroblasts to SPI/PEO.

3) Evaluate electrospun SPI/PEO scaffolds *in vivo* using a rat wound healing model.

Specific Aim 1 was fulfilled by optimization of a solvent system, component ratios and electrospinning parameters in order to develop an electrospun fibrous scaffold based on soy protein isolate (SPI) as a renewable, abundant raw material with well-documented bioactive properties, with minimal addition of synthetic poly(ethylene oxide) (PEO) to increase chain entanglements in solution and facilitate polymerization. Parametric studies revealed an optimal concentration of 7% (w/v) SPI with 0.05% (w/v) PEO, using 1,1,1,3,3,3 Hexafluoro-2-propanol (HFP) as a solvent. This solvent system provided the benefits of producing protein solutions with

an indefinite shelf life, a reduction in the concentration of PEO required to produce consistent electrospun fibers compared to aqueous solvents such as NaOH, and ductile fibrous scaffolds that possess the important advantage of being stable in aqueous media without the need for further cross-linking. Just as importantly, they are capable of being degraded proteolytically. Also, the process of electrospinning does not alter the molecular weight distribution of native SPI, suggesting that the molecular structure remains intact throughout the simple fabrication process using HFP as a solvent. Electrospinning is the preferred fabrication method for our application of creating a scaffold for skin tissue regeneration due to its ability to generate a fibrous structure in the sub-micron to micron range that mimics the structure of native ECM, as well as its potential for scaling up in manufacturing. Electrospinning is highly suitable when a thin (~0.1 – 0.2 mm thickness) scaffold with a large surface area is desired, such as for skin repair.

The differential behavior of soy protein in HFP compared to NaOH may be at least partially attributed to HFP being a more effective solvent than NaOH, allowing for enhanced opening of the soy protein structure followed by the formation of more intricate physical bonds that serve to crosslink the fibers in the electrospun SPI/PEO scaffold. While stable physical crosslinking is not observed among other proteins electrospun from solutions in HFP, the presence of disulfide bridges that is characteristic of soy protein may contribute to this phenomenon. The presence of

disulfide bridges increases the size of aggregating peptides (Kuipers and Gruppen, 2008), and the breaking of these bonds may expose more surface area for chain entanglements to form.

Electrospun SPI/PEO scaffolds had fiber diameters in the range of 852 ± 373 nm when dry and 1473 ± 328 nm when hydrated for 3 h in 1X PBS. The tensile properties of electrospun SPI/PEO scaffolds are compatible with those of human skin. When dry, SPI/PEO scaffolds have an ultimate tensile strength (UTS) of 0.91 ± 0.39 MPa and strain to break of 7.53 ± 1.29 %. When wet, they have a UTS of 0.10 ± 0.05 MPa and ductility increases with a strain to break of 83.33 ± 21.18 %. These values are comparable to those reported for human skin, with a UTS of approx. 7.7 MPa (Adekogbe and Ghanem, 2005) and strain to break of approx. 100% (Diridollou et al., 2000). The tensile properties of SPI/PEO scaffolds remain similar after 14 days of hydration in aqueous media. Macroscopically, hydrated electrospun SPI/PEO scaffolds are “skin-like” in appearance and easy to handle, store and sterilize, making them attractive for use in a clinical setting.

In vitro, electrospun SPI/PEO scaffolds were shown to be biocompatible with human dermal fibroblasts alone and in co-culture with human epidermal fibroblasts. The proliferation rate and cytotypic morphology of fibroblasts were similar on SPI/PEO scaffolds as on other well-characterized biomaterials such as electrospun PLGA (synthetic) and gelatin (natural, animal

protein-derived), as well as on electrospun zein, another plant protein-derived scaffold. Fibroblasts attached and spread on all substrates, apparently receiving directional cues from each other instead of their randomly oriented fibrous substrates. Fibroblasts deposited their native extracellular matrix (ECM) onto SPI/PEO scaffolds, a response that is crucial to the tissue remodeling process. Thus, electrospun SPI/PEO scaffolds have been shown to be biocompatible as a scaffold for skin tissue regeneration, and a suitable platform for organotypic skin equivalent co-culture in *in vitro* models of skin.

Specific Aim 2 was approached by a global analysis of gene expression related to human ECM and adhesion molecules, using targeted PCR arrays, followed by validation with PCR analysis of specific genes up-regulated or highly expressed by fibroblasts on SPI and collagen I coated substrates after 2 h and 24 h of seeding. No substrate-significant differences were found at either time point. However, on both substrates, certain genes were similarly up-regulated at 24 h compared to 2 h. MMP-10 was the most highly up-regulated, approx. 1152-fold on SPI and 471-fold on collagen I. MMP-1 was also very highly up-regulated, although by orders of magnitude lower than MMP-10, 54-fold on SPI and 37-fold on collagen I. Tissue inhibitors of MMPs (TIMPs) were not significantly up-regulated at these time points. ECM proteins collagen and laminin, as well as integrin subunit α2, the predominant cell surface receptor for collagen,

were also up-regulated at 24 h. Taken together, these results point to an aggressive remodeling response by the fibroblasts to their immediate extracellular environment, a process necessary in the early stages of wound healing that is usually aided by macrophages and neutrophils that infiltrate the wound site. Importantly, SPI elicited a similar cellular response as the native ECM protein collagen and synthetic PLGA, suggesting that SPI as a biomaterial may be as suitable as these other well-established materials.

In the initial phase of remodeling, degradation occurs more rapidly than deposition of new ECM (Badylak et al., 2009). This is reflected in the cellular response observed in our experiments. However, it is not known whether the upregulation of integrin subunit α2 is in response to the substrate material directly, or to the presence of newly synthesized ECM proteins adsorbed onto the substrates. In the case of SPI, it may be possible that the intrinsic RGD motif contained in the peptide lunasin provides a specific adhesion site for the fibroblasts; however, unless this integrin-ligand interaction is specifically investigated, it cannot be assumed, and the very similar adhesion behavior across the substrates we tested suggests that adsorption of new ECM secreted by the fibroblasts may play a large role in the initial adhesion process.

Specific Aim 3 was fulfilled at a preliminary level in evaluations that were carried out to the end of study at complete wound closure. Electrospun SPI/PEO scaffolds were evaluated against Tegaderm™ wound dressing, a standard in wound care, as a control in a full-thickness excision wound model in the hairless rat. SPI/PEO scaffolds promoted a slightly but not significantly faster initial wound closure than the control, although wounds in both groups healed completely by post-operative day 18, while the neodermis continued to be replaced by thicker scar tissue up to the end of our study at day 31. The similar quantitative response in both groups was corroborated by non-invasive optical measurements using functional near infrared spectroscopy (fNIR). SPI/PEO scaffolds were optically transparent to the fNIR sensors and did not present any background signal, which was a desirable advantage in using optical techniques for measurement as absorbance at the wound site could be measured directly through the scaffold without the need to remove the scaffold.

Electrospun SPI/PEO scaffolds provided qualitative benefits over the control, by virtue of its natural, plant protein-derived material and electrospun fibrous structure. The tensile properties of SPI/PEO scaffolds were a much closer match to native skin than those of Tegaderm™, and SPI/PEO scaffolds were much more compliant to the wound shape, absorbing wound exudates and thus preventing irritation at the wound site. SPI/PEO scaffolds integrated well with the

wound and detached naturally with the formed encrustation at day 7 that occurred in both treatment groups.

Clinically, electrospun SPI/PEO scaffolds would be applied in a single procedure, avoiding the complications of repeat applications such as with commercial composite skin substitutes. The presence of the scaffold may aid in retaining moisture; however, as it dries, it becomes part of the encrustation or scab that forms, and this may or may not interfere with granulation tissue formation underneath the scaffold and keratinocyte migration into the healing wound. If the wound needs to be surgically cleaned regularly, the scaffold may need to be removed with the debrided tissue, and a fresh scaffold re-applied, until the wound is sufficiently healed to continue the process without the support of the scaffold.

These scaffolds provide a “breathable” interface between the wound and the external environment, which allow for a normal course of healing without the disadvantages of occlusive dressings that do not come in direct contact with the open wound. By design as a permanent scaffold, electrospun SPI/PEO is able to present structural and molecular cues to the cells in a regenerating wound environment. It is therefore promising as a new type of treatment for non-healing wounds, and further studies will help to elucidate potential mechanisms by which it

promotes wound healing at a cellular and/or molecular level.

SPI as a raw material provides several advantages over other materials such as collagen, as it bypasses the concerns raised with animal-derived proteins, is abundantly available and renewable, and comes at a significantly lower cost. Its versatility in processing, its biodegradability and bioactivity also render it preferable to synthetic materials. Therefore, it serves as a viable alternative to currently available, more expensive materials used in wound healing scaffolds.

7.2. Recommendations for future work

While our results have been encouraging in that electrospun SPI/PEO scaffolds promote a similar response from human dermal fibroblasts *in vitro* and in a full-thickness excision wound *in vivo* in comparison to well-established standard materials, further investigation is needed to correlate cellular responses to the properties of the scaffold. *In vitro*, function-blocking studies may be performed using disintegrins (Marcinkiewicz, 2005; Surażyński et al., 2005; Sarkar, 2006) or antibodies to specific integrins (e.g. Choi et al., 2007; Kim et al., 2008) identified as potentially highly involved in mediating initial cellular adhesion to foreign substrates, as discussed in Chapter 5. Since integrin $\alpha 2\beta 1$ is the predominant receptor for collagen (Sethi et al., 2002) and

α2 was the most highly up-regulated integrin subunit on SPI and collagen at 24 h, this integrin is a worthwhile target for inhibition assays. *In vitro*, integrin α2β1 mediates collagen gel contraction, and application anti-α2β1 antibody to fibroblasts reverts their attached morphology from elongated and bipolar to rounded within 1 h (Fujimura et al., 2007). It would be valuable to investigate whether blocking integrins produces such a significant effect on fibroblast attachment to SPI.

It would also be worthwhile to clarify whether fibroblasts are attaching to foreign substrates via integrins directly or to ECM adsorbed onto the substrates. The rate of deposition of new ECM by fibroblasts onto SPI and other foreign substrates, including glass (which is inert and hydrophilic but without biochemical cues), would first need to be established, and this time course would then be correlated with the time progression of expression of integrin receptor subunits by fibroblasts attaching on these substrates.

In vivo, the wound healing events occurring at the early stage of inflammation, during the first 2 days, needs to be investigated in more detail to identify the differences between SPI/PEO treated and control groups. Acute inflammatory responses, if they occur, could be detected within 24 hours post-wounding (Birch et al., 2005). IL-6 and IL-1β are commonly targeted as measures of

inflammatory response, important for cell recruitment (e.g. de Mejia and Dia, 2009; Valsecchi et al., 2010), as is tumor necrosis factor alpha (TNF-α) (e.g. Hernández-Ledesma et al., 2009). These cytokines may be assayed from wound fluids or supernatants of homogenized wound tissue using enzyme-linked immunosorbent assays (ELISA) or RT-PCR. Analysis time points may be extended to encompass days 1, 2, 4, 7, 14 and 21 post-wounding as well as end of study, to track the progression of wound healing (Birch et al., 2005). Recruitment of inflammatory cells may be detected from histological biopsies by staining for CD45-positive cells (Scherer et al., 2009).

As discussed in Chapter 6, vascularization should be assessed at the same time points to determine whether SPI/PEO scaffolds promote this response to a greater extent than the control. While fNIR provides indirect measurements of vascularity by correlating optical absorbance to hemoglobin concentration, more direct methods may also be employed, such as RT-PCR analysis of VEGF expression in wound tissue homogenate (Scherer et al., 2009; Wong et al., 2010), or immunofluorescent staining for platelet endothelial cell adhesion molecule 1 (PECAM-1) (Scherer et al., 2009) or lectin (Papazoglou et al., 2008).

Further experiments in the rat should also be done incorporating the splinted ring model (Shinzawa et al., 2007; Wong et al., 2010) in order to prevent contraction and allow for healing

by granulation tissue formation and re-epithelialization. This model not only simulates the human wound scenario more closely, but also increases the time window in which to detect differences between treatment groups at each of the stages in wound healing that might be missed in the regular rat model where contraction is the dominant mechanism of healing.

Histological biopsies at earlier time points would also show the formation of granulation tissue and the migration of keratinocytes in wounds treated with or without the scaffold, to detect whether the new growth integrates with the scaffold, and whether the rate of new growth is affected by the presence of the scaffold. Image analysis of the biopsies would show whether the scaffold serves as a support structure to enhance growth or whether it acts as a physical barrier to slow down growth of new skin tissue in the wound.

While beyond the scope of this thesis, a larger animal model, especially the pig, is highly encouraged in further evaluations of electrospun SPI/PEO scaffolds in wound healing. The pig is a desirable model in simulating human wound healing because pig skin and human skin have a comparable dermal-epidermal thickness ratio ranging from 10:1 to 13:1, with similar epidermal turnover time (Sullivan et al., 2001). The large surface of pigs allows them to receive multiple experimental wounds, which along with frequent handling causes great physiological stress,

which may also simulate the condition of wounded patients with severe illnesses (Sullivan et al., 2001). Data from a pig model may also correlate better with a human scenario, as comparisons of animal models revealed that out of 25 wound therapies, the pig model was in agreement with human studies 78% of the time compared with 53% for small-mammal studies (Sullivan et al., 2001).

List of References

Adekogbe I, Ghanem A. Fabrication and characterization of DTBP-crosslinked chitosan scaffolds for skin tissue engineering. Biomaterials. 2005 Dec;26(35):7241-50.

Amano S, Ogura Y, Akutsu N, Nishiyama T. Quantitative analysis of the synthesis and secretion of type VII collagen in cultured human dermal fibroblasts with a sensitive sandwich enzyme-linked immunoassay. Exp Dermatol. 2007 Feb;16(2):151-5.

Armstrong WB, Wan XS, Kennedy AR, Taylor TH, Meyskens FL Jr. Development of the Bowman-Birk inhibitor for oral cancer chemoprevention and analysis of Neu immunohistochemical staining intensity with Bowman-Birk inhibitor concentrate treatment. Laryngoscope. 2003 Oct;113(10):1687-702.

Assoian RK, Klein EA. Growth control by intracellular tension and extracellular stiffness. Trends Cell Biol. 2008, 18:347-352.

Ayres CE, Jha BS, Sell SA, Bowlin GL, Simpson DG. Nanotechnology in the design of soft tissue scaffolds: innovations in structure and function. Wiley Interdiscip Rev Nanomed Nanobiotechnol. 2010 Jan;2(1):20-34.

Badylak SF, Freytes DO, Gilbert TW. Extracellular matrix as a biological scaffold material: Structure and function. Acta Biomater. 2009 Jan;5(1):1-13.

Baum CL, Arpey CJ. Normal cutaneous wound healing: clinical correlation with cellular and molecular events. Dermatol Surg. 2005 Jun;31(6):674-86; discussion 686.

Bawadi HA, Antunes TM, Shih F, Losso JN. In vitro inhibition of the activation of Pro-matrix Metalloproteinase 1 (Pro-MMP-1) and Pro-matrix metalloproteinase 9 (Pro-MMP-9) by rice and soybean Bowman-Birk inhibitors. J Agric Food Chem. 2004 Jul 28;52(15):4730-6.

Bell E, Ivarsson B, Merrill C. Production of a tissue-like structure by contraction of collagen lattices by human fibroblasts of different proliferative potential in vitro. Proc. Natl. Acad. Sci. USA Vol. 76, No. 3, pp. 1274-1278, March 1979.

Bell E, Ehrlich HP, Buttle DJ, Nakatsuji T. Living tissue formed in vitro and accepted as skin-equivalent tissue of full thickness. Science. 1981 Mar 6;211(4486):1052-4.

Bhardwaj N, Kundu SC. Electrospinning: a fascinating fiber fabrication technique. Biotechnol Adv. 2010 May-Jun;28(3):325-47.

Birch M, Tomlinson A, Ferguson MW. Animal models for adult dermal wound healing. Methods Mol Med. 2005, 117:223-235.

Bischofs IB, Schwarz US. Cell organization in soft media due to active mechanosensing. Proc Natl Acad Sci USA 100 (2003), pp. 9274–9279.

Blackwood KA, McKean R, Canton I, Freeman CO, Franklin KL, Cole D, Brook I, Farthing P, Rimmer S, Haycock JW, Ryan AJ, MacNeil S. Development of biodegradable electrospun scaffolds for dermal replacement. Biomaterials. 2008, 29:3091-3104.

Boehnke K, Mirancea N, Pavesio A, Fusenig NE, Boukamp P, Stark HJ. Effects of fibroblasts and microenvironment on epidermal regeneration and tissue function in long-term skin equivalents. Eur J Cell Biol. 2007, 86:731-746.

Bott K, Upton Z, Schrobback K, Ehrbar M, Hubbell JA, Lutolf MP, Rizzi SC. The effect of matrix characteristics on fibroblast proliferation in 3D gels. Biomaterials. 2010 Nov;31(32):8454-64.

Böttcher-Haberzeth S, Biedermann T, Reichmann E. Tissue engineering of skin. Burns. 2010 Jun;36(4):450-60.

Brownlee C. Role of the extracellular matrix in cell-cell signalling: paracrine paradigms. Curr Opin Plant Biol. 2002 Oct;5(5):396-401.

Cai N, Wong CC, Tan SC, Chan V, Liao K. Temporal effect of functional blocking of beta1 integrin on cell adhesion strength under serum depletion. Langmuir. 2009 Sep 15;25(18):10939-47.

Caillard R, Remondetto GE, Mateescu MA, Subirade M. Characterization of amino cross-linked soy protein hydrogels. J Food Sci. 2008 Jun;73(5):C283-91.

Caillard R, Mateescu MA, Subirade M. Maillard-type cross-linked soy protein hydrogels as devices for the release of ionic compounds: an in vitro study. Food Res Int. 2010 Dec;43(10):2349-55.

Cao B, Yin J, Yan S, Cui L, Chen X, Xie Y. Porous scaffolds based on cross-linking of poly(L-glutamic acid). Macromol Biosci. DOI: 10.1002/mabi.201000389

Carrino DA, Sorrell JM, Caplan AI. Age-related changes in the proteoglycans of human skin. Arch Biochem Biophys. 2000 Jan 1;373(1):91-101.

Chastain SR, Kundu AK, Dhar S, Calvert JW, Putnam AJ. Adhesion of mesenchymal stem cells to polymer scaffolds occurs via distinct ECM ligands and controls their osteogenic differentiation. J Biomed Mater Res A. 2006, 78:73-85.

Chen H, Huang J, Yu J, Liu S, Gu P. Electrospun chitosan-graft-poly (ε-caprolactone)/poly (ε-caprolactone) cationic nanofibrous mats as potential scaffolds for skin tissue engineering. Int J Biol Macromol. 2011 Jan 1;48(1):13-9.

Chen L, Remondetto G, Rouabhia M, Subirade M. Kinetics of the breakdown of cross-linked soy protein films for drug delivery. Biomaterials. 2008, 29:3750-56.

Chen L, Subirade M. Elaboration and characterization of soy/zein protein microspheres for controlled nutraceutical delivery. Biomacromolecules. 2009 Dec 14;10(12):3327-34.

Chen L, Hébrard G, Beyssac E, Denis S, Subirade M. In vitro study of the release properties of soy-zein protein microspheres with a dynamic artificial digestive system. J Agric Food Chem. 2010 Sep 8;58(17):9861-7.

Chen P, Parks WC. Role of matrix metalloproteinases in epithelial migration. J Cell Biochem. 2009 Dec 15;108(6):1233-43.

Choi S, Vilaire G, Marcinkiewicz C, Winkler JD, Bennett JS, DeGrado WF. Small molecule inhibitors of integrin alpha2beta1. J Med Chem. 2007, 50:5457-62.

Chung TW, Chang YL. Silk fibroin/chitosan-hyaluronic acid versus silk fibroin scaffolds for tissue engineering: promoting cell proliferations in vitro. J Mater Sci Mater Med. 2010 Apr;21(4):1343-51.

Clark GB, Thompson G Jr, Roux SJ. Signal transduction mechanisms in plants: an overview. Curr Sci. 2001 Jan 25;80(2):170-7.

Coimbra P, Ferreira P, de Sousa HC, Batista P, Rodrigues MA, Correia IJ, Gil MH. Preparation and chemical and biological characterization of a pectin/chitosan polyelectrolyte complex scaffold for possible bone tissue engineering applications. Int J Biol Macromol. 2011 Jan 1;48(1):112-8.

Cross SE, Naylor IL, Coleman RA, Teo TC. An experimental model to investigate the dynamics of wound contraction. Br J Plast Surg. 1995 Jun;48(4):189-97.

Cui W, Zhou Y, Chang J. Electrospun nanofibrous materials for tissue engineering and drug delivery. Sci. Technol. Adv. Mater. 11 (2010) 014108 (11pp) doi:10.1088/1468-6996/11/1/014108

Curciarello R, Lareu JF, Fossati CA, Docena GH, Petruccelli S. Immunochemical characterization of Glycine max L. Merr. var Raiden, as a possible hypoallergenic substitute for cow's milk-allergic patients. Clin Exp Allergy. 2008 Sep;38(9):1559-65.

Curt S, Subirade M, Rouabhia M. Production and in vitro evaluation of soy protein–based biofilms as a support for human keratinocyte and fibroblast culture. Tissue Eng Part A. 2009 Jun;15(6):1223-32.

Curtis AS, Dalby MJ, Gadegaard N. Nanoprinting onto cells. J R Soc Interface. 2006 Jun 22;3(8):393-8.

Davidson JM. Animal models for wound repair. Arch Dermatol Res. 1998, 290 Suppl:S1-11.

de Lumen BO. Lunasin: a cancer-preventive soy peptide. Nutr Rev. 2005 Jan;63(1):16-21.

de Lumen BO, Galvez AF. Soybean protein nutraceuticals. Patent US 6,391,848 B1 (May 21, 2002)

de Mejia EG, Dia VP. Lunasin and lunasin-like peptides inhibit inflammation through suppression of NF-kappaB pathway in the macrophage. Peptides. 2009 Dec;30(12):2388-98.

Derrick KL, Norbury K, Kieswetter K, Skaf J, McNulty AK. Comparative analysis of global gene expression profiles between diabetic rat wounds treated with vacuum-assisted closure therapy, moist wound healing or gauze under suction. Int Wound J 2008;5:615–624.

Dhandayuthapani B, Krishnan UM, Sethuraman S. Fabrication and characterization of chitosan-gelatin blend nanofibers for skin tissue engineering. J Biomed Mater Res B Appl Biomater. 2010 Jul;94(1):264-72.

Di Toro R, Betti V, Spampinato S. Biocompatibility and integrin-mediated adhesion of human osteoblasts to poly(DL-lactide-co-glycolide) copolymers. Eur J Pharm Sci. 2004, 21:161-169.

Dia VP, Berhow MA, Gonzalez De Mejia E. Bowman-Birk inhibitor and genistein among soy compounds that synergistically inhibit nitric oxide and prostaglandin E2 pathways in lipopolysaccharide-induced macrophages. J Agric Food Chem. 2008 Dec 24;56(24):11707-17.

Diridollou S, Patat F, Gens F, Vaillant L, Black D, Lagarde JM, Gall Y, Berson M. In vivo model of the mechanical properties of the human skin under suction Skin Res Technol. 2000 Nov;6(4):214-221.

Dittmann K, Löffler H, Bamberg M, Rodemann HP. Bowman-Birk proteinase inhibitor (BBI) modulates radiosensitivity and radiation-induced differentiation of human fibroblasts in culture. Radiother Oncol. 1995 Feb;34(2):137-43.

Dorsett-Martin WA, Wysocki AB. 2008, ‘Rat models of skin wound healing’, in Sourcebook of Models for Biomedical Research, ed. Conn PM, Humana Press Inc., Totowa, NJ; 631-638.

Emmerson E, Campbell L, Ashcroft GS, Hardman MJ. The phytoestrogen genistein promotes wound healing by multiple independent mechanisms. Mol Cell Endocrinol. 2010 Jun 10;321(2):184-93.

Enoch S, Shaaban H, Dunn KW. Informed consent should be obtained from patients to use products (skin substitutes) and dressings containing biological material. J Med Ethics. 2005 Jan;31(1):2-6.

Fernández P, Pullarkat PA, Ott A. A master relation defines the nonlinear viscoelasticity of single fibroblasts. Biophys J. 2006 May 15;90(10):3796-805.

Fisher GJ, Quan T, Purohit T, Shao Y, Cho MK, He T, Varani J, Kang S, Voorhees JJ. Collagen fragmentation promotes oxidative stress and elevates matrix metalloproteinase-1 in fibroblasts in aged human skin. Am J Pathol. 2009 Jan;174(1):101-14.

Fonder MA, Lazarus GS, Cowan DA, Aronson-Cook B, Kohli AR, Mamelak AJ. Treating the chronic wound: A practical approach to the care of nonhealing wounds and wound care dressings. J Am Acad Dermatol. 2008 Feb;58(2):185-206.

Fong H, Chun I, Reneker DH. Beaded nanofibers formed during electrospinning. Polymer 40 (1999) 4585–4592.

Fujimura T, Moriwaki S, Imokawa G, Takema Y. Crucial role of fibroblast integrins alpha2 and beta1 in maintaining the structural and mechanical properties of the skin. J Dermatol Sci. 2007 Jan;45(1):45-53.

Fung WY, Yuen KH, Liong MT. Characterization of fibrous residues from agrowastes and the production of nanofibers. J Agric Food Chem. 2010 Jul 14;58(13):8077-84.

Gailit J, Clark RA. Studies in vitro on the role of alpha v and beta 1 integrins in the adhesion of human dermal fibroblasts to provisional matrix proteins fibronectin, vitronectin, and fibrinogen. J Invest Dermatol. 1996, 106:102-108.

Gailit J, Clarke C, Newman D, Tonnesen MG, Mosesson MW, Clark RA. Human fibroblasts bind directly to fibrinogen at RGD sites through integrin alpha(v)beta3. Exp Cell Res. 1997, 232:118-126.

Galiano RD, Michaels J 5th, Dobryansky M, Levine JP, Gurtner GC. Quantitative and reproducible murine model of excisional wound healing. Wound Repair Regen. 2004 Jul-Aug;12(4):485-92.

Galvez AF, Chen N, Macasieb J, de Lumen BO. Chemopreventive property of a soybean peptide (lunasin) that binds to deacetylated histones and inhibits acetylation. Cancer Res. 2001 Oct 15;61(20):7473-8.

Gangatirkar P, Paquet-Fifield S, Li A, Rossi R, Kaur P. Establishment of 3D organotypic cultures using human neonatal epidermal cells. Nat Protoc. 2007, 2:178-186.

Garcia Y, Wilkins B, Collighan RJ, Griffin M, Pandit A. Towards development of a dermal rudiment for enhanced wound healing response. Biomaterials. 2008, 29:857-868.

García-Esteo F, Pascual G, Gallardo A, San-Román J, Buján J, Bellón JM. A biodegradable copolymer for the slow release of growth hormone expedites scarring in diabetic rats. J Biomed Mater Res B Appl Biomater. 2007, 81:291-304.

Gelse K, Pöschl E, Aigner T. Collagens--structure, function, and biosynthesis. Adv Drug Deliv Rev. 2003 Nov 28;55(12):1531-46.

Gilliver SC, Ruckshanthi JP, Hardman MJ, Zeef LA, Ashcroft GS. 5alpha-dihydrotestosterone (DHT) retards wound closure by inhibiting re-epithelialization. J Pathol. 2009 Jan;217(1):73-82.

Gong S, Wang H, Sun Q, Xue ST, Wang JY. Mechanical properties and in vitro biocompatibility of porous zein scaffolds. Biomaterials. 2006 Jul;27(20):3793-9.

Gong SJ, Sun SX, Sun QS, Wang JY, Liu XM, Liu GY. Tablets Based on Compressed Zein Microspheres for Sustained Oral Administration: Design, Pharmacokinetics, and Clinical Study. J Biomater Appl. 2010 Apr 23. DOI: 10.1177/0885328210363504

Gottrup F, Apelqvist J, Price P. Outcomes in controlled and comparative studies on non-healing wounds: recommendations to improve the quality of evidence in wound management. J Wound Care. 2010 Jun;19(6):237-68.

Gran B, Tabibzadeh N, Martin A, Ventura ES, Ware JH, Zhang GX, Parr JL, Kennedy AR, Rostami AM. The protease inhibitor, Bowman-Birk Inhibitor, suppresses experimental autoimmune encephalomyelitis: a potential oral therapy for multiple sclerosis. Mult Scler. 2006 Dec;12(6):688-97.

Groth T, Seifert B, Malsch G, Albrecht W, Paul D, Kostadinova A, Krasteva N, Altankov G. Interaction of human skin fibroblasts with moderate wettable polyacrylonitrile--copolymer membranes. J Biomed Mater Res. 2002 Aug;61(2):290-300.

Guo R, Xu S, Ma L, Huang A, Gao C. The healing of full-thickness burns treated by using plasmid DNA encoding VEGF-165 activated collagen-chitosan dermal equivalents. Biomaterials. 2011 Feb;32(4):1019-31.

Guo Y, Li M, Mylonakis A, Han J, MacDiarmid AG, Chen X, Lelkes PI, Wei Y. Electroactive oligoaniline-containing self-assembled monolayers for tissue engineering applications. Biomacromolecules. 2007 Oct;8(10):3025-34.

Hadjipanayi E, Mudera V, Brown RA. Close dependence of fibroblast proliferation on collagen scaffold matrix stiffness. J Tissue Eng Regen Med. 2009 Feb;3(2):77-84.

Hakki SS, Hakki EE, Nohutcu RM. Regulation of matrix metalloproteinases and tissue inhibitors of matrix metalloproteinases by basic fibroblast growth factor and dexamethasone in periodontal ligament cells. J Periodontal Res. 2009 Dec;44(6):794-802.

Han CM, Zhang LP, Sun JZ, Shi HF, Zhou J, Gao CY. Application of collagen-chitosan/fibrin glue asymmetric scaffolds in skin tissue engineering. J Zhejiang Univ Sci B. 2010 Jul;11(7):524-30.

Han J, Lazarovici P, Pomerantz C, Chen X, Wei Y, Lelkes PI. Co-Electrospun Blends of PLGA, Gelatin, and Elastin as Potential Nonthrombogenic Scaffolds for Vascular Tissue Engineering. Biomacromolecules. 2011 Feb 14;12(2):399-408.

Hannafin JA, Attia EA, Henshaw R, Warren RF, Bhargava MM. Effect of cyclic strain and plating matrix on cell proliferation and integrin expression by ligament fibroblasts. J Orthop Res. 2006 Feb;24(2):149-58.

Helary C, Bataille I, Abed A, Illoul C, Anglo A, Louedec L, Letourneur D, Meddahi-Pellé A, Giraud-Guille MM. Concentrated collagen hydrogels as dermal substitutes. Biomaterials. 2010 Jan;31(3):481-90.

Henderson PW, Nagineni VV, Harper A, Bavinck N, Sohn AM, Krijgh DD, Jimenez N, Weinstein AL, Spector JA. Development of an acellular bioengineered matrix with a dominant vascular pedicle. J Surg Res. 2010 Nov;164(1):1-5.

Hernández-Ledesma B, Hsieh CC, de Lumen BO. Lunasin, a novel seed peptide for cancer prevention. Peptides. 2009, 30:426-30.

Holzbeierlein JM, McIntosh J, Thrasher JB. The role of soy phytoestrogens in prostate cancer. Curr Opin Urol. 2005, 15:17-22.

Hua Y, Yuang Y, Qiu A, Liu X. Properties of soy protein isolate prepared from aqueous alcohol washed soy flakes, Food Res Int. 2005, 38: 273-9.

Hynes RO. Integrins: bidirectional, allosteric signaling machines. Cell. 2002 Sep 20;110(6):673-87.

Ingber D. Integrins as mechanochemical transducers. Curr Opin Cell Biol. 1991, 3:841-8.

Jiang G, Huang AH, Cai Y, Tanase M, Sheetz MP. Rigidity sensing at the leading edge through alphavbeta3 integrins and RPTPalpha. Biophys J. 2006 Mar 1;90(5):1804-9.

Jiang H, Zhao P, Zhu K. Fabrication and characterization of zein-based nanofibrous scaffolds by an electrospinning method. Macromol Biosci. 2007 Apr 10;7(4):517-25.

Jiang Q, Reddy N, Yang Y. Cytocompatible cross-linking of electrospun zein fibers for the development of water-stable tissue engineering scaffolds. Acta Biomater. 2010 Oct;6(10):4042-51.

Jiang Y, Tang C-H, Wen Q-B, Li L, Yang X-Q. Effect of processing parameters on the properties of transglutaminase-treated soy protein isolate films, Innovat Food Sci Emerg Tech. 2007, 8: 218-25

Kao B, Kadomatsu K, Hosaka Y. Construction of synthetic dermis and skin based on a self-assembled peptide hydrogel scaffold. Tissue Eng Part A. 2009 Sep;15(9):2385-96.

Kim HK, Oh DS, Lee SB, Ha JM, Joe YA. Antimigratory effect of TK1-2 is mediated in part by interfering with integrin alpha2beta1. Mol Cancer Ther. 2008, 7:2133-41.

Kluger PJ, Wyrwa R, Weisser J, Maierle J, Votteler M, Rode C, Schnabelrauch M, Walles H, Schenke-Layland K. Electrospun poly(D/L-lactide-co-L-lactide) hybrid matrix: a novel scaffold material for soft tissue engineering. J Mater Sci Mater Med. 2010 Sep;21(9):2665-71.

Koombhongse S, Liu W, Reneker DH. Flat polymer ribbons and other shapes by electrospinning, J Polymer Sci: Part B: Polymer Phys. 2001, 39: 2598–2606.

Koskela A, Engström K, Hakelius M, Nowinski D, Ivarsson M. Regulation of fibroblast gene expression by keratinocytes in organotypic skin culture provides possible mechanisms for the antifibrotic effect of reepithelialization. Wound Repair Regen. 2010 Sep-Oct;18(5):452-9.

Kuipers BJ, Gruppen H. Identification of strong aggregating regions in soy glycinin upon enzymatic hydrolysis. J Agric Food Chem. 2008 May 28;56(10):3818-27.

Kumbar SG, Nukavarapu SP, James R, Nair LS, Laurencin CT. Electrospun poly(lactic acid-co-glycolic acid) scaffolds for skin tissue engineering. Biomaterials. 2008 Oct;29(30):4100-7.

Lai LF, Guo HX. Preparation of new 5-fluorouracil-loaded zein nanoparticles for liver targeting. Int J Pharm. 2011 Feb 14;404(1-2):317-23.

Lazopoulos KA, Stamenović D. Durotaxis as an elastic stability phenomenon. J Biomech. 2008;41(6):1289-94.

Lee JW, Serna F, Nickels J, Schmidt CE. Carboxylic acid-functionalized conductive polypyrrole as a bioactive platform for cell adhesion. Biomacromolecules. 2006 Jun;7(6):1692-5.

Lee YK, Kim SY, Kim KH, Chun BH, Lee KH, Oh DJ, Chung N. Use of soybean protein hydrolysates for promoting proliferation of human keratinocytes in serum-free medium. Biotechnol Lett. 2008 Nov;30(11):1931-6.

Lelkes PI, Li M, Perets A, Lin L, Han J, Woerdeman DL. 2008, ‘Electrospinning of natural proteins for tissue engineering scaffolding’ in Handbook of Natural-based Polymers for Biomedical Applications, ed. Reis RL, Woodhead Publishing Ltd, Cambridge, UK; 446-482.

Leong MF, Lim TC, Chian KS. Manufacturing three-dimensional scaffolds using electrospinning at low temperatures. Patent Cooperation Treaty (PCT) Application, PCT/SG2007/000413, 2006.

Leong MF, Rasheed MZ, Lim TC, Chian KS. In vitro cell infiltration and in vivo cell infiltration and vascularization in a fibrous, highly porous poly(D,L-lactide) scaffold fabricated by cryogenic electrospinning technique. J Biomed Mater Res A. 2009 Oct;91(1):231-40.

Leong MF, Chan WY, Chian KS, Rasheed MZ, Anderson JM. Fabrication and in vitro and in vivo cell infiltration study of a bilayered cryogenic electrospun poly(D,L-lactide) scaffold. J Biomed Mater Res A. 2010 Sep 15;94(4):1141-9.

Li B, Davidson JM, Guelcher SA. The effect of the local delivery of platelet-derived growth factor from reactive two-component polyurethane scaffolds on the healing in rat skin excisional wounds. Biomaterials. 2009 Jul;30(20):3486-94.

Li M, Mondrinos MJ, Gandhi MR, Ko FK, Weiss AS, Lelkes PI. Electrospun protein fibers as matrices for tissue engineering. Biomaterials. 2005 Oct;26(30):5999-6008.

Li M, Guo Y, Wei Y, MacDiarmid AG, Lelkes PI. Electrospinning polyaniline-contained gelatin nanofibers for tissue engineering applications. Biomaterials. 2006 May;27(13):2705-15.

Liang WH, Kienitz BL, Penick KJ, Welter JF, Zawodzinski TA, Baskaran H. Concentrated collagen-chondroitin sulfate scaffolds for tissue engineering applications. J Biomed Mater Res A. 2010 Sep 15;94(4):1050-60.

Lindblad WJ. Considerations for selecting the correct animal model for dermal wound-healing studies. J Biomater Sci Polym Ed. 2008;19(8):1087-96.

Liu BS, Yao CH, Fang SS. Evaluation of a non-woven fabric coated with a chitosan bi-layer composite for wound dressing. Macromol Biosci. 2008 May 13;8(5):432-40.

Liu X, Sun Q, Wang H, Zhang L, Wang JY. Microspheres of corn protein, zein, for an ivermectin drug delivery system. Biomaterials. 2005 Jan;26(1):109-15.

Liu Y, Dammann C, Bhattacharyya MK. The matrix metalloproteinase gene GmMMP2 is activated in response to pathogenic infections in soybean. Plant Physiol. 2001 Dec;127(4):1788-97.

Losso JN, Munene CN, Bansode RR, Bawadi HA. Inhibition of matrix metalloproteinase-1 activity by the soybean Bowman-Birk inhibitor. Biotechnol Lett. 2004 Jun;26(11):901-5.

Lowery JL, Datta N, Rutledge GC. Effect of fiber diameter, pore size and seeding method on growth of human dermal fibroblasts in electrospun poly(ε -caprolactone) fibrous mats. Biomaterials 31 (2010) 491–504.

Luo LH, Zhang YF, Wang XM, Wan YQ, Chang PC, Anderson DR, Chen Y. Preparation, characterization, and in vitro and in vivo evaluation of cellulose/soy protein isolate composite sponges. J Biomater Appl. 2010 Feb;24(6):503-26.

Ma L, Shi Y, Chen Y, Zhao H, Gao C, Han C. In vitro and in vivo biological performance of collagen-chitosan/silicone membrane bilayer dermal equivalent. J Mater Sci Mater Med. 2007 Nov;18(11):2185-91.

Machida-Sano I, Matsuda Y, Namiki H. In vitro adhesion of human dermal fibroblasts on iron cross-linked alginate films. Biomed Mater. 2009 Apr;4(2):025008.

Magee PJ, Rowland IR. Phyto-oestrogens, their mechanism of action: current evidence for a role in breast and prostate cancer. Br J Nutr. 2004 Apr;91(4):513-31.

Mallikarjun Gouda KG, Gowda LR, Rao AG, Prakash V. Angiotensin I-converting enzyme inhibitory peptide derived from glycinin, the 11S globulin of soybean (Glycine max). J Agric Food Chem. 2006 Jun 28;54(13):4568-73.

Maltais A, Remondetto GE, Subirade M. Mechanisms involved in the formation and structure of soya protein cold-set gels: A molecular and supramolecular investigation. Food Hydrocolloids. 2007, 22: 550-9.

Maltais A, Remondetto GE, Subirade M. Tabletted soy protein cold-set hydrogels as carriers of nutraceutical substances. Food Hydrocolloids. 2010 Jul;24(5):518-24.

Marcinkiewicz C. Functional characteristic of snake venom disintegrins: potential therapeutic implication. Curr Pharm Des. 2005, 11:815-27.

Margadant C, Charafeddine RA, Sonnenberg A. Unique and redundant functions of integrins in the epidermis. FASEB J. 2010 Nov;24(11):4133-52.

Mauri A N, Añon M C. Effect of solution pH on solubility and some structural properties of soybean protein isolate films. J Sci Food Agric. 2006, 86:1064-72.

McGrath JA, Eady RAJ, Pope FM. 2004, 'Anatomy and organization of human skin' in Rook's textbook of dermatology, 7th Ed., eds. Burns T, Breathnach S, Cox N, Griffiths C, Blackwell Publishing, Oxford, UK; 45-128.

Medina A, Ghaffari A, Kilani RT, Ghahary A. The role of stratifin in fibroblast-keratinocyte interaction. Mol Cell Biochem. 2007 Nov;305(1-2):255-64.

Menke NB, Ward KR, Witten TM, Bonchev DG, Diegelmann RF. Impaired wound healing. Clin Dermatol. 2007 Jan-Feb;25(1):19-25.

Metcalfe AD, Ferguson MW. Tissue engineering of replacement skin: the crossroads of biomaterials, wound healing, embryonic development, stem cells and regeneration. J R Soc Interface. 2007 Jun 22;4(14):413-37.

Milleret V, Simonet M, Bittermann AG, Neuenschwander P, Hall H. Cyto- and hemocompatibility of a biodegradable 3D-scaffold material designed for medical applications. J Biomed Mater Res B Appl Biomater. 2009 Oct;91(1):109-21.

Miyoshi S, Ishikawa H, Kaneko T, Fukui F, Tanaka H, Maruyama S. Structures and activity of angiotensin-converting enzyme inhibitors in an alpha-zein hydrolysate. Agric Biol Chem. 1991 May;55(5):1313-8.

Morihara K, Takai S, Takenaka H, Sakaguchi M, Okamoto Y, Morihara T, Miyazaki M, Kishimoto S. Cutaneous tissue angiotensin-converting enzyme may participate in pathologic scar formation in human skin. J Am Acad Dermatol. 2006 Feb;54(2):251-7.

Nielsen, NC. 1985, ‘Structure of soy proteins’ in New protein foods (Vol. 5), eds. Altschul AA, Wilcke HL, Academic Press, NY, USA; 27-64.

Nikolaychik VV, Samet MM, Lelkes PI. A new method for continual quantitation of viable cells on endothelialized polyurethanes. J Biomater Sci Polym Ed. 1996;7(10):881-91.

Nolte SV, Xu W, Rennekampff HO, Rodemann HP. Diversity of fibroblasts--a review on implications for skin tissue engineering. Cells Tissues Organs. 2008;187(3):165-76.

Noszczyk BH, Klein E, Holtkoetter O, Krieg T, Majewski S. Integrin expression in the dermis during scar formation in humans. Exp Dermatol. 2002 Aug;11(4):311-8.

Oliveira LO, Nam YW, Jung R, Nielsen NC. Processing and assembly in vitro of engineered soybean beta-conglycinin subunits with the asparagine-glycine proteolytic cleavage site of 11S globulins. Mol Cells. 2002 Feb 28;13(1):43-51.

Papazoglou ES, Zubkov L, Zhu L, Weingarten MS, Tyagi S, Pourrezaei K. Monitoring diabetic wound healing by NIR spectroscopy. Conf Proc IEEE Eng Med Biol Soc. 2005, 6:6662-6664.

Papazoglou ES, Weingarten MS, Zubkov L, Neidrauer M, Zhu L, Tyagi S, Pourrezaei K. Changes in optical properties of tissue during acute wound healing in an animal model. J Biomed Opt. 2008 Jul-Aug;13(4):044005.

Pardo A, Selman M. MMP-1: the elder of the family. Int J Biochem Cell Biol. 2005 Feb;37(2):283-8.

Park JH, Jeong HJ, Lumen BO. In vitro digestibility of the cancer-preventive soy peptides lunasin and BBI. J Agric Food Chem. 2007 Dec 26;55(26):10703-6.

Pickard BG. "Second extrinsic organizational mechanism" for orienting cellulose: modeling a role for the plasmalemmal reticulum. Protoplasma. 2008;233(1-2):7-29.

Powell HM, Supp DM, Boyce ST. Influence of electrospun collagen on wound contraction of engineered skin substitutes. Biomaterials. 2008 Mar;29(7):834-43.

Powell HM, Boyce ST. Engineered human skin fabricated using electrospun collagen-PCL blends: morphogenesis and mechanical properties. Tissue Eng Part A. 2009 Aug;15(8):2177-87.

Prost-Squarcioni C. [Histology of skin and hair follicle]. Med Sci (Paris). 2006 Feb;22(2):131-7.

Pukstad BS, Ryan L, Flo TH, Stenvik J, Moseley R, Harding K, Thomas DW, Espevik T. Non-healing is associated with persistent stimulation of the innate immune response in chronic venous leg ulcers. J Dermatol Sci. 2010 Aug;59(2):115-22.

Reddy N, Yang Y. Novel protein fibers from wheat gluten. Biomacromolecules. 2007 Feb;8(2):638-43.

Reddy N, Yang Y. Soyprotein fibers with high strength and water stability for potential medical applications. Biotechnol Prog. 2009 Nov-Dec;25(6):1796-802.

Reddy N, Jiang Q, Yang Y. Novel wheat protein films as substrates for tissue engineering. J Biomater Sci Polym Ed. 2010 Oct 27. PMID: 21029519

Reed CC, Iozzo RV. The role of decorin in collagen fibrillogenesis and skin homeostasis. Glycoconj J. 2002 May-Jun;19(4-5):249-55.

Reed MJ, Ferara NS, Vernon RB. Impaired migration, integrin function, and actin cytoskeletal organization in dermal fibroblasts from a subset of aged human donors. Mech Ageing Dev. 2001 Aug;122(11):1203-20.

Reid RR, Said HK, Mogford JE, Mustoe TA. The future of wound healing: pursuing surgical models in transgenic and knockout mice. J Am Coll Surg. 2004 Oct;199(4):578-85.

Rnjak J, Li Z, Maitz PK, Wise SG, Weiss AS. Primary human dermal fibroblast interactions with open weave three-dimensional scaffolds prepared from synthetic human elastin. Biomaterials. 2009 Nov;30(32):6469-77.

Saeed AI, Bhagabati NK, Braisted JC, Liang W, Sharov V, Howe EA, Li J, Thiagarajan M, White JA, Quackenbush J. TM4 microarray software suite. Methods Enzymol. 2006;411:134-93.

Salmela MT, Pender SL, Karjalainen-Lindsberg ML, Puolakkainen P, Macdonald TT, Saarialho-Kere U. Collagenase-1 (MMP-1), matrilysin-1 (MMP-7), and stromelysin-2 (MMP-10) are expressed by migrating enterocytes during intestinal wound healing. Scand J Gastroenterol. 2004 Nov;39(11):1095-104.

Sarkar S. Fibronectin mediated ES-D3 differentiation. Unpublished thesis (M.S.). 2006, Drexel University.

Scherer SS, Pietramaggiori G, Matthews J, Perry S, Assmann A, Carothers A, Demcheva M, Muise-Helmericks RC, Seth A, Vournakis JN, Valeri RC, Fischer TH, Hechtman HB, Orgill DP. Poly-N-acetyl glucosamine nanofibers: a new bioactive material to enhance diabetic wound healing by cell migration and angiogenesis. Ann Surg. 2009 Aug;250(2):322-30.

Schindler M, Meiners S, Cheresh DA. RGD-dependent linkage between plant cell wall and plasma membrane: consequences for growth. J Cell Biol. 1989 May;108(5):1955-65.

Sell SA, McClure MJ, Garg K, Wolfe PS, Bowlin GL. Electrospinning of collagen/biopolymers for regenerative medicine and cardiovascular tissue engineering. Adv Drug Deliv Rev. 2009 Oct 5;61(12):1007-19.

Selling GW, Sessa DJ, Palmquist DE. Effect of water and tri(ethylene) glycol on the rheological properties of zein. Polymer. 2004, 45(12):4249-55.

Selling GW, Biswas A, Patel A, Walls DJ, Dunlap C, Wei Y. Impact of solvent on electrospinning of zein and analysis of resulting fibers. Macromol Chem Phys. 2007, 208:1002-10.

Sethi KK, Yannas IV, Mudera V, Eastwood M, McFarland C, Brown RA. Evidence for sequential utilization of fibronectin, vitronectin, and collagen during fibroblast-mediated collagen contraction. Wound Repair Regen. 2002, 10:397-408.

Shenoy SL, Bates WD, Frisch HL, Wnek GE. Role of chain entanglements on fiber formation during electrospinning of polymer solutions: good solvent, non-specific polymer–polymer interaction limit. Polymer. 2005, 46:3372-84.

Shevchenko RV, James SL, James SE. A review of tissue-engineered skin bioconstructs available for skin reconstruction. J R Soc Interface. 2010 Feb 6;7(43):229-58.

Shinzawa H, Takeda A, Sone Y, Murashita K, Uchinuma E. Wound healing process of a full-thickness skin wound model in rats. Int Surg. 2007 Mar-Apr;92(2):63-72.

Shukla R, Cheryan M. Zein: the industrial protein from corn. Ind Crop Prod. 2001, 13:171-92.

Shutov AD, Kakhovskaya IA, Bastrygina AS, Bulmaga VP, Horstmann C, Müntz K. Limited proteolysis of beta-conglycinin and glycinin, the 7S and 11S storage globulins from soybean [Glycine max (L.) Merr.]. Structural and evolutionary implications. Eur J Biochem. 1996 Oct 1;241(1):221-8.

Siebers MC, Walboomers XF, van den Dolder J, Leeuwenburgh SC, Wolke JG, Jansen JA. The behavior of osteoblast-like cells on various substrates with functional blocking of integrin-beta1 and integrin-beta3. J Mater Sci Mater Med. 2008 Feb;19(2):861-8.

Sienkiewicz P, Surazyński A, Pałka J, Miltyk W. Nutritional concentration of genistein protects human dermal fibroblasts from oxidative stress-induced collagen biosynthesis inhibition through IGF-I receptor-mediated signaling. Acta Pol Pharm. 2008 Mar-Apr;65(2):203-11.

Silva GA, Vaz CM, Coutinho OP, Cunha AM, Reis RL. In vitro degradation and cytocompatibility evaluation of novel soy and sodium caseinate-based membrane biomaterials. J Mater Sci Mater Med. 2003 Dec;14(12):1055-66.

Silva SS, Santos MI, Coutinho OP, Mano JF, Reis RL. Physical properties and biocompatibility of chitosan/soy blended membranes. J Mater Sci Mater Med. 2005 Jun;16(6):575-9.

Sirén V, Salmenperä P, Kankuri E, Bizik J, Sorsa T, Tervahartiala T, Vaheri A. Cell-cell contact activation of fibroblasts increases the expression of matrix metalloproteinases. Ann Med. 2006;38(3):212-20.

Snyders R, Shingel KI, Zabeida O, Roberge C, Faure MP, Martinu L, Klemberg-Sapieha JE. Mechanical and microstructural properties of hybrid poly(ethylene glycol)-soy protein hydrogels for wound dressing applications. J Biomed Mater Res A. 2007 Oct;83(1):88-97.

Solon J, Levental I, Sengupta K, Georges PC, Janmey PA. Fibroblast adaptation and stiffness matching to soft elastic substrates. Biophys J. 2007 Dec 15;93(12):4453-61.

Sousa FF, Luzardo-Alvarez A, Pérez-Estévéz A, Seoane-Prado R, Blanco-Méndez J. Development of a novel AMX-loaded PLGA/zein microsphere for root canal disinfection. Biomed Mater. 2010 Oct;5(5):055008.

Stark HJ, Boehnke K, Mirancea N, Willhauck MJ, Pavesio A, Fusenig NE, Boukamp P. Epidermal homeostasis in long-term scaffold-enforced skin equivalents. J Investig Dermatol Symp Proc. 2006 Sep;11(1):93-105.

Stauffer WR, Cui XT. Polypyrrole doped with 2 peptide sequences from laminin. Biomaterials. 2006, 27:2405-2413.

Sullivan TP, Eaglstein WH, Davis SC, Mertz P. The pig as a model for human wound healing. Wound Repair Regen. 2001 Mar-Apr;9(2):66-76.

Sun QS, Dong J, Lin ZX, Yang B, Wang JY. Comparison of cytocompatibility of zein film with other biomaterials and its degradability in vitro. Biopolymers. 2005 Aug 5;78(5):268-74.

Sun LP, Wang S, Zhang ZW, Wang XY, Zhang QQ. Biological evaluation of collagen-chitosan scaffolds for dermis tissue engineering. Biomed Mater. 2009 Oct;4(5):055008.

Surazyński A, Sienkiewicz P, Wołczyński S, Pałka J. Differential effects of echistatin and thrombin on collagen production and prolidase activity in human dermal fibroblasts and their possible implication in beta1-integrin-mediated signaling. Pharmacol Res. 2005 Mar;51(3):217-21.

Szulgit G, Rudolph R, Wandel A, Tenenhaus M, Panos R, Gardner H. Alterations in fibroblast alpha1beta1 integrin collagen receptor expression in keloids and hypertrophic scars. J Invest Dermatol. 2002 Mar;118(3):409-15.

Taubenberger A, Cisneros DA, Friedrichs J, Puech PH, Muller DJ, Franz CM. Revealing early steps of alpha2beta1 integrin-mediated adhesion to collagen type I by using single-cell force spectroscopy. Mol Biol Cell. 2007 May;18(5):1634-44.

Thélu J, Rossio P, Favier B. Notch signalling is linked to epidermal cell differentiation level in basal cell carcinoma, psoriasis and wound healing. BMC Dermatol. 2002 Apr 29;2:7.

Toriseva M, Kähäri VM. Proteinases in cutaneous wound healing. Cell Mol Life Sci. 2009 Jan;66(2):203-24.

Tsuruki T, Kishi K, Takahashi M, Tanaka M, Matsukawa T, Yoshikawa M. Soymetide, an immunostimulating peptide derived from soybean beta-conglycinin, is an fMLP agonist. FEBS Lett. 2003 Apr 10;540(1-3):206-10.

Tu J, Wang H, Li H, Dai K, Wang J, Zhang X. 2009, The in vivo bone formation by mesenchymal stem cells in zein scaffolds. Biomaterials. 2009 Sep;30(26):4369-76.

Valsecchi AE, Franchi S, Panerai AE, Rossi A, Sacerdote P, Colleoni M. The soy isoflavone genistein reverses oxidative and inflammatory state, neuropathic pain, neurotrophic and vasculature deficits in diabetes mouse model. Eur J Pharmacol. 2011 Jan 15;650(2-3):694-702.

van Aalst JA, Reed CR, Han L, Andrady T, Hromadka M, Bernacki S, Kolappa K, Collins JB, Loboa EG. Cellular incorporation into electrospun nanofibers: retained viability, proliferation, and function in fibroblasts. Ann Plast Surg. 2008 May;60(5):577-83.

van der Valk P, van Pelt AW, Busscher HJ, de Jong HP, Wildevuur CR, Arends J. 1983, Interaction of fibroblasts and polymer surfaces: relationship between surface free energy and fibroblast spreading. J Biomed Mater Res. 1983 Sep;17(5):807-17.

Van Tomme SR, Storm G, Hennink WE. In situ gelling hydrogels for pharmaceutical and biomedical applications. Int J Pharm. 2008 May 1;355(1-2):1-18.

Vaz CM, De Graaf LA, Reis RL, Cunha AM. 2003a, Effect of crosslinking, thermal treatment and UV irradiation on the mechanical properties and in vitro degradation behavior of several natural proteins aimed to be used in the biomedical field. J Mater Sci Mater Med. 2003 Sep;14(9):789-96.

Vaz CM, De Graaf LA, Reis RL, Cunha AM. 2003b, In vitro degradation behaviour of biodegradable soy plastics: effects of crosslinking with glyoxal and thermal treatment, Polymer Degrad and Stabil. 2003, 81:65–74.

Vaz CM, van Doeveren PF, Reis RL, Cunha AM. 2003c, Soy matrix drug delivery systems obtained by melt-processing techniques. Biomacromolecules. 2003 Nov-Dec;4(6):1520-9.

Vaz CM, van Doeveren PF, Dias GR, Reis RL, Cunha AM. Controlled delivery achieved with bi-layer matrix devices produced by co-injection moulding. Macromol Biosci. 2004 Aug 9;4(8):795-801.

Vega-Lugo A, Lim L. Electrospinning of soy protein isolate nanofibers, J Biobased Materials and Bioenergy. 2008, 2:223-30.

Waldeck H, Chung AS, Kao WJ. Interpenetrating polymer networks containing gelatin modified with PEGylated RGD and soluble KGF: synthesis, characterization, and application in in vivo critical dermal wound. J Biomed Mater Res A. 2007 Sep 15;82(4):861-71.

Waller JM, Maibach HI. Age and skin structure and function, a quantitative approach (II): protein, glycosaminoglycan, water, and lipid content and structure. Skin Res Technol. 2006 Aug;12(3):145-54.

Walter N, Selhuber C, Kessler H, Spatz JP. Cellular unbinding forces of initial adhesion processes on nanopatterned surfaces probed with magnetic tweezers. Nano Lett. 2006 Mar;6(3):398-402.

Wang F, Li Z, Tamama K, Sen CK, Guan J. Fabrication and characterization of prosurvival growth factor releasing, anisotropic scaffolds for enhanced mesenchymal stem cell survival/growth and orientation. Biomacromolecules. 2009 Sep 14;10(9):2609-18.

Wang HJ, Gong SJ, Lin ZX, Fu JX, Xue ST, Huang JC, Wang JY. In vivo biocompatibility and mechanical properties of porous zein scaffolds. Biomaterials. 2007 Sep;28(27):3952-64.

Wang Q, Zheng YP. Ultrasound biomicroscopy imaging for monitoring progressive trypsin digestion and inhibition in articular cartilage. Ultrasound Med Biol. 2009 Sep;35(9):1535-45.

Wang W, Bringe NA, Berhow MA, Gonzalez de Mejia E. beta-Conglycinins among sources of bioactives in hydrolysates of different soybean varieties that inhibit leukemia cells in vitro. J Agric Food Chem. 2008 Jun 11;56(11):4012-20.

Wang W, Dia VP, Vasconez M, de Mejia EG, Nelson RL. Analysis of soybean protein-derived peptides and the effect of cultivar, environmental conditions, and processing on lunasin concentration in soybean and soy products. J AOAC Int. 2008 Jul-Aug;91(4):936-46.

Wang W, Zhang M, Lu W, Zhang X, Ma D, Rong X, Yu C, Jin Y. Cross-linked collagen-chondroitin sulfate-hyaluronic acid imitating extracellular matrix as scaffold for dermal tissue engineering. Tissue Eng Part C Methods. 2010 Apr;16(2):269-79.

Wang YY, Lü LX, Feng ZQ, Xiao ZD, Huang NP. Cellular compatibility of RGD-modified chitosan nanofibers with aligned or random orientation. Biomed Mater. 2010 Oct;5(5):054112.

Weingarten MS, Papazoglou E, Zubkov L, Zhu L, Vorona G, Walchack A. Measurement of optical properties to quantify healing of chronic diabetic wounds. Wound Repair Regen. 2006 May-Jun;14(3):364-70.

Weingarten MS, Papazoglou ES, Zubkov L, Zhu L, Neidrauer M, Savir G, Peace K, Newby JG, Pourrezaei K. Correlation of near infrared absorption and diffuse reflectance spectroscopy scattering with tissue neovascularization and collagen concentration in a diabetic rat wound healing model. Wound Repair Regen. 2008 Mar-Apr;16(2):234-42.

Weingarten MS, Neidrauer M, Mateo A, Mao X, McDaniel JE, Jenkins L, Bouraee S, Zubkov L, Pourrezaei K, Papazoglou ES. Prediction of wound healing in human diabetic foot ulcers by diffuse near-infrared spectroscopy: a pilot study. Wound Repair Regen. 2010 Mar;18(2):180-5.

Woerdeman DL, Ye P, Shenoy S, Parnas RS, Wnek GE, Trofimova O. Electrospun fibers from wheat protein: investigation of the interplay between molecular structure and the fluid dynamics of the electrospinning process. Biomacromolecules. 2005 Mar-Apr;6(2):707-12.

Wong T, Gammon L, Liu L, Mellerio JE, Dopping-Hepenstal PJ, Pacy J, Elia G, Jeffery R, Leigh IM, Navsaria H, McGrath JA. Potential of fibroblast cell therapy for recessive dystrophic epidermolysis bullosa. J Invest Dermatol. 2008 Sep;128(9):2179-89.

Wong VW, Rustad KC, Galvez MG, Neofyotou E, Glotzbach JP, Januszyk M, Major MR, Sorkin M, Longaker MT, Rajadas J, Gurtner GC. Engineered pullulan-collagen composite dermal hydrogels improve early cutaneous wound healing. Tissue Eng Part A. 2011 Mar;17(5-6):631-44.

Wood MA, Bagnaninchi P, Dalby MJ. The beta integrins and cytoskeletal nanoimprinting. Exp Cell Res. 2008 Feb 15;314(4):927-35.

Woodfield TB, Miot S, Martin I, van Blitterswijk CA, Riesle J. The regulation of expanded human nasal chondrocyte re-differentiation capacity by substrate composition and gas plasma surface modification. Biomaterials. 2006 Mar;27(7):1043-53.

Woodley DT, Remington J, Huang Y, Hou Y, Li W, Keene DR, Chen M. Intravenously injected human fibroblasts home to skin wounds, deliver type VII collagen, and promote wound healing. Mol Ther. 2007 Mar;15(3):628-35.

Xiao J, Addabbo RM, Lauer JL, Fields GB, Baum J. Local conformation and dynamics of isoleucine in the collagenase cleavage site provide a recognition signal for matrix metalloproteinases. J Biol Chem. 2010 Oct 29;285(44):34181-90.

Xu YZ, Wu JJ, Chen YP, Liu J, Li N, Yang FY. The use of zein and Shuanghuangbu for periodontal tissue engineering. Int J Oral Sci. 2010 Sep;2(3):142-8.

Yang X, Shah JD, Wang H. Nanofiber enabled layer-by-layer approach toward three-dimensional tissue formation. Tissue Eng Part A. 2009 Apr;15(4):945-56.

Yao C, Li X, Song T. Electrospinning and crosslinking of zein nanofiber mats. J Appl Polymer Sci. 2007, 103:380-5.

Zabrodin, I. Design and characterization of a biodegradable, nanofibrous scaffold incorporating microspheres for sustained release of soluble proteins. Unpublished thesis (M.S.). 2009, Drexel University.

Zawko SA, Schmidt CE. Crystal templating dendritic pore networks and fibrillar microstructure into hydrogels. Acta Biomater. 2010 Jul;6(7):2415-21.

Zhang X, Min B G, Kumar S. Solution spinning and characterization of poly(vinyl alcohol)/soybean protein blend fibers. J Appl Polymer Sci. 2003, 90:716-21.

Zlatanov I, Groth T, Lendlein A, Altankov G. Dynamics of beta1-integrins in living fibroblasts--effect of substratum wettability. Biophys J. 2005 Nov;89(5):3555-62.

Znoyko I, Trojanowska M, Reuben A. Collagen binding alpha2beta1 and alpha1beta1 integrins play contrasting roles in regulation of Ets-1 expression in human liver myofibroblasts. Mol Cell Biochem. 2006 Jan;282(1-2):89-99.

http://en.wikipedia.org/wiki/Image:3DScience_skin_section_labeled.jpg

http://www.che.vt.edu/Wilkes/electrospinning/electrspinning.html

Appendix. Human ECM and cell adhesion related genes

96-well PCR array of human extracellular matrix and cell adhesion molecules:

ADAMTS1 A01	ADAMTS13 A02	ADAMTS8 A03	CD44 A04	CDH1 A05	CNTN1 A06	COL11A1 A07	COL12A1 A08	COL14A1 A09	COL15A1 A10	COL16A1 A11	COL1A1 A12
COL4A2 B01	COL5A1 B02	COL6A1 B03	COL6A2 B04	COL7A1 B05	COL8A1 B06	VCAN B07	CTGF B08	CTNNA1 B09	CTNNB1 B10	CTNND1 B11	CTNND2 B12
ECM1 C01	FN1 C02	HAS1 C03	ICAM1 C04	ITGA1 C05	ITGA2 C06	ITGA3 C07	ITGA4 C08	ITGA5 C09	ITGA6 C10	ITGA7 C11	ITGA8 C12
ITGAL D01	ITGAM D02	ITGAV D03	ITGB1 D04	ITGB2 D05	ITGB3 D06	ITGB4 D07	ITGB5 D08	KAL1 D09	LAMA1 D10	LAMA2 D11	LAMA3 D12
LAMB1 E01	LAMB3 E02	LAMC1 E03	MMP1 E04	MMP10 E05	MMP11 E06	MMP12 E07	MMP13 E08	MMP14 E09	MMP15 E10	MMP16 E11	MMP2 E12
MMP3 F01	MMP7 F02	MMP8 F03	MMP9 F04	NCAM1 F05	PECAM1 F06	SELE F07	SELL F08	SELP F09	SGCE F10	SPARC F11	SPG7 F12
SPP1 G01	TGFBI G02	THBS1 G03	THBS2 G04	THBS3 G05	TIMP1 G06	TIMP2 G07	TIMP3 G08	CLEC3B G09	TNC G10	VCAM1 G11	VTN G12
B2M H01	HPRT1 H02	RPL13A H03	GAPDH H04	ACTB H05	HGDC H06	RTC H07	RTC H08	RTC H09	PPC H10	PPC H11	PPC H12

The molecules are functionally grouped as follows:

<u>Cell Adhesion Molecules:</u>

Transmembrane Molecules: CD44, CDH1, HAS1, ICAM1, ITGA1, ITGA2, ITGA3, ITGA4, ITGA5, ITGA6, ITGA7, ITGA8, ITGAL, ITGAM, ITGAV, ITGB1, ITGB2, ITGB3, ITGB4, ITGB5, MMP14, MMP15, MMP16, NCAM1, PECAM1, SELE, SELL, SELP, SGCE, SPG7, VCAM1.

Cell-Cell Adhesion: CD44, CDH1, COL11A1, COL14A1, COL6A2, CTNND1, ICAM1, ITGA8, VCAM1.

Cell-Matrix Adhesion: ADAMTS13, CD44, ITGA1, ITGA2, ITGA3, ITGA4, ITGA5, ITGA6, ITGA7, ITGA8, ITGAL, ITGAM, ITGAV, ITGB1, ITGB2, ITGB3, ITGB4, ITGB5, SGCE, SPP1, THBS3.

Other Adhesion Molecules: CNTN1, COL12A1, COL15A1, COL16A1, COL5A1, COL6A1, COL7A1, COL8A1, VCAN, CTGF, CTNNA1, CTNNB1, CTNND2, FN1, KAL1, LAMA1, LAMA2, LAMA3, LAMB1, LAMB3, LAMC1, THBS1, THBS2, CLEC3B, TNC, VTN.

Extracellular Matrix Proteins:

Basement Membrane Constituents: COL4A2, COL7A1, LAMA1, LAMA2, LAMA3, LAMB1, LAMB3, LAMC1, SPARC.

Collagens & ECM Structural Constituents: COL11A1, COL12A1, COL14A1, COL15A1, COL16A1, COL1A1, COL4A2, COL5A1, COL6A1, COL6A2, COL7A1, COL8A1, FN1, KAL1.

ECM Proteases: ADAMTS1, ADAMTS13, ADAMTS8, MMP1, MMP10, MMP11, MMP12, MMP13, MMP14, MMP15, MMP16, MMP2, MMP3, MMP7, MMP8, MMP9, SPG7, TIMP1.

ECM Protease Inhibitors: COL7A1, KAL1, THBS1, TIMP1, TIMP2, TIMP3.

Other ECM Molecules: VCAN, CTGF, ECM1, HAS1, SPP1, TGFBI, THBS2, THBS3, CLEC3B, TNC, VTN.

http://www.sabiosciences.com/rt_pcr_product/HTML/PAHS-013A.html

Vita

Leko Lin

Education

Ph.D. in Biomedical Engineering - Drexel University, Philadelphia, PA (February 2011).

BSc(Eng) (1st Class Honours) in Engineering with Medical Engineering - Queen Mary College, University of London, UK (June 2003).

Teaching and Professional Experience

Teaching Assistant - Drexel University (2006, 2008-2009)

-Tissue Engineering (I, II, III); The Body Synthetic; Engineering Principles of Living Systems I

Test Technician - DePuy International, Leeds, UK (2003 – 2004)

Publications and Presentations

Lin L, Varma D, Perets, A, Li M, Lazarovici P, Woerdeman DL, Lelkes PI. Alimentary "Green" Proteins as Electrospun Scaffolds for Regenerative Engineering. *Journal of Tissue Engineering and Regenerative Medicine*. (in review)

Lelkes PI, Li M, Perets A, Lin L, Han J, Woerdeman DL. 2008, 'Electrospinning of natural proteins for tissue engineering scaffolding' in Handbook of Natural-based Polymers for Biomedical Applications, ed. Reis RL, Woodhead Publishing Ltd, Cambridge, UK; 446-482

Lin L, Varma D, Perets, A, Li M, Woerdeman DL, Lelkes PI. Oral presentation at the 8th World Biomaterials Congress, Amsterdam, The Netherlands, May 28 – June 1, 2008.

Lin L, Varma D, Perets, A, Li M, Woerdeman DL, Lelkes PI. Oral presentation at the ACS 236th National Meeting, Philadelphia, August 17 – 21, 2008.

Lin L, Perets A, Woerdeman DL, Wasko K, Mao X, Samuels J, Weingarten MS, Papazoglou ES, Lelkes PI. Oral presentation at the Tissue Engineering and Regenerative Medicine International Society Asia-Pacific (TERMIS-AP) Chapter Meeting, Sydney, Australia, September 15-17, 2010.

Awards

(2006 – 2008) National Science Foundation Integrative Graduate Education and Research Traineeship (NSF-IGERT) (Grant nos. DGE-0221664 and DGE-0654313)